

Molecular mechanisms of alarmones during bacterial stress responses

Kumulative Dissertation

zur Erlangung des Grades eines

Doktor der Naturwissenschaften

(Dr. rer.nat.)

des Fachbereichs Chemie der Philipps-Universität Marburg

Vorgelegt von

MSc, Pietro Ivan, Giammarinaro

Aus Mazara del Vallo, Italien

Marburg, 2023

Die vorliegende Dissertation wurde von Februar/2017 bis August/2022 am
Fachbereich Chemie, unter Leitung von Prof. Dr. Gert Bange angefertigt.

Vom Fachbereich Chemie der Philipps-Universität Marburg
(Hochschulkennziffer 1180) als Dissertation angenommen am _____

Erstgutachter: Prof. Dr. Gert Bange

Zweitgutachter: Dr. Georg Hochberg

Drittgutachter: Prof. Dr. Andreas Seubert

Viertgutachter: Prof. Dr. Olalla Vázquez

Tag der Disputation: _____

Statutory Declaration

I hereby declare that the present dissertation is entirely of my own intellectual conception. To the best of my knowledge no part of this work has been submitted or presented to other institutions in fulfilment of an academic degree. In the following pages all the sources are referenced, and the contributions are acknowledged.

Pietro Ivan Giammarinaro

Heidelberg, 12th September 2022

Eidesstattliche Erklärung

Hiermit versichere ich, Pietro Ivan Giammarinaro, dass ich meine Dissertation selbständig ohne unerlaubte Hilfe angefertigt habe, mich dabei keiner anderen als der von mir ausdrücklich bezeichneten Quellen und Hilfen bediene und alle vollständigen oder sinngemäß übernommenen Zitate als solche gekennzeichnet habe. Die Dissertation wurde in der jetzigen oder einer ähnlichen Form noch bei keiner anderen Hochschule eingereicht und hat noch keinen sonstigen Prüfungszwecken gedient.

Pietro Ivan Giammarinaro

Heidelberg, 12th September 2022

Academic records

Pietro Ivan Giammarinaro

Date of birth 09/01/1991, Mazara del Vallo (TP), Italy.

ORCID: 0000-0002-0356-8481

Marburg University, Chemistry Department, AG Bange

Feb. 2017 - Aug. 2022

- PhD Candidate.

GlaxoSmithKline Vaccines (GSK), Siena (Italy)

May 2016 – Oct. 2016

- Internship at the Proteomics and Antigen Design Lab.

Jun 2015 - Apr. 2016

- Master's student at the Proteomics and Antigen Design Lab.

Università degli Studi di Siena, (Siena, Italy)

2010 - Apr 2016

- Degree course in Pharmaceutical Chemistry and Technology

Title of the Msc. degree thesis: *A new strategy for conformational analysis of membrane antigens in native environment by Hydrogen-Deuterium Exchange Mass Spectrometry.*

Academic Mentor: Pr. Lorenza Trabalzini

In situ Mentors: Dr. Nathalie Norais and Dr. Danilo Donnarumma

Final score: 106/110.

Publications discussed in the thesis

#1 **Giammarinaro, P. I.**, M. K. M. Young, W. Steinchen, C. N. Mais, G. Hochberg, J. Yang, D. M. Stevenson, D. Amador-Noguez, A. Paulus, J. D. Wang, and G. Bange. 2022. '**Diadenosine tetraphosphate regulates biosynthesis of GTP in *Bacillus subtilis***', Nat Microbiol, 7: 1442-52.

#2 Czech, L., C. N. Mais, H. Kratzat, P. Sarmah, **P. Giammarinaro**, S. A. Freibert, H. F. Esser, J. Musial, O. Berninghausen, W. Steinchen, R. Beckmann, H. G. Koch, and G. Bange. 2022. '**Inhibition of SRP-dependent protein secretion by the bacterial alarmone (p)ppGpp**', Nat Commun, 13: 1069.

#3 Steinchen, W., M. S. Vogt, F. Altegoer, **P. I. Giammarinaro**, P. Horvatek, C. Wolz, and G. Bange. 2018. '**Structural and mechanistic divergence of the small (p)ppGpp synthetases RelP and RelQ**', Sci Rep, 8: 2195.

Publications not discussed in the thesis

Altegoer, F., T. E. F. Quax, P. Weiland, P. Nussbaum, **P. I. Giammarinaro**, M. Patro, Z. Li, D. Oesterhelt, M. Grininger, S. V. Albers, and G. Bange. 2022. 'Structural insights into the mechanism of archaeellar rotational switching', *Nat Commun*, 13: 2857.

Feyh, R., N. B. Waeber, S. Prinz, **P. I. Giammarinaro**, G. Bange, G. Hochberg, R. K. Hartmann, and F. Altegoer. 2021. 'Structure and mechanistic features of the prokaryotic minimal RNase P', *Elife*, 10.

Osorio-Valeriano, M., F. Altegoer, C. K. Das, W. Steinchen, G. Panis, L. Connolley, G. Giacomelli, H. Feddersen, L. Corrales-Guerrero, **P. I. Giammarinaro**, J. Hanssmann, M. Bramkamp, P. H. Viollier, S. Murray, L. V. Schafer, G. Bange, and M. Thanbichler. 2021. 'The CTPase activity of ParB determines the size and dynamics of prokaryotic DNA partition complexes', *Mol Cell*, 81: 3992-4007 e10.

Altegoer, F., P. Weiland, **P. I. Giammarinaro**, S. A. Freibert, L. Binnebesel, X. Han, A. Lepak, R. Kahmann, M. Lechner, and G. Bange. 2020. 'The two paralogous kiwellin proteins KWL1 and KWL1-b from maize are structurally related and have overlapping functions in plant defense', *J Biol Chem*, 295: 7816-25.

Han, X., F. Altegoer, W. Steinchen, L. Binnebesel, J. Schuhmacher, T. Glatter, **P. I. Giammarinaro**, A. Djamei, S. A. Rensing, S. Reissmann, R. Kahmann, and G. Bange. 2019. 'A kiwellin disarms the metabolic activity of a secreted fungal virulence factor', *Nature*, 565: 650-53.

Donnarumma, D., C. Maestri, **P. I. Giammarinaro**, L. Capriotti, E. Bartolini, D. Veggi, R. Petracca, M. Scarselli, and N. Norais. 2018. 'Native State Organization of Outer Membrane Porins Unraveled by HDx-MS', *J Proteome Res*, 17: 1794-800.

Acknowledgements

As first I need to express my deep gratitude to Prof. Dr. Gert Bange when in 2017 gave me the opportunity to join his group. At that time, I only had the desire to learn more about structural biology and I could not imagine what was waiting for me. Of course, most of what makes me as a scientist today is due to my scientific maturation in the Bange's lab. Especially I am grateful to Prof. Dr. Bange for the attitude towards science he transmitted to me: be brave and challenge the consolidated knowledge. He made me look at biological questions with a pragmatic approach when they were enigmatic and obscure.

Looking back in time I cannot neglect any of the experiences lived in the Bange's lab and I will bring them always with me. A very long list of people should be present in this page of acknowledgements. But in this moment, I feel to remember few names for their consistent contribution to my personal carrier and life.

Dr. Wieland Steinchen and Dr. Florian Altegoer were always a present figure when I needed to share doubts and hesitations while I was facing biochemistry or structural biology.

Dr. Patricia Bedrunka, Dr. Marino Moretti, Dr. Laura Czech and Dr. Felix Dempwolff were as well extremely significant during my PhD.

The rest of the Bange's crew is going to be in my heart forever. Mohamad, Devid, Liu, Itzel, Victor, Anita, Marvin, Nils, Paul and Eslam. I can only tell you thanks for all the emotions and keep rocking.

I am also grateful to Mrs Karin Sievers, Dr. Jan Kellmann and Dr. Jan Pane-Farre. I won't forget your support over the last years.

Dr. Georg Hochberg has been a friend and a mentor for me. I am genuinely jealous of his group, and I wish him all the best.

Enrica, mamma *e* papà, we are each other's extension and no words in line can describe us. Thanks to be me so many times.

*A Giulio Regeni, anche se
non ci siamo mai conosciuti.*

Table of Contents

<i>Abstract</i> _____	<i>xiv</i>
<i>Zusammenfassung</i> _____	<i>xvi</i>
<i>List of abbreviations</i> _____	<i>19</i>
<i>Introduction</i> _____	<i>21</i>
<i>The Heat Shock Response</i> _____	<i>21</i>
<i>Bacillus subtilis' protein actors in HSR</i> _____	<i>22</i>
<i>Ap4A as signal molecule during stress</i> _____	<i>23</i>
<i>(p)ppGpp in the Stress Response</i> _____	<i>26</i>
<i>Stringent response and membrane protein biogenesis</i> _____	<i>28</i>
<i>Regulation of (p)ppGpp pools</i> _____	<i>29</i>
<i>References of the Introduction</i> _____	<i>30</i>
<i>Publication #1</i> _____	<i>38</i>
<i>Publication #2</i> _____	<i>64</i>
<i>Publication #3</i> _____	<i>79</i>
<i>Discussion</i> _____	<i>90</i>
<i>Ap4A is a central component in thermoresistance of Bacillus subtilis</i>	<i>90</i>
<i>Regulation of eukaryotic and prokaryotic IMPDH enzymes</i> _____	<i>92</i>
<i>IMPDH and (p)ppGpp</i> _____	<i>93</i>
<i>Priorities in Stringent Response</i> _____	<i>96</i>
<i>Diversification in (p)ppGpp production</i> _____	<i>98</i>
<i>References of the Discussion</i> _____	<i>100</i>

Abstract

In the incessant effort of living and propagating, bacterial cells cope with environmental stress via the release of second messengers and/or alarmones that allow them to adapt swiftly. Such molecules are nucleotide-based and can be promptly generated when stress stimuli occur. According to the cellular concentration of stress mediators, specific molecular targets would be activated to modulate vital processes for bacterial survival and proliferation. As soon as the stress is over, cells would reconstitute the initial concentration of the stress-coping mediators with deputed enzymes. Overall, the aforementioned mechanisms fall in the definition of Bacterial Stress Response (BSR).

The aim of the present doctoral thesis is to illustrate and discuss three published scientific articles that contributed to the understanding of the BSR in bacterial cells and the role of the stress mediators 5',5''-diadenosine tetraphosphate (Ap4A) and ppGpp and pppGpp (collectively (p)ppGpp).

The Publication #1 described how Ap4A could restrict the activity of the essential enzyme inosine monophosphate dehydrogenase (IMPDH) in *Bacillus subtilis* in order to reprogram the levels of purine nucleotides during heat shock. The present publication proposed IMPDH as the first physiologically confirmed target of Ap4A in prokaryotes and characterized the molecular mechanisms of how Ap4A inhibits IMPDH. The biological relevance of the interaction Ap4A-IMPDH was further analyzed and proven with *in vivo* experiments.

The Publication #2 aimed to expand the knowledge of the membrane proteins insertion and translocation dynamics during Stringent Response (SR) in *Bacillus subtilis* and *Escherichia coli*. In many organisms, the Signal Recognition Particle (SRP) complex, composed of the 4.5s RNA and the GTPase Ffh, facilitates protein insertion and translocation through membranes co- or post-translationally. Since the SR induces the conversion of GDP and GTP to the alarmones ppGpp and pppGpp respectively, such molecules could inhibit Ffh and its receptor Ftsy. Ffh and Ftsy are known to form a heterodimer supported by a symmetrical GTP coordination in their active sites. The Publication #2 offered a variety of *in vitro* data that demonstrated how ppGpp and pppGpp could both substitute GTP in the nucleotide binding sites of Ffh and Ftsy and impede their functional heterodimer complex. This study shows how wide is the spectrum of (p)ppGpp's targets in the 'protein production chain'.

The enzymes responsible for the formation of (p)ppGpp are known to be RelA/SpoT like Homology proteins (RSH) in both bacteria and plants. The typical RSH protein possesses a synthetase domain and/or a hydrolase domain, plus other domains crucial for tRNA and ribosome association. In multiple genomes also shorter RSH proteins were found, called small alarmone synthetases (SAS) consisting just of a small synthetase domain. Such proteins contribute in the (p)ppGpp production during SR. In the Publication #3, enzymatic and crystallographic studies of bacterial SAS proteins – RelP and RelQ – are presented showing how (p)ppGpp formation can be orchestrated in the Gram-positives *Bacillus subtilis* and *Staphylococcus aureus*.

Zusammenfassung

Zwecks der ständigen Bemühung zum Existieren und der Vermehrung gehen Bakterienzellen mit Stress in der Umgebung um, indem sie sich mithilfe von Second Messengern und/oder Alarmones anpassen. Solche Moleküle sind Nuklotide basiert und können beim Auftreten von Stress-Stimuli schnell generiert werden.

Der Zellkonzentrationen von Stressmediatoren entsprechend können bestimmte molekulare Ziele beeinflusst werden, um bedeutende physiologische Prozesse, die zum Überleben und zur Vermehrung beitragen, fein zu modulieren.

Sobald die Stressquelle zu Ende ist, können die Zellen mithilfe von übertragenen Enzymen ihre physiologischen Niveaus der Mediatoren wiederbeleben. Im Großen und Ganzen fallen Mechanismen, wie oben erwähnt, in die Definition *Bacterial Stress Response* (BSF).

Ziel der vorliegenden Dissertation ist es, drei publizierte Artikel aufzuzeigen und darüber zu diskutieren. Die drei erwähnten Veröffentlichungen sollen zum Verständnis der BSF in bakteriellen Zellen und der Rolle des Stressmediators 5',5"-diadenosine tetraphosphate (Ap4A), ppGpp sowie pppGpp (kollektiv (p)ppGpp) beitragen.

Die erste Publikation vorschlägt, wie Ap4A die Aktivität des essenziellen Enzyms inosine monophosphate dehydrogenase (IMPDH) in *Bacillus subtilis* einschränken kann, um die Niveaus von purine nucleotides während Hitzeschocks umzuprogrammieren. Die vorliegende Veröffentlichung zeigt IMPDH als das erste physiologisch bestätigte Ziel von Ap4A in Prokaryota und beschreibt die molekularen Mechanismen, wie Ap4A IMPDH hindert. Zudem wurde die biologische Relevanz der Interaktion zwischen

Ap4A und IMPDH analysiert und anhand der *in vivo* Experimente überprüft.

Die zweite Publikation zielt darauf, die Erkenntnisse des Einfügens der Membranproteine sowie der Translokationsdynamik während der Stringent Response (SR) in *Bacillus subtilis* und *Escherichia coli* zu erweitern. In vielen Organismen fördert der Signal Recognition Particle (SRP) Komplex, der aus der 4.5s RNA und den GTPase Ffh besteht, co- oder post-translational den Einschub von Proteinen und die Ortsveränderung durch Membrane. Dadurch, dass die SR die Umwandlung von GDP und GTP in die Alarmone ppGpp and pppGpp dementsprechend veranlasst, konnten solche Moleküle Ffh und dessen Empfänger Ftsy hindern. Ffh sowie Ftsy sind dafür bekannt, dass sie mithilfe der aktiven Seite einer symmetrischen GTP-Koordination einen Heterodimer formen. Die zweite Veröffentlichung bietet vielfältige *in vitro* Daten, die zeigen, wie sowohl ppGpp als auch pppGpp GTP bei der Nukleotidbindestelle von Ffh sowie Ftsy ersetzen konnten und dabei ihren funktionalen Heterodimerkomplex erschweren. Dieser Artikel zeigt, wie weit das Spektrum von Zielen der (p)ppGpp in der "Produktionskette von Proteinen".

Die Enzyme, die das Formen von (p)ppGpp verantworten, sind als RelA/SpoT wie homologe Proteine (RSH) in sowohl Bakterien als auch Pflanzen bekannt. Das typische RSH-Protein besitzt eine Synthetase Domäne und/oder eine Hydrolase Domäne und zusätzlich dazu andere Domänen, die für tRNA sowie eine ribosome Assoziation wichtig sind. In zahlreichen Genomen wurden ebenso kurze RSH-Proteine, sogenannte Alarmone Synthetasen (SAS), gefunden. Diese bestehen lediglich aus einer kleinen Synthetase Domäne. Solche Proteine tragen zur Produktion von (p)ppGpp während SR bei. In der dritten Publikation werden enzymatische und kristallographische Charakterisierungen eines bakteriellen SAS-Proteins, RelP zwecks Aufklärung aufgezeigt, wie unterschiedlich die

(p)ppGpp Bildung in die Gram-positive *Bacillus subtilis* und *Staphylococcus aureus*.

List of abbreviations

aaRSs	Aminoacyl tRNA synthetases
ADP	Adenosine diphosphate
AMP	Adenosine monophosphate
Ap ₄ A	Diadenosine 5',5''-P ₁ ,P ₄ -tetraphosphate
ATP	Adenosine triphosphate
<i>B. subtilis</i> or <i>Bs</i>	<i>Bacillus subtilis</i>
CBS	Cystathionine β-synthetase
CryoEM	Cryogenic electron microscopy
GDP	Guanosine diphosphate
GMP	Guanosine monophosphate
GTP	Guanosine triphosphate
HIT	Histidine triad
HS	Heat shock
HSP	Heat shock proteins
HSR	Heat shock response
IMP	Inosine-5'-monophosphate
IMPDH	Inosine-5'-monophosphate dehydrogenase
ITC	Isothermal titration calorimetry
K _D	Dissociation constant
K _i	Inhibitory constant
MST	MicroScale thermophoresis
N _p xN	Dinucleotides bridged with n phosphates
Nudix	Nucleoside diphosphate linked moiety X
Nudt2	Nudix hydrolase 2
ppGpp	Guanosine tetraphosphate

pppGpp	Guanosine pentaphosphate
PQCS	Protein quality control system
RNA	Ribonucleic acid
rpoH	Sigma factor σ^{32}
RSH	RelA/SpoT homology enzyme
SAS	Small alarmone synthetases
SR	Stringent response
SRP	Signal recognition particle
tRNA	Transfer Ribonucleic acid
XMP	Xanthosine-5'-monophosphate

Introduction

The Heat Shock Response

Typically, when a cell is exposed to a higher temperature, its proteome is under risk of unfolding. In such situation, hydrophobic regions of proteins become exposed to the surrounding solvent and, thus, prone to aggregation. Moreover, the nascent chains emerging from ribosomes might not reach the ideal functional folding. Other cellular components could also be highly compromised like membranes, but a non-functional pool of proteins is lethal for any cell because they are the only tools to rescue physiological conditions during stress situations.

In order to fight temperature fluctuations, eukaryotes and prokaryotes evolved over billions of years common mechanisms that are nowadays described as heat shock response (HSR)^{1,2}. The HSR signaling components were first observed and described in *Drosophila melanogaster*³. Similar processes were later characterized also in prokaryotes. There, a set of genes is up regulated during heat stress (or shock, HS) and they code for chaperones and proteases (heat shock proteins, HSP) that contribute in a global reaction to proteotoxic stress⁴ or to oxidation stress⁵.

***Bacillus subtilis*' protein actors in HSR**

Bacillus subtilis (*B. subtilis*) is a soil-ubiquitous gram-positive bacterium, and like many other prokaryotes, sustains HS thanks to chaperones and proteases that all together contribute to a general 'protein quality control system' (PQCS). In many bacteria, the sigma factor σ^{32} (rpoH) is the trigger for the transcription of the PQCS, but in *B. subtilis* diverse factors orchestrate the transcriptions of the HS genes. The vegetative σ^A and the transcriptional repressors HrcA and CtsR maneuver the transcription of many Hsp in *B. subtilis*⁷ while other Hsp are controlled by the factors σ^B and SPX^{8,9}.

GroEL is a chaperonin part of the PQCS and it is the bacterial homolog of the eukaryotic Hsp60¹⁰. GroEL is essential in *B. subtilis* to restrain and re-fold small, unfolded proteins inside its barrel-like structure through ATP-hydrolysis cycles. The chaperone DnaK and its stimulator DnaJ can also recognize unfolded substrates. Similarly to GroEL, DnaK utilizes ATP¹¹ to properly bind its substrates (unfolded proteins) and the nucleotide-exchange factor GrpE facilitates the DnaK folding processes removing the bound ADP and competing for its substrate binding site¹².

The repressor HrcA regulates two of the HS operons *hrcA-dnaK-dnaJ-grpE-yqeT-yqeU-yqeV* and *groES-groEL*¹³. Since HrcA tends to aggregate, during HS, it loses functionality and the transcription of the Hsps can occur. Upon reduction of the overall pool of misfolded cellular proteins, GroEL can bind and refold HrcA, which in turn inhibits the transcription of some Hsps¹³.

AAA+ ATPase/protease complexes are as well part of the PQCS in *B. subtilis* and they are crucial to target and process protein aggregates during HS¹⁴. Despite the absence of the protease ClpB¹⁵ in *Bacillus subtilis* genome, the ClpC gene can complement its function, together with the adaptor protein MecA¹⁶. While many other genes are found to be upregulated during HS and governed by the σ^B ¹⁷, their functions remain largely elusive.

Ap4A as signal molecule during stress

The HS does not only perturb the protein pool, in fact DNA repairing proteins also are produced together with HSP¹⁸ in times of stress. Moreover, σ^B regulates multiple genes that help bacterial cells to mitigate oxygen-reacting compound¹⁹ and ribosomal protectors are also expressed upon HS^{20,21}.

Even though all the aforementioned key players in the HS are proteins, the study of the bacterial stress response has brought to attention nucleotide species accumulating during HS and other situations. In fact, over the last 50 years, different studies have reported the increase in concentration of some nucleotides and dinucleotides, especially the diadenosine tetraphosphate (Ap4A)²²⁻²⁴ upon different stimuli. The Ap4A molecule consists in a couple of adenosine moieties bridged by four phosphates at their 5' terminus (**fig. 1**).

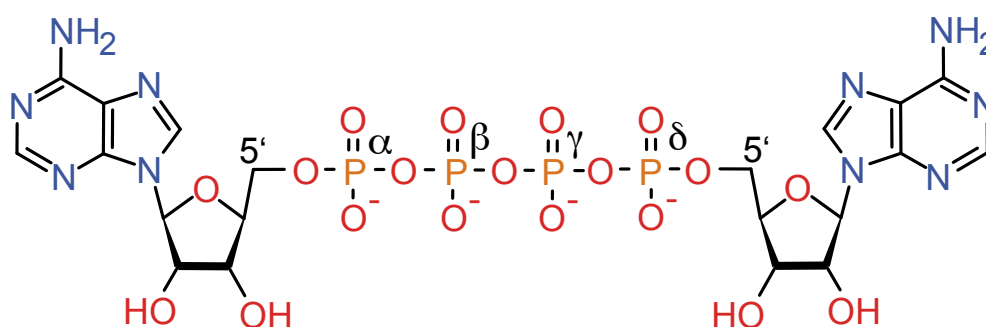


Fig. 1: The diadenosine tetraphosphate molecule (Ap4A). Two adenosines are bridged by four phosphates between their ribose moieties. Aminoacyl tRNA synthetases are the main producers of dinucleotides as Ap4A.

Ap4A is produced by the aminoacyl tRNA synthetases (aaRSs) theoretically in every single form of life. aaRSs are known to load their cognate tRNAs with the deputed amino acids in a two-step reaction that involves the formation of the intermediate aminoacyl-AMP that can subsequently react with the specific tRNA. In absence of the cognate tRNA, the aminoacyl-AMP could react with the γ -phosphate of an extra ATP molecule, forming then Ap4A²⁵. Dinucleotides in general (NpxN) are primarily synthesized by aaRSs in prokaryotes and eukaryotes, but different enzymes can generate Ap4A and other NpxN upon stimuli or spontaneously (reviewed in²⁶).

Different enzymes have evolved to hydrolase Ap4A. The Nudix- (nucleoside diphosphate linked moiety X) -hydrolases are a superfamily responsible for the scission of diverse nucleotides in order to repress cellular signaling or to prevent the accumulation of certain nucleotides²⁷. In human, for instance the the nudix hydrolase, Nudt2, cleaves Ap4A asymmetrically²⁸. Some other hydrolases share sequence homology with the histidine triad (HIT) protein family. One example was characterized in *Schizosaccharomyces pombe*²⁹. In *Escherichia coli* the enzyme ApaH can cleave Ap4A,

and it is also found to be an RNA decapping enzyme after disulfide stress³⁰. Instead in *Bacillus subtilis*, PrpE was identified as a specific Ap4A hydrolase that can cleave it both symmetrically and asymmetrically³¹.

The discovery of Ap4A dates back almost 60 years ago, when Paul Zamecnik and co-workers³², studying conformation changes of the lysyl tRNA synthetase, observed an unexpected formation of a high phosphorylated compound, that was indeed Ap4A.

To this day, Ap4A remains an obscure molecule. Even though the Ap4A has diverse sources of origin and dedicated enzymes to dispose it, no clear target has been characterized thus far in bacteria. Over the last decades, literature has been enriched with possible pleiotropic roles of Ap4A in the bacterial kingdom. In *Escherichia coli*, Ap4A seems to affect the timing of cell division, motility, catabolite repression, the response to heat/oxidative stress and aminoglycoside antibiotics^{22,24,33}. Moreover, Ap4A and/or Ap5A were correlated with the sporulation of *Myxococcus xanthus*³⁴. Heat shock, ethanol stress and cell oxidation trigger the production of dinucleotides in the pathogen *Salmonella typhimurium*²². Other studies reported how Ap4A could impact the biofilm formation of *Pseudomonas aeruginosa*³⁵ and in the survival of *Helicobacter pylori* to oxidative stress³⁶.

Interestingly enough, opposite fronts emerged in the latest literature regarding possible roles of Ap4A. Since no clear bacterial targets have been identified and characterized until recently, some authors considered Ap4A as damage metabolite and a side reaction product³⁷. Others, instead, support the idea that Ap4A is a *bona fide* a stress signal molecule²⁶ due to the discrete numbers of correlations observed in the bacterial kingdom. Despite

not direct correlations have been observed between the accumulation of dinucleotides and the HSP, some chaperones have been proposed to be targets of Ap4A³⁸ and many other new targets were recently proposed in human and in *Escherichia coli*³⁹.

One of the aims of this thesis is to demonstrate how Ap4A target and inhibit the inosine monophosphate dehydrogenase enzyme in *Bacillus subtilis*. Based on this work and in the data presented in the Publication #1, I propose Ap4A to be part of the heat shock response.

(p)ppGpp in the Stress Response

Nucleotide molecules like ppGpp/pppGpp⁴⁰, cyclic-di-GMP⁴¹ and cyclic-di-AMP⁴² recur in biology and act as key players mediating stress signaling. In nature, uni- and multicellular organisms are continuously exposed to diverse stimuli from their environment that sometimes impose an evolutionary pressure onto the organisms. In fact, predation, starvation, pH or temperature variations are typical factors that affect cellular metabolisms. A living cell must adapt or has already built-in system designed to cope with various stresses, in this sense the aforementioned nucleotides (p)ppGpp, cyclic-di-GMP and cyclic-di-AMP, have been widely characterized over the last five decades and all the three species possess defined enzymatic sources, acclaimed molecular targets (protein or nucleic acids) and dedicated enzyme to dispose of them. In particular, (p)ppGpp is produced in bacterial cells⁴³ or in plant chloroplasts⁴⁴ by RelA/SpoT homology (RSH)-type proteins, moreover some procaryotes also encode small alarmone synthetases (SAS)⁴⁵⁻⁴⁷ genes. SAS enzymes are shorter versions of the RSH

(long multi-domains proteins) and possess only a synthetase domain (as RSH) that exploit ATP to transfer a pyrophosphate group onto the 3'OH of the GDP or GTP ribose moiety, yielding, respectively ppGpp and pppGpp⁴⁸ (**Fig. 2**).

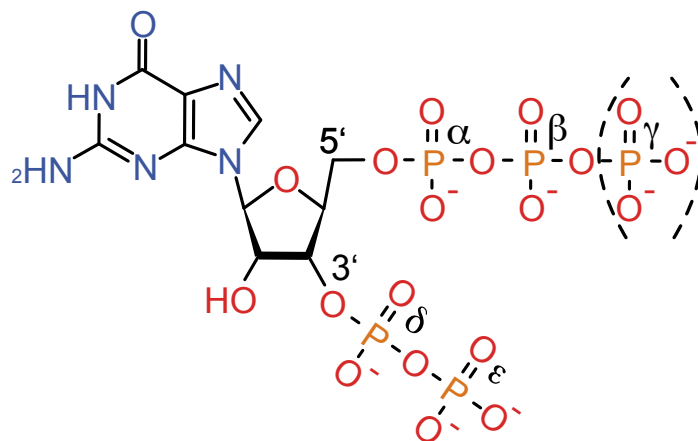


Fig. 2: (p)ppGpp is produced mainly by RelA/SpoT homology proteins when stalled ribosome lack of loaded tRNAs. One ATP molecule donates a pyrophosphate group to the 3' of a GDP or GTP molecule.

Especially during amino acid starvation RSH enzymes sense stalled ribosomes with uncharged tRNA bound to the A-site⁴⁹⁻⁵², and such dramatic scenario triggers (p)ppGpp production as nicely described in Pausch *et al.* (2020)⁵² and in Hogg *et al.* (2004)⁴⁸. Increasing (p)ppGpp concentrations have been observed not only in amino acid starvation^{53,54} but in multiple bacterial stresses like: fatty acid starvation⁵⁵, cell wall stresses⁵⁶, and carbon depletion⁵⁷.

Since the discovery of (p)ppGpp⁵⁴ multiple of its targets had been identified⁵⁸ and characterized^{59,60}, spanning from diverse GTPases in ribosome biogenesis and translation, DNA replication factors and high (p)ppGpp concentrations had been observed during different biological phenomena: bio-film formation⁶¹, bacterial motility⁶², virulence^{63,64} and general GTP depletion in cell⁶⁵.

Stringent response and membrane protein biogenesis

Insertion of membrane proteins is a highly conserved process. It is supported by the signal recognition particle (SRP) together with its membrane receptor FtsY, and it can happen co- or post-translationally⁶⁶. Hydrophobic nascent chains can be targeted by SRP during translation and handed over to the translocation site *via* SRP-FtsY interaction. In bacterial cells SRP consists of the GTPase Ffh and the 4.5S RNA⁶⁷. Like Ffh, FtsY is a GTPase and together with Ffh forms a heterodimer at the membrane level. Dimer formation and hydrolysis of GTP are the driving force to ensure proper delivery of the nascent chain to SecYEG translocon.

During the stringent response, the GDP and GTP pools are in large part converted to (p)ppGpp (reviewed in ⁶⁸) and as direct consequence, many GTPases, especially involved in translation processes, are inhibited by it. Ffh and FtsY already appeared in a wide screen of (p)ppGpp targets⁶⁹, but detailed molecular mechanism on the possible interaction were still missing. In the Publication #2 included in the present dissertation, Czech L., Mais C.N. and coworkers explored how (p)ppGpp binds both Ffh and FtsY in compatible scenarios with the stringent response. In particular, (p)ppGpp

prevents the heterodimer formation since it binds both FtsY and Ffh at their interaction surface. Moreover, inhibition in the translocation was observed in presence of (p)ppGpp. Detailed structural insights were also explored by crystallography and cryogenic electron-microscopy.

Regulation of (p)ppGpp pools

RelA/StopT enzymes are not the unique (p)ppGpp sources. In fact, small alarmone synthetases (SAS) are also present in many bacterial genomes⁴⁵. SAS are divided into two subclasses: RelQ (also: SAS1) and RelP (also: SAS2). An exception is a third class of SAS, called RelV, present in *Vibrio cholerae*⁷⁰. Both classes of SAS share a similar amino acid sequence, but their transcription is differently regulated, and it may depend on diverse stress stimuli. Additionally, both SAS lack sensory domains for stress. Deletion mutants of both SAS hardly show any phenotype⁷¹⁻⁷³.

Precedent studies already described *Bacillus subtilis* and *Enterococcus faecalis* RelQ as homotetramer^{74,75}. Each monomer of RelQ binds one ATP molecule in its active site and subsequently GDP or GTP. More is known about the allosteric regulation of RelQ, in fact, aside its active site, it possesses an additional domain where pppGpp can bind and stimulates allosterically the enzymatic activity⁷⁴. In the same allosteric site, a sequence specific RNA can compete with pppGpp to instead inhibit the transfer of a pyrophosphate from ATP to GDP or GTP⁷⁶.

Despite (p)ppGpp is the main secondary messenger in amino acid starvation for gram-positive, and gram-negative bacteria, as well as plant

chloroplast⁴³, the control mechanisms for its production are different and poorly understood among kingdoms and species. Clearer biochemical characterizations are still necessary for the different alarmone producers. In this sense, the Publication #3, present in this thesis, expands the knowledge on the fundamental molecular mechanisms of (p)ppGpp production in *Bacillus subtilis* and *Staphylococcus aureus*.

References of the Introduction

- 1 Morimoto, R. I. Regulation of the heat shock transcriptional response: cross talk between a family of heat shock factors, molecular chaperones, and negative regulators. *Genes Dev* **12**, 3788-3796 (1998). <https://doi.org:10.1101/gad.12.24.3788>
- 2 Richter, K., Haslbeck, M. & Buchner, J. The heat shock response: life on the verge of death. *Mol Cell* **40**, 253-266 (2010). <https://doi.org:10.1016/j.molcel.2010.10.006>
- 3 Ritossa, F. A new puffing pattern induced by temperature shock and DNP in drosophila. *Experientia* **18**, 571-573 (1962). <https://doi.org:10.1007/BF02172188>
- 4 Mogk, A., Huber, D. & Bukau, B. Integrating protein homeostasis strategies in prokaryotes. *Cold Spring Harb Perspect Biol* **3** (2011). <https://doi.org:10.1101/cshperspect.a004366>
- 5 Santra, M., Dill, K. A. & de Graff, A. M. R. How Do Chaperones Protect a Cell's Proteins from Oxidative Damage? *Cell Syst* **6**, 743-751 e743 (2018). <https://doi.org:10.1016/j.cels.2018.05.001>
- 6 Grossman, A. D., Straus, D. B., Walter, W. A. & Gross, C. A. Sigma 32 synthesis can regulate the synthesis of heat shock proteins in *Escherichia coli*. *Genes Dev* **1**, 179-184 (1987). <https://doi.org:10.1101/gad.1.2.179>
- 7 Schulz, A. & Schumann, W. hrcA, the first gene of the *Bacillus subtilis* dnaK operon encodes a negative regulator of class I heat shock genes. *J Bacteriol* **178**, 1088-1093 (1996). <https://doi.org:10.1128/jb.178.4.1088-1093.1996>

- 8 Hecker, M., Schumann, W. & Völker, U. Heat-shock and general stress response in *Bacillus subtilis*. *Mol Microbiol* **19**, 417-428 (1996). <https://doi.org:10.1046/j.1365-2958.1996.396932.x>
- 9 Rochat, T. *et al.* Genome-wide identification of genes directly regulated by the pleiotropic transcription factor Spx in *Bacillus subtilis*. *Nucleic Acids Res* **40**, 9571-9583 (2012). <https://doi.org:10.1093/nar/gks755>
- 10 Fayet, O., Ziegelhoffer, T. & Georgopoulos, C. The groES and groEL heat shock gene products of *Escherichia coli* are essential for bacterial growth at all temperatures. *J Bacteriol* **171**, 1379-1385 (1989). <https://doi.org:10.1128/jb.171.3.1379-1385.1989>
- 11 Kityk, R., Kopp, J. & Mayer, M. P. Molecular Mechanism of J-Domain-Triggered ATP Hydrolysis by Hsp70 Chaperones. *Mol Cell* **69**, 227-237.e224 (2018). <https://doi.org:10.1016/j.molcel.2017.12.003>
- 12 Wetzstein, M. *et al.* Cloning, sequencing, and molecular analysis of the dnaK locus from *Bacillus subtilis*. *J Bacteriol* **174**, 3300-3310 (1992). <https://doi.org:10.1128/jb.174.10.3300-3310.1992>
- 13 Mogk, A. *et al.* The GroE chaperonin machine is a major modulator of the CIRCE heat shock regulon of *Bacillus subtilis*. *Embo j* **16**, 4579-4590 (1997). <https://doi.org:10.1093/emboj/16.15.4579>
- 14 Elsholz, A. K. W., Birk, M. S., Charpentier, E. & Turgay, K. Functional Diversity of AAA+ Protease Complexes in *Bacillus subtilis*. *Front Mol Biosci* **4**, 44 (2017). <https://doi.org:10.3389/fmolb.2017.00044>
- 15 Eriksson, M. J. & Clarke, A. K. The *Escherichia coli* heat shock protein ClpB restores acquired thermotolerance to a cyanobacterial clpB deletion mutant. *Cell Stress Chaperones* **5**, 255-264 (2000). [https://doi.org:10.1379/1466-1268\(2000\)005<0255:techsp>2.0.co;2](https://doi.org:10.1379/1466-1268(2000)005<0255:techsp>2.0.co;2)
- 16 Schlothauer, T., Mogk, A., Dougan, D. A., Bukau, B. & Turgay, K. MecA, an adaptor protein necessary for ClpC chaperone activity. *Proc Natl Acad Sci U S A* **100**, 2306-2311 (2003). <https://doi.org:10.1073/pnas.0535717100>
- 17 Hecker, M., Pané-Farré, J. & Völker, U. SigB-dependent general stress response in *Bacillus subtilis* and related gram-positive bacteria. *Annu Rev Microbiol* **61**, 215-236 (2007). <https://doi.org:10.1146/annurev.micro.61.080706.093445>
- 18 Krüger, E., Msadek, T., Ohlmeier, S. & Hecker, M. The *Bacillus subtilis* clpC operon encodes DNA repair and competence proteins. *Microbiology (Reading)* **143** (Pt 4), 1309-1316 (1997). <https://doi.org:10.1099/00221287-143-4-1309>

- 19 Reder, A., Höper, D., Gerth, U. & Hecker, M. Contributions of individual σ B-dependent general stress genes to oxidative stress resistance of *Bacillus subtilis*. *J Bacteriol* **194**, 3601-3610 (2012). <https://doi.org:10.1128/jb.00528-12>
- 20 Schmalisch, M., Langbein, I. & Stülke, J. The general stress protein Ctc of *Bacillus subtilis* is a ribosomal protein. *J Mol Microbiol Biotechnol* **4**, 495-501 (2002).
- 21 Shin, J. H. & Price, C. W. The SsrA-SmpB ribosome rescue system is important for growth of *Bacillus subtilis* at low and high temperatures. *J Bacteriol* **189**, 3729-3737 (2007). <https://doi.org:10.1128/jb.00062-07>
- 22 Lee, P. C., Bochner, B. R. & Ames, B. N. AppppA, heat-shock stress, and cell oxidation. *Proc Natl Acad Sci U S A* **80**, 7496-7500 (1983). <https://doi.org:10.1073/pnas.80.24.7496>
- 23 VanBogelen, R. A., Kelley, P. M. & Neidhardt, F. C. Differential induction of heat shock, SOS, and oxidation stress regulons and accumulation of nucleotides in *Escherichia coli*. *J Bacteriol* **169**, 26-32 (1987). <https://doi.org:10.1128/jb.169.1.26-32.1987>
- 24 Lee, P. C., Bochner, B. R. & Ames, B. N. Diadenosine 5',5'''-P1,P4-tetraphosphate and related adenylylated nucleotides in *Salmonella typhimurium*. *J Biol Chem* **258**, 6827-6834 (1983).
- 25 Charlier, J. & Sanchez, R. Lysyl-tRNA synthetase from *Escherichia coli* K12. Chromatographic heterogeneity and the lysU-gene product. *Biochem J* **248**, 43-51 (1987). <https://doi.org:10.1042/bj2480043>
- 26 Ferguson, F., McLennan, A. G., Urbaniak, M. D., Jones, N. J. & Copeland, N. A. Re-evaluation of Diadenosine Tetraphosphate (Ap(4)A) From a Stress Metabolite to Bona Fide Secondary Messenger. *Front Mol Biosci* **7**, 606807 (2020). <https://doi.org:10.3389/fmolb.2020.606807>
- 27 Swarbrick, J. D. *et al.* Structure and substrate-binding mechanism of human Ap4A hydrolase. *J Biol Chem* **280**, 8471-8481 (2005). <https://doi.org:10.1074/jbc.M412318200>
- 28 Marriott, A. S. *et al.* NUDT2 Disruption Elevates Diadenosine Tetraphosphate (Ap4A) and Down-Regulates Immune Response and Cancer Promotion Genes. *PLoS One* **11**, e0154674 (2016). <https://doi.org:10.1371/journal.pone.0154674>
- 29 Huang, Y., Garrison, P. N. & Barnes, L. D. Cloning of the *Schizosaccharomyces pombe* gene encoding diadenosine 5',5'''-P1,P4-tetraphosphate (Ap4A) asymmetrical hydrolase: sequence

- similarity with the histidine triad (HIT) protein family. *Biochem J* **312 (Pt 3)**, 925-932 (1995). <https://doi.org:10.1042/bj3120925>
- 30 Luciano, D. J., Levenson-Palmer, R. & Belasco, J. G. Stresses that Raise Np(4)A Levels Induce Protective Nucleoside Tetraphosphate Capping of Bacterial RNA. *Mol Cell* **75**, 957-966.e958 (2019). <https://doi.org:10.1016/j.molcel.2019.05.031>
- 31 Iwanicki, A., Herman-Antosiewicz, A., Pierechod, M., Séror, S. J. & Obuchowski, M. PrpE, a PPP protein phosphatase from *Bacillus subtilis* with unusual substrate specificity. *Biochem J* **366**, 929-936 (2002). <https://doi.org:10.1042/bj20011591>
- 32 Zamecnik, P. G., Stephenson, M. L., Janeway, C. M. & Randerath, K. Enzymatic synthesis of diadenosine tetraphosphate and diadenosine triphosphate with a purified lysyl-sRNA synthetase. *Biochemical and Biophysical Research Communications* **24**, 91-97 (1966). [https://doi.org:https://doi.org/10.1016/0006-291X\(66\)90415-3](https://doi.org:https://doi.org/10.1016/0006-291X(66)90415-3)
- 33 Farr, S. B., Arnosti, D. N., Chamberlin, M. J. & Ames, B. N. An apaH mutation causes AppppA to accumulate and affects motility and catabolite repression in *Escherichia coli*. *Proc Natl Acad Sci US A* **86**, 5010-5014 (1989). <https://doi.org:10.1073/pnas.86.13.5010>
- 34 Kimura, Y., Tanaka, C., Sasaki, K. & Sasaki, M. High concentrations of intracellular Ap4A and/or Ap5A in developing *Myxococcus xanthus* cells inhibit sporulation. *Microbiology (Reading)* **163**, 86-93 (2017). <https://doi.org:10.1099/mic.0.000403>
- 35 Monds, R. D. *et al.* Di-adenosine tetraphosphate (Ap4A) metabolism impacts biofilm formation by *Pseudomonas fluorescens* via modulation of c-di-GMP-dependent pathways. *J Bacteriol* **192**, 3011-3023 (2010). <https://doi.org:10.1128/jb.01571-09>
- 36 Lundin, A. *et al.* The NudA protein in the gastric pathogen *Helicobacter pylori* is an ubiquitous and constitutively expressed dinucleoside polyphosphate hydrolase. *J Biol Chem* **278**, 12574-12578 (2003). <https://doi.org:10.1074/jbc.M212542200>
- 37 Despotović, D. *et al.* Diadenosine tetraphosphate (Ap4A) - an *E. coli* alarmone or a damage metabolite? *Febs j* **284**, 2194-2215 (2017). <https://doi.org:10.1111/febs.14113>
- 38 Johnstone, D. B. & Farr, S. B. AppppA binds to several proteins in *Escherichia coli*, including the heat shock and oxidative stress proteins DnaK, GroEL, E89, C45 and C40. *Embo j* **10**, 3897-3904 (1991). <https://doi.org:10.1002/j.1460-2075.1991.tb04959.x>
- 39 Krüger, L. *et al.* Chemical proteomic profiling reveals protein interactors of the alarmones diadenosine triphosphate and

- tetraphosphate. *Nature Communications* **12**, 5808 (2021). <https://doi.org:10.1038/s41467-021-26075-4>
- 40 Zegarra, V., Bedrunka, P., Bange, G. & Czech, L. How to save a bacterial ribosome in times of stress. *Semin Cell Dev Biol* (2022). <https://doi.org:10.1016/j.semcdb.2022.03.015>
- 41 Jenal, U., Reinders, A. & Lori, C. Cyclic di-GMP: second messenger extraordinaire. *Nat Rev Microbiol* **15**, 271-284 (2017). <https://doi.org:10.1038/nrmicro.2016.190>
- 42 Stulke, J. & Kruger, L. Cyclic di-AMP Signaling in Bacteria. *Annu Rev Microbiol* **74**, 159-179 (2020). <https://doi.org:10.1146/annurev-micro-020518-115943>
- 43 Steinchen, W. & Bange, G. The magic dance of the alarmones (p)ppGpp. *Mol Microbiol* **101**, 531-544 (2016). <https://doi.org:10.1111/mmi.13412>
- 44 Masuda, S. *et al.* The Bacterial Stringent Response, Conserved in Chloroplasts, Controls Plant Fertilization. *Plant and Cell Physiology* **49**, 135-141 (2008). <https://doi.org:10.1093/pcp/pcm177>
- 45 Atkinson, G. C., Tenson, T. & Hauryliuk, V. The RelA/SpoT Homolog (RSH) Superfamily: Distribution and Functional Evolution of ppGpp Synthetases and Hydrolases across the Tree of Life. *PLOS ONE* **6**, e23479 (2011). <https://doi.org:10.1371/journal.pone.0023479>
- 46 Gaca, A. O. *et al.* From (p)ppGpp to (pp)pGpp: Characterization of Regulatory Effects of pGpp Synthesized by the Small Alarmone Synthetase of *Enterococcus faecalis*. *J Bacteriol* **197**, 2908-2919 (2015). <https://doi.org:10.1128/JB.00324-15>
- 47 Das, B., Pal, R. R., Bag, S. & Bhadra, R. K. Stringent response in *Vibrio cholerae*: genetic analysis of spoT gene function and identification of a novel (p)ppGpp synthetase gene. *Mol Microbiol* **72**, 380-398 (2009). <https://doi.org:10.1111/j.1365-2958.2009.06653.x>
- 48 Hogg, T., Mechold, U., Malke, H., Cashel, M. & Hilgenfeld, R. Conformational antagonism between opposing active sites in a bifunctional RelA/SpoT homolog modulates (p)ppGpp metabolism during the stringent response [corrected]. *Cell* **117**, 57-68 (2004). [https://doi.org:10.1016/s0092-8674\(04\)00260-0](https://doi.org:10.1016/s0092-8674(04)00260-0)
- 49 Arenz, S. *et al.* The stringent factor RelA adopts an open conformation on the ribosome to stimulate ppGpp synthesis. *Nucleic Acids Res* **44**, 6471-6481 (2016). <https://doi.org:10.1093/nar/gkw470>

- 50 Loveland, A. B. *et al.* Ribosome*RelA structures reveal the mechanism of stringent response activation. *Elife* **5** (2016). <https://doi.org:10.7554/eLife.17029>
- 51 Wendrich, T. M., Blaha, G., Wilson, D. N., Marahiel, M. A. & Nierhaus, K. H. Dissection of the mechanism for the stringent factor RelA. *Mol Cell* **10**, 779-788 (2002). [https://doi.org:10.1016/s1097-2765\(02\)00656-1](https://doi.org:10.1016/s1097-2765(02)00656-1)
- 52 Pausch, P. *et al.* Structural Basis for Regulation of the Opposing (p)ppGpp Synthetase and Hydrolase within the Stringent Response Orchestrator Rel. *Cell Rep* **32**, 108157 (2020). <https://doi.org:10.1016/j.celrep.2020.108157>
- 53 Stent, G. S. & Brenner, S. A genetic locus for the regulation of ribonucleic acid synthesis. *Proc Natl Acad Sci U S A* **47**, 2005-2014 (1961). <https://doi.org:10.1073/pnas.47.12.2005>
- 54 Cashel, M. The control of ribonucleic acid synthesis in Escherichia coli. IV. Relevance of unusual phosphorylated compounds from amino acid-starved stringent strains. *J Biol Chem* **244**, 3133-3141 (1969).
- 55 Battesti, A. & Bouveret, E. Bacteria possessing two RelA/SpoT-like proteins have evolved a specific stringent response involving the acyl carrier protein-SpoT interaction. *J Bacteriol* **191**, 616-624 (2009). <https://doi.org:10.1128/jb.01195-08>
- 56 Zweers, J. C., Nicolas, P., Wiegert, T., van Dijl, J. M. & Denham, E. L. Definition of the sigma(W) regulon of Bacillus subtilis in the absence of stress. *PLoS One* **7**, e48471 (2012). <https://doi.org:10.1371/journal.pone.0048471>
- 57 Battesti, A. & Bouveret, E. Bacteria Possessing Two RelA/SpoT-Like Proteins Have Evolved a Specific Stringent Response Involving the Acyl Carrier Protein-SpoT Interaction. *Journal of Bacteriology* **191**, 616-624 (2009). <https://doi.org:doi:10.1128/JB.01195-08>
- 58 Wang, B. *et al.* Affinity-based capture and identification of protein effectors of the growth regulator ppGpp. *Nat Chem Biol* **15**, 141-150 (2019). <https://doi.org:10.1038/s41589-018-0183-4>
- 59 Irving, S. E., Choudhury, N. R. & Corrigan, R. M. The stringent response and physiological roles of (pp)pGpp in bacteria. *Nat Rev Microbiol* **19**, 256-271 (2021). <https://doi.org:10.1038/s41579-020-00470-y>
- 60 Steinchen, W., Zegarra, V. & Bange, G. (p)ppGpp: Magic Modulators of Bacterial Physiology and Metabolism. *Front Microbiol* **11**, 2072 (2020). <https://doi.org:10.3389/fmicb.2020.02072>

- 61 He, H., Cooper, J. N., Mishra, A. & Raskin, D. M. Stringent response regulation of biofilm formation in *Vibrio cholerae*. *J Bacteriol* **194**, 2962-2972 (2012). <https://doi.org:10.1128/JB.00014-12>
- 62 Ababneh, Q. O. & Herman, J. K. RelA inhibits *Bacillus subtilis* motility and chaining. *J Bacteriol* **197**, 128-137 (2015). <https://doi.org:10.1128/JB.02063-14>
- 63 Weiss, L. A. & Stallings, C. L. Essential roles for *Mycobacterium tuberculosis* Rel beyond the production of (p)ppGpp. *J Bacteriol* **195**, 5629-5638 (2013). <https://doi.org:10.1128/JB.00759-13>
- 64 Vogt, S. L. *et al.* The stringent response is essential for *Pseudomonas aeruginosa* virulence in the rat lung agar bead and *Drosophila melanogaster* feeding models of infection. *Infect Immun* **79**, 4094-4104 (2011). <https://doi.org:10.1128/IAI.00193-11>
- 65 Ababneh, Q. O. & Herman, J. K. CodY Regulates SigD Levels and Activity by Binding to Three Sites in the *fla/che* Operon. *J Bacteriol* **197**, 2999-3006 (2015). <https://doi.org:10.1128/JB.00288-15>
- 66 Akopian, D., Shen, K., Zhang, X. & Shan, S.-o. Signal Recognition Particle: An Essential Protein-Targeting Machine. *Annual Review of Biochemistry* **82**, 693-721 (2013). <https://doi.org:10.1146/annurev-biochem-072711-164732>
- 67 Kuhn, P. *et al.* The bacterial SRP receptor, SecA and the ribosome use overlapping binding sites on the SecY translocon. *Traffic* **12**, 563-578 (2011). <https://doi.org:10.1111/j.1600-0854.2011.01167.x>
- 68 Steinchen, W., Zegarra, V. & Bange, G. (p)ppGpp: Magic Modulators of Bacterial Physiology and Metabolism. *Frontiers in Microbiology* **11** (2020). <https://doi.org:10.3389/fmicb.2020.02072>
- 69 Wang, B. *et al.* Affinity-based capture and identification of protein effectors of the growth regulator ppGpp. *Nature Chemical Biology* **15**, 141-150 (2019). <https://doi.org:10.1038/s41589-018-0183-4>
- 70 Das, B., Pal, R. R., Bag, S. & Bhadra, R. K. Stringent response in *Vibrio cholerae*: genetic analysis of *spoT* gene function and identification of a novel (p)ppGpp synthetase gene. *Molecular Microbiology* **72**, 380-398 (2009). <https://doi.org:https://doi.org/10.1111/j.1365-2958.2009.06653.x>
- 71 Abranches, J. *et al.* The molecular alarmone (p)ppGpp mediates stress responses, vancomycin tolerance, and virulence in *Enterococcus faecalis*. *J Bacteriol* **191**, 2248-2256 (2009). <https://doi.org:10.1128/jb.01726-08>
- 72 Lemos, J. A., Nascimento, M. M., Lin, V. K., Abranches, J. & Burne, R. A. Global regulation by (p)ppGpp and CodY in *Streptococcus*

-
- mutans. *J Bacteriol* **190**, 5291-5299 (2008).
<https://doi.org:10.1128/jb.00288-08>
- 73 Natori, Y. *et al.* Transcription Activity of Individual *rrn* Operons in *Bacillus subtilis* Mutants Deficient in (p)ppGpp Synthetase Genes, *relA*, *yjbM*, and *ywaC*. *Journal of Bacteriology* **191**, 4555-4561 (2009).
<https://doi.org:doi:10.1128/JB.00263-09>
- 74 Steinchen, W. *et al.* Catalytic mechanism and allosteric regulation of an oligomeric (p)ppGpp synthetase by an alarmone. *Proceedings of the National Academy of Sciences* **112**, 13348-13353 (2015).
<https://doi.org:doi:10.1073/pnas.1505271112>
- 75 Gaca, A. O. *et al.* From (p)ppGpp to (pp)pGpp: Characterization of Regulatory Effects of pGpp Synthesized by the Small Alarmone Synthetase of *Enterococcus faecalis*. *Journal of Bacteriology* **197**, 2908-2919 (2015). <https://doi.org:doi:10.1128/JB.00324-15>
- 76 Hauryliuk, V. & Atkinson, G. C. Small Alarmone Synthetases as novel bacterial RNA-binding proteins. *RNA Biol* **14**, 1695-1699 (2017). <https://doi.org:10.1080/15476286.2017.1367889>

Publication #1

Title: **Diadenosine tetraphosphate regulates biosynthesis of GTP in *Bacillus subtilis***

Authors: Pietro I. Giammarinaro, Megan K. M. Young, Wieland Steinchen, Christopher-Nils Mais, Georg Hochberg, Jin Yang, David M. Stevenson, Daniel Amador-Noguez, Anja Paulus, Jue D. Wang and Gert Bange.

Journal: Nature Microbiology

Year: 2022

Contributions: J.D.W. and G.B. conceptualized the project. G.H. and D.A.-N. developed the methodology. P.I.G., M.K. M.Y., W.S., C.-N.M., J.Y. and A.P. conducted the experimental investigations. J.D.W. and G.B. acquired funding. J.D.W. and G.B. supervised the project. P.I.G., M.Y., W.S., J.D.W. and G.B. wrote the original draft. All authors read and commented on the manuscript.



Diadenosine tetraphosphate regulates biosynthesis of GTP in *Bacillus subtilis*

Pietro I. Giammarinaro^{1,4}, Megan K. M. Young^{2,4}, Wieland Steinchen¹, Christopher-Nils Mais¹, Georg Hochberg^{1,3}, Jin Yang², David M. Stevenson², Daniel Amador-Noguez², Anja Paulus¹, Jue D. Wang²✉ and Gert Bange^{1,3}✉

Diadenosine tetraphosphate (Ap4A) is a putative second messenger molecule that is conserved from bacteria to humans. Nevertheless, its physiological role and the underlying molecular mechanisms are poorly characterized. We investigated the molecular mechanism by which Ap4A regulates inosine-5'-monophosphate dehydrogenase (IMPDH, a key branching point enzyme for the biosynthesis of adenosine or guanosine nucleotides) in *Bacillus subtilis*. We solved the crystal structure of BslMPDH bound to Ap4A at a resolution of 2.45 Å to show that Ap4A binds to the interface between two IMPDH subunits, acting as the glue that switches active IMPDH tetramers into less active octamers. Guided by these insights, we engineered mutant strains of *B. subtilis* that bypass Ap4A-dependent IMPDH regulation without perturbing intracellular Ap4A pools themselves. We used metabolomics, which suggests that these mutants have a dysregulated purine, and in particular GTP, metabolome and phenotypic analysis, which shows increased sensitivity of *B. subtilis* IMPDH mutant strains to heat compared with wild-type strains. Our study identifies a central role for IMPDH in remodelling metabolism and heat resistance, and provides evidence that Ap4A can function as an alarmone.

Nucleotide-based second messengers, for example, (p)ppGpp^{1,2}, c-di-GMP^{3,4} or c-di-AMP⁵, are essential for bacterial responses to changing environmental and stress conditions. Diadenosine polyphosphate molecules such as diadenosine 5',5''-P1,P4-tetraphosphate (Ap4A) have been known since the 1960s⁶ and are found in all domains of life⁷. There is ongoing debate on whether they are damage metabolites⁸ or bona fide second messengers⁷.

Ap4A is composed of two adenosines bridged at their 5' ends by four phosphates (Fig. 1a). It is primarily produced by aminoacyl-transfer RNA (tRNA) synthetases, with lysyl-tRNA synthetase (LysRS) being a prominent example, under heat shock and oxidative stress conditions through the transfer of the aminoacylated AMP onto the 5' γ -phosphate of ATP^{6,9–11}. The promiscuous utilization of other aminoacyl-AMP acceptors by LysRS, such as ADP, GDP or GTP leading to the synthesis of the even more enigmatic Ap3A, Ap3G and Ap4G, respectively, broadens the spectrum of dinucleoside polyphosphate molecules¹⁰.

Several studies have reported pleiotropic roles for Ap4A in bacteria. In *Escherichia coli* Ap4A has been implicated in cell division¹², motility¹³ and responses to heat/oxidative stress¹⁴ and aminoglycoside antibiotics¹⁵. Ap4A has been associated with sporulation in *Myxococcus xanthus*¹⁶; heat shock, ethanol stress and cell oxidation in *Salmonella typhimurium*¹⁰; biofilm formation in *Pseudomonas aeruginosa* (*Pa*)¹⁷; and survival of *Helicobacter pylori* in response to oxidative stress¹⁸.

Our knowledge about Ap4A-binding partners in bacteria and a mere understanding of the mechanisms by which Ap4A regulates the above-mentioned processes is currently limited to *E. coli*^{8,14,19,20}. Proposed targets include the chaperones DnaK, ClpB and GroEL^{14,21} and the de novo purine nucleotide biosynthesis

enzyme inosine-5'-monophosphate dehydrogenase (IMPDH)^{8,19}. These screens employed biotin and/or aziridine-modified Ap4A to enrich Ap4A-binding proteins, which may have potentially biased the target spectrum due to the size of the modifier groups.

Results

Identification of Ap4A targets in *Bacillus anthracis*. To identify further Ap4A targets in an unbiased manner, we used a radioactively labelled but otherwise chemically unmodified Ap4A as bait in a differential radial capillary action of ligand assay (DRaCALA)²². Simultaneously, we aimed to expand knowledge on Ap4A regulation to the Firmicutes phylum. Having a library for all *B. anthracis* proteins available, we screened for Ap4A-binding targets in this organism and then continued our mechanistic and physiological analyses in *Bacillus subtilis*. We employed two *B. anthracis* overexpression libraries, each including 5,341 open reading frames (ORFs) N-terminally fused to either hexahistidine (His) or His-maltose binding protein (His-MBP)²³. Both libraries were overexpressed in *E. coli*, and the binding of radiolabelled ³²P-Ap4A to the lysates assayed by DRaCALA²². This screen identified inosine-5'-monophosphate dehydrogenase (IMPDH, gene: *guaB*) as putative Ap4A-binding partner (Fig. 1b).

IMPDH catalyses the nicotinamide adenine dinucleotide (NAD⁺)-dependent conversion of inosine-5'-monophosphate (IMP) into xanthosine-5'-monophosphate (XMP)²⁴. XMP represents the start for the generation of GMP, GDP and GTP. Moreover, IMPDH represents the branching point in the biosynthesis of adenosine and guanosine nucleotides (Fig. 1c).

To further probe the Ap4A-IMPDH interaction, we investigated IMPDH from *B. subtilis* (*Bs*) because this bacterium is broadly studied and is a close relative of *B. anthracis*. Isothermal titration

¹Department of Chemistry and Center for Synthetic Microbiology, Philipps University Marburg, Marburg, Germany. ²Department of Bacteriology, University of Wisconsin-Madison, Madison, WI, USA. ³Max Planck Institute for Terrestrial Microbiology, Marburg, Germany. ⁴These authors contributed equally: Pietro I. Giammarinaro, Megan K. M. Young. ✉e-mail: wang@bact.wisc.edu; gert.bange@synmikro.uni-marburg.de

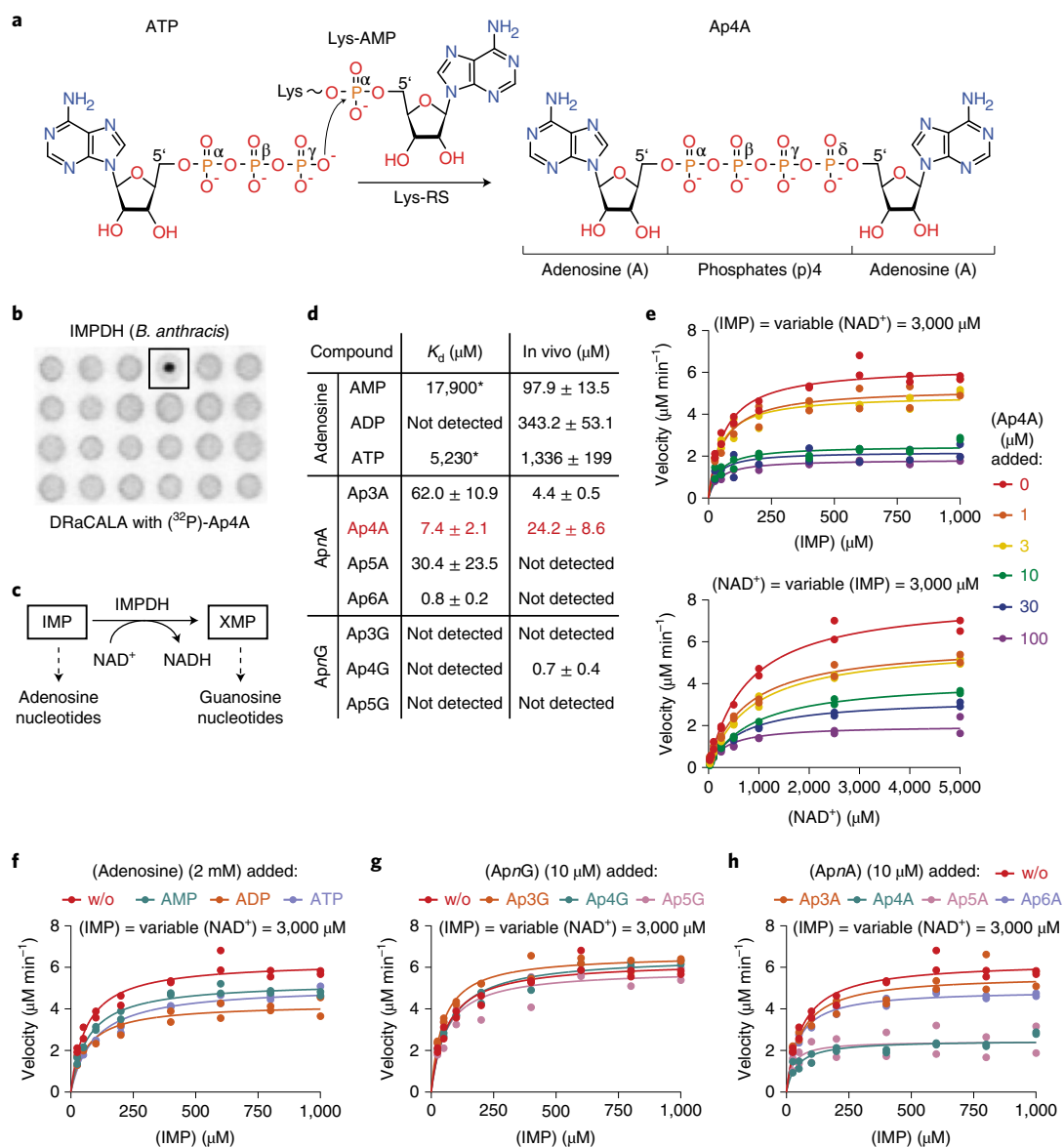


Fig. 1 | Ap4A inhibits IMPDH in a non-competitive manner. **a**, Scheme of Ap4A formation by lysyl-tRNA synthetase (LysRS) from ATP and lysyl-AMP (Lys-AMP). **b**, DRaCALA assay with ^{32}P -labelled Ap4A employing a *B. anthracis* library suggests IMPDH as a target of Ap4A. **c**, Scheme of the enzymatic reaction catalysed by IMPDH, the NAD^+ -dependent conversion of IMP into XMP, which represent the starting points in the de novo biosynthesis of adenosine and guanosine nucleotides, respectively. **d**, Binding of adenosine nucleotides, and AprnA and AprnG dinucleotides (n =variable number of phosphates) to BsIMPDH determined by ITC and their intracellular concentrations determined by LC-MS. Asterisks denote bad binding curve-fitting. LC-MS data represent the mean \pm s.d. of $n=3$ biological replicates. The error of the K_d derived from ITC data represents unambiguity in the curve fitting. **e-h**, Enzyme-kinetic behaviour of BsIMPDH for its conversion of the IMP substrate into XMP dependent on Ap4A (**e**), adenosine nucleotides (**f**), AprnG dinucleotides (**g**) and AprnA dinucleotides (**h**). In **e** (top panel) and **f-h**, NAD^+ was constant at 3,000 μM and IMP variable (25–1,000 μM). In **e** (bottom panel) IMP was constant at 3,000 μM and NAD^+ variable (25–5,000 μM). Individual data points of $n=2$ technical replicates are shown, and parameters of the fits are given in Extended Data Fig. 2.

calorimetry (ITC) revealed a dissociation constant (K_d) of $7.4 \pm 2.1 \mu\text{M}$ for the Ap4A-BsIMPDH interaction (Fig. 1d and Extended Data Fig. 1e). This K_d is within the range of Ap4A concentration determined by liquid chromatography coupled to mass spectrometry (LC-MS) for exponentially growing *B. subtilis* (Fig. 1d). We also tested the binding of the adenosine nucleotides AMP, ADP and ATP to BsIMPDH due to their structural similarity to Ap4A and because an ATP-dependent stimulation of IMPDH activity in *P. aeruginosa* was reported²⁵. Binding of AMP and ATP to BsIMPDH proceeds with low affinity evidenced by K_d values of

approximately 18 and 5 mM, respectively. No interaction was found for ADP (Fig. 1d and Extended Data Fig. 1a–c). Furthermore, we tested the specificity of BsIMPDH for the nucleobases linked by the phosphates in the dinucleotides and the length of this phosphate linker by probing the binding of AprnA and AprnG compounds. AprnA dinucleotides Ap3A, Ap5A and Ap6A bound to BsIMPDH with K_d s of $62.0 \pm 10.9 \mu\text{M}$, $30.4 \pm 23.5 \mu\text{M}$ and $0.8 \pm 0.2 \mu\text{M}$, respectively (Fig. 1d and Extended Data Fig. 1d,f,g). No binding was found for the AprnG dinucleotides Ap3G, Ap4G and Ap5G (Fig. 1d and Extended Data Fig. 1h–j). Collectively, BsIMPDH had a strong

preference (≥ 100 -fold higher affinity) for ApnA dinucleotides with varying phosphor-linker lengths over the related adenosine mononucleotides.

Ap4A is a non-competitive inhibitor of IMPDH. Next, we probed whether Ap4A and ApnA would affect IMPDH activity by an assay based on the reduction of the NAD⁺ cofactor to NADH detectable at a wavelength of 340 nm. At constant saturating NAD⁺ and variable IMP concentrations without Ap4A supplemented, BsIMPDH showed a Michaelis-Menten-like kinetic behaviour, with maximal velocity (V_{\max}) and Michaelis-Menten constant (K_m) values of $6.3 \mu\text{M min}^{-1}$ and $63 \mu\text{M}$, respectively (Fig. 1e and Extended Data Fig. 2a). With increasing Ap4A concentration, V_{\max} decreased while K_m remained unaltered, suggesting an allosteric mode of inhibition. BsIMPDH inhibition by Ap4A proceeded with an inhibitory constant (K_i) of $15.8 \mu\text{M}$, roughly reflecting the K_d between Ap4A and BsIMPDH (Fig. 1e and Extended Data Fig. 2a). At constant saturating IMP and variable NAD⁺ concentrations, BsIMPDH activity showed a similar decline of V_{\max} dependent on increasing Ap4A concentrations (Fig. 1e and Extended Data Fig. 2b). In contrast to Ap4A, which potently reduced BsIMPDH activity, adenosine mononucleotides only moderately inhibited BsIMPDH (Fig. 1f and Extended Data Fig. 2a). ApnG dinucleotides did not alleviate BsIMPDH activity and out of the ApnA dinucleotides tested by us, only Ap5A and Ap6A resulted in BsIMPDH inhibition (Fig. 1g,h and Extended Data Fig. 2a). Despite Ap5A and Ap6A being the most potent inhibitors of BsIMPDH, we focused our further studies on Ap4A because it was more abundant than other dinucleotides in *B. subtilis* in vivo (Fig. 1d). Likewise, Ap4A was approximately 3-fold more abundant than Ap5A under various stress conditions and throughout growth in *M. xanthus*¹⁶. Collectively, our data show that Ap4A inhibits IMPDH in vitro at concentrations that roughly match those present in vivo.

Ap4A binds to the CBS domains of IMPDH. Next, we determined the structure of Ap4A-bound BsIMPDH (Table 1). BsIMPDH consists of the catalytic triose isomerase (TIM)-barrel with two cystathionine- β -synthase (CBS) domains forming the disc-like Bateman module inserted into the TIM-barrel (Fig. 2a–c and Extended Data Fig. 3a). Four IMPDH molecules form a tetramer through their catalytic domains, with each CBS domain pointing outward from the centre of the tetramer (Fig. 2b). Electron density, which could be unambiguously attributed to Ap4A, was present in between the two CBS domains of each IMPDH monomer (Extended Data Fig. 3b). It binds into a cleft formed by the two CBS domains constituting the Bateman module (Fig. 2c and Extended Data Fig. 3c). Binding of Ap4A to BsIMPDH closely resembles that of Ap5G to *Ashbya gossypii* IMPDH²⁶ as well as that of the adenosine nucleoside moieties of two ATP molecules to *P. aeruginosa* IMPDH²⁵ (Extended Data Fig. 3d).

The crystal structures of the IMPDH Apo states from *B. anthracis*, *P. aeruginosa* and *A. gossypii* show a high degree of disorder in their CBS domains, which diminishes in the presence of a ligand (Extended Data Fig. 4). Thus, we probed the impact of Ap4A and ATP (as control) on the conformational flexibility of BsIMPDH by hydrogen/deuterium exchange-mass spectrometry (HDX-MS). Decrease in HDX with either ligand was exclusively present in the CBS domains, substantiating binding to this entity (Extended Data Fig. 5a). The progression of HDX in peptides from the CBS1 (residues 113–136) and CBS2 (residues 172–200) domains of the Bateman module evidenced bimodal distributions of deuterated peptide ions (Extended Data Fig. 5b–d), which are thought to arise from partial unfolding or conformational flexibility^{27,28}. Bimodal behaviour is less pronounced in the presence of Ap4A and ATP, suggesting ligand-induced rigidification of the CBS domains. Thus,

Table 1 | Data collection and refinement statistics of crystallographic datasets

	Ap4A-bound BsIMPDH	BsIMPDH- Δ CBS
Data collection		
Space group	I4	I422
Cell dimensions		
<i>a</i> , <i>b</i> , <i>c</i> (Å)	133.75 133.75 149.68	110.91 110.91 156.85
α , β , γ (°)	90 90 90	90 90 90
Wavelength (Å)	0.978561	0.918400
Resolution (Å)	66.88–2.442 (2.53–2.442)	45.28–1.76 (1.823–1.76)
R_{merge}	0.067 (0.2841)	0.03072 (0.2892)
$I/\sigma I$	6.55 (2.58)	13.79 (2.43)
Completeness (%)	99.58 (99.82)	99.95 (100.00)
Redundancy	1.9 (1.9)	2.0 (2.0)
CC1/2	0.992 (0.641)	0.999 (0.708)
Refinement		
Resolution (Å)	66.88–2.442	45.28–1.76
No. reflections	48,533 (4,865)	48,580 (4,794)
$R_{\text{work}} / R_{\text{free}}$	0.27/0.29	0.17/0.19
No. atoms	6,255	2,868
Protein	6,112	2,868
Ligand/ion	108	17
Water	35	200
B-factors	71.44	29.89
Protein	70.65	29.45
Ligand/ion	120.22	36.30
Water	58.99	35.20
R.m.s. deviations		
Bond lengths (Å)	0.006	0.016
Bond angles (°)	1.02	1.78
Ramachandran		
Favoured (%)	95.01	97.98
Allowed (%)	4.37	2.02
Outliers (%)	0.62	0.00

Data were collected on ID23-1 (ESRF, Grenoble, France) and P14.2 (BESSY II, Berlin, Germany). Values in parentheses are for the highest-resolution shell.

Ap4A and ATP restrict the conformational flexibility of the CBS domains of IMPDH.

Ap4A induces formation of a less active IMPDH octamer. Bacterial IMPDH enzymes are grouped into classes I and II depending on their oligomeric states and catalytic properties²⁹. Class I enzymes (for example, PaIMPDH) are octameric irrespective of their bound ligand, exhibit comparably low but positive cooperative enzymatic activity, and increase catalytic efficiency accompanied by loss of cooperativity when ATP is present²⁵. Class II enzymes (for example, BsIMPDH) can be tetrameric (apo or IMP-bound) or octameric

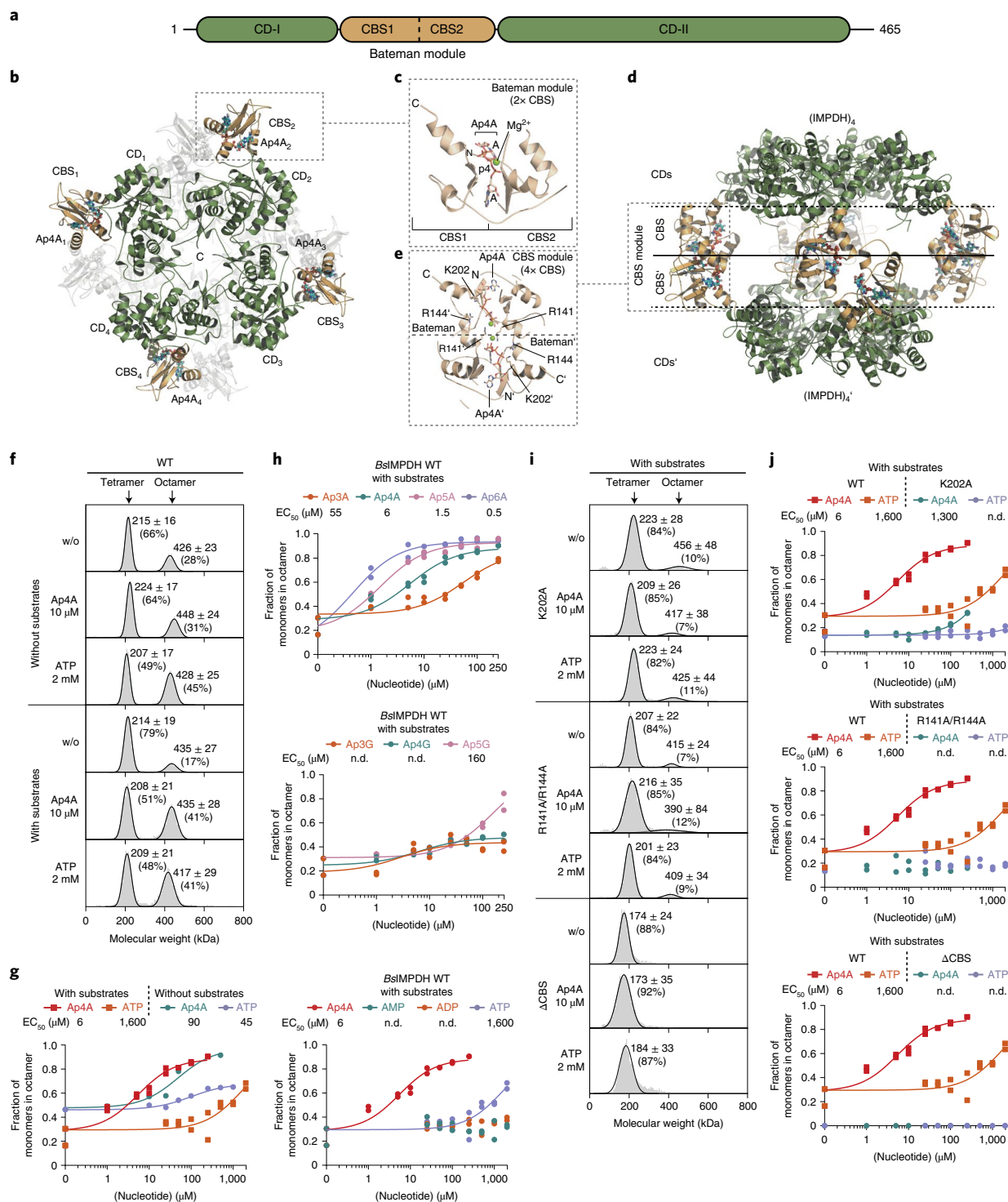


Fig. 2 | Mechanism of the Ap4A-dependent inhibition of IMPDH. **a**, Domain organization of IMPDH enzymes. The CBS domains forming a Bateman module (orange) are inserted into the catalytic domain (CD, green). **b**, Top view on the IMPDH structure bound to Ap4A, which binds into the CBS domains of the IMPDH oligomer. **c**, Close-up view showing that Ap4A binds in a horseshoe-like manner into a cavity formed by the two CBS domains (Bateman module) of an IMPDH monomer. **d**, Side view on the Ap4A-dependent IMPDH octamer showing that two tetramers of IMPDH form an octamer via their CBS domains. **e**, Close-up view into a CBS module established by two IMPDH monomers belonging to different tetrameric rings. The interaction of the Bateman modules is mainly enforced by interactions between R141 and R144 residues of one monomer with the Ap4A bound in the Bateman module of the opposing monomer. **f-i**, Influence of substrates and ligands on the oligomeric state of *Bsl*IMPDH (tetramer or octamer) analysed by mass photometry. **f,i**, Representative distributions of tetrameric and octameric *Bsl*IMPDH species for *Bsl*IMPDH-WT (**f**), or *Bsl*IMPDH CBS domain variants (K202A, R141A/R144A, Δ CBS) (**i**), dependent on substrates and/or ligands to the sample. Numbers in the diagrams reflect the molecular weight of the observed oligomeric species (mean \pm s.d.) and their percentage of all observed molecules in the sample. **g-h,j**, The fraction of *Bsl*IMPDH monomers in the octameric state in the absence or presence of indicated substrates displayed as a function of nucleotide or dinucleotide concentration. Individual data points of $n=2$ technical replicates are displayed, and their means used for curve fitting. Where possible, EC_{50} values (in μ M) were derived from the dose-response curves. n.d., not determined.

(NAD⁺ or ATP-bound). Both states show Michaelis-Menten-like kinetic properties²⁹. Our biochemical experiments revealed that Ap4A and ATP, albeit binding with approximately 700-fold different affinity, share their interaction site in the CBS domains and similarly restrict its conformational flexibility. Thus, both ligands may affect the tetramer/octamer equilibrium of *Bs*IMPDH. If true, this also raises the question of why Ap4A strongly restricts the enzymatic activity of *Bs*IMPDH while ATP does so only moderately, if at all (Fig. 1f).

Analysis of the crystal structure of Ap4A-bound *Bs*IMPDH suggests that two IMPDH tetramers engage into an octamer through their Ap4A-bound CBS domains (Fig. 2d). This *Bs*IMPDH octamer is stabilized by the arginines 141 and 144 of the CBS domains of one tetramer, these arginines interacting with the phosphates of the Ap4A molecules of the other tetramer, and vice versa (Fig. 2e). Thus, our structure suggests that Ap4A promotes the joining of two *Bs*IMPDH tetramers via their CBS domains into an octamer.

Next, we employed mass photometry, which enables direct mass determination of single molecules in solution by interferometric scattering microscopy³⁰. In the absence of substrates, *Bs*IMPDH predominantly appeared as a tetramer, the portion of which is further enlarged in the presence of NAD⁺ and IMP (Fig. 2f,g). Ap4A promoted formation of *Bs*IMPDH octamers in a dose-dependent manner, with EC₅₀ values of 90 μM and 6 μM in the absence and presence of substrates, respectively (Fig. 2g and Extended Data Fig. 6a,b). The addition of ATP enforced octamer formation, with comparable EC₅₀ in the absence (that is, 45 μM ATP) but with a roughly 250-fold higher EC₅₀ than that exhibited by Ap4A in the presence of substrates (Fig. 2g), in agreement with the higher inhibitory potency of Ap4A for *Bs*IMPDH activity (Fig. 1f,h). We presume that the discrepancies in EC₅₀ related to the presence of substrate are a consequence of their impact on the oligomerization state of the enzyme²⁹. The observed fraction of *Bs*IMPDH octamers induced by other ApnA and ApnG dinucleotides and adenosine mononucleotides (Fig. 2h and Extended Data Fig. 6f) correlated well with their impact on enzymatic activity (Fig. 1f–h).

Guided by the structure (Fig. 2e), we conceived several variants that should not bind Ap4A anymore, that is, K202A, R141A/R144A and ΔCBS, in which the CBS domains from residues Val95 to Ile208 were replaced by a Ser–Gly–Ser linker. The K202A variant was still able to octamerize, dependent on Ap4A, albeit higher concentrations were required (Fig. 2i and Extended Data Fig. 6c), and showed a modest Ap4A-dependent reduction in activity (Extended Data Figs. 2c and 6g). The R141A/R144A and ΔCBS variants were insensitive to Ap4A-dependent regulation in enzymatic activity (Extended Data Figs. 2c and 6a) and tetramer-to-octamer equilibrium (Fig. 2i and Extended Data Fig. 6d,e). The ΔCBS variants exhibited a higher V_{max} of enzymatic activity than the wild type (Extended Data Figs. 2c and 6g). Plotting the fraction of active sites residing in the octameric form versus the V_{max} yielded a reasonable correlation, implying that the *Bs*IMPDH tetramer would exhibit a roughly 10-fold higher activity than the octamer (Extended Data Fig. 6h). Collectively, these data indicate that the promotion of *Bs*IMPDH octamers, which are enzymatically less active than the tetrameric form, represents the underlying mechanistic principle of Ap4A-dependent inhibition of *Bs*IMPDH activity. Of note, all assays were conducted at 25 °C for technical reasons instead of, for example, 51 °C (*B. subtilis* heat shock temperature, see below). Nevertheless, we expect that these in vitro characteristics of IMPDH would also apply to the enzyme in vivo.

Octamerization by Ap4A alters catalytic elements in IMPDH.

Next, we wanted to understand why the Ap4A-induced octamer was catalytically less active than the tetramer. In solution employing HDX–MS, we could not detect Ap4A-dependent changes in IMPDH's active site, marked by the catalytically essential cysteine

residue 308²⁴, probably because of the high HDX rate of this region (peptides 297–308 and 297–310, see Source Data) or due to the enzyme fraction being octameric even in the absence of Ap4A (Fig. 2f). We thus made use of the exclusively tetrameric ΔCBS variant (Fig. 3a) and determined its crystal structure (Table 1). The structure of ΔCBS shows an identical tetrameric arrangement of the catalytic domains as the wild type (Fig. 3a). In-depth comparison between the individual monomers of ΔCBS and Ap4A-bound *Bs*IMPDH revealed that the catalytic flap (that is, Glu376–Glu398 and Phe413–Pro423) and the C-terminal residues (that is, Gly467–Tyr485) were resolved in the ΔCBS structure, but not in that of the Ap4A-bound wild type (Fig. 3b). Moreover, we spotted differences in the conformation of the active site loop containing the catalytic cysteine 308 (Fig. 3c). In the Ap4A-bound *Bs*IMPDH structure, this Cys308-containing loop points away from the catalytic site but orients towards the active centre in the ΔCBS suited to execute its catalytic duty (Fig. 3c). Similar changes were also observed in the crystal structures of *P. aeruginosa* and *A. gossypii* IMPDH ΔCBS variants in the presence of the substrate IMP (Extended data Fig. 7), and the additional function of the C-terminal residue and catalytic flaps in establishing IMPDH tetramer-to-tetramer interfaces (forming IMPDH octamers) implied that octamerization may influence IMPDH activity allosterically^{31,32}. Collectively, our data suggest that the Ap4A-induced octamerization has direct consequences on the conformational geometry of the active site elements, and thus IMPDH activity.

IMPDH and nucleotide metabolism in *B. subtilis*. To assess whether our in vitro findings would have physiological relevance, we constructed a series of *B. subtilis* strains carrying mutations in the IMPDH-encoding gene *guaB* at its endogenous locus, using CRISPR-mediated gene editing. In the resulting mutant strains (K202A, the R141A/R144A double mutant and ΔCBS), we examined the levels of adenosine and guanosine nucleotides as well as their precursors by LC–MS. LC–MS profiling of *B. subtilis* grown at 30 °C revealed dysregulation of the purine nucleotide metabolism for all IMPDH mutant strains (Fig. 4). Specifically, the levels of IMP and its precursors PRPP, FGAR and SAICAR were elevated, and similarly increased levels of XMP, GMP, GDP and GTP, all of which derive from the IMPDH-dependent conversion of IMP to XMP, were apparent. In contrast, LC–MS suggested fewer perturbations in pools of adenylosuccinate and adenosine nucleotides. Collectively, the IMPDH mutants showed ~3- to 7-fold higher GTP:ATP ratios than the wild type, in good agreement with our in vitro results. Collectively, our data suggest that dysregulation of IMPDH results in increased flux from the common ATP/GTP intermediate IMP towards GTP.

IMPDH activity and *B. subtilis* heat tolerance. Given the profound effects of our IMPDH mutations on *B. subtilis* nucleotide metabolism at 30 °C (Fig. 4), we wondered whether these would translate to phenotypic differences at elevated temperatures that should promote Ap4A accumulation. First, we grew wildtype *B. subtilis* and the mutant strains at 30 °C in liquid minimal medium (S7) whereupon the mutants displayed a higher doubling time of ~46 min compared with 40 min for the wild type during logarithmic growth, which probably resulted from their disarrayed metabolome (Fig. 5a). Second, to probe temperature resistance and tolerance (Fig. 5b,c) phenotypes of the IMPDH mutant strains, the cultures grown to mid-log phase in S7 medium at 30 °C were used as inoculum for phenotypic characterization at elevated temperatures. On agar plates incubated with serial dilutions at various temperatures (that is, 22, 37, 45 and 51 °C), the site-directed mutants and the ΔCBS strain displayed strongly compromised growth at 51 °C, whereas at all other temperatures below 51 °C, the mutants grew similarly as the wildtype cells. The K202A mutant, in contrast to R141A/R144A

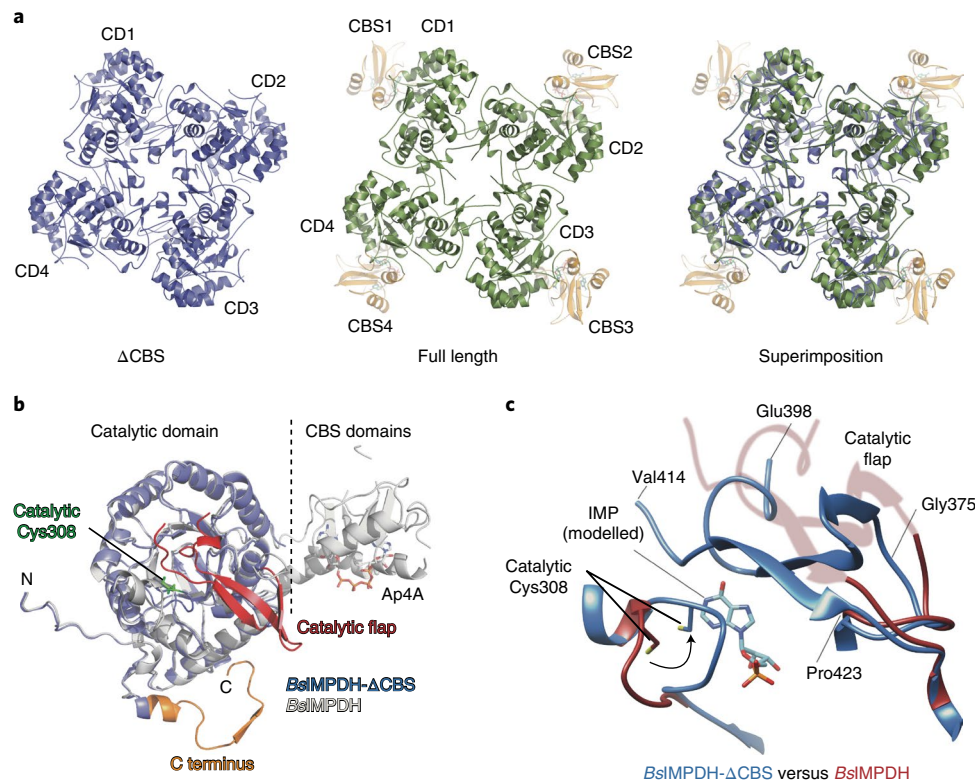


Fig. 3 | Crystal structure and conformational changes in *BslIMPDH* Δ CBS. **a**, Cartoon representation of the crystal structures of *BslIMPDH*- Δ CBS (blue, left), full-length *BslIMPDH* (green and orange for the catalytic (CD) and CBS domains, respectively, middle) and the superimposition of both structures (right). *BslIMPDH*- Δ CBS constitutes only one tetrameric ring through its catalytic domains in contrast to CBS-dependent octamerization in full-length *BslIMPDH*. **b**, The catalytic flap (red) and C termini (orange) could be located in *BslIMPDH*- Δ CBS (blue) but not in full-length *BslIMPDH* bound to Ap4A (white), evidencing a different conformation. **c**, Close-up view into the Cys308-containing catalytic loop and catalytic flap regions of *BslIMPDH*- Δ CBS (blue) and full-length *BslIMPDH* in complex with Ap4A (red). The position of the IMP substrate was approximated on the basis of an overlay with IMP-bound *P. aeruginosa* IMPDH- Δ CBS (PDB-ID: 5AHM³¹). Cys308 is dislocated in the Ap4A-bound state but oriented towards the IMP substrate-binding site of *BslIMPDH*- Δ CBS, thus probably representing the active conformation of IMPDH.

and Δ CBS, still afforded very weak growth even at 51 °C. These data indicate that the protective effect conferred by intact CBS domains for temperature resistance of *B. subtilis* is only required at higher temperatures (Fig. 5b). We further investigated heat shock tolerance of our strains in liquid culture by rapidly shifting cells from 30 °C to 53 °C, a potentially lethal temperature inducing strong heat shock response³⁵. Collectively, all investigated variants showed a mild trend towards lower survival rates than the wildtype strain, although there was high variation between the biological replicates (Fig. 5c). The K202A and R141A/R144A mutants were least affected and displayed a lower median of survival rate versus wild type only after 60 min at 53 °C. This trend was more pronounced for the Δ CBS mutant strain. The gradation in the survival rates of the mutant strains coincides with the impact of Ap4A on oligomerization and activity of IMPDH variants in vitro (Fig. 2j) and Extended Data Fig. 6g). We also quantified the intracellular Ap4A concentrations at 51 °C, which showed a significant increase induced by heat shock (Extended data Fig. 8). These results suggest that regulation of IMPDH activity is critical to *B. subtilis* heat shock response.

Discussion

Ap4A is conserved across the domains of life⁷. In eukaryotes, Ap4A is involved in activating the microphthalmia-associated transcription factor during allergic-response-IgE^{34,35} and inhibiting the cGAS-STING pathway³⁶. Diverse dinucleotides can also serve as protective messenger RNA (mRNA) caps during disulfide stress³⁷.

Even before the discovery of the molecular chaperones, Ap4A has been considered as a heat stress signal¹¹ and has been proposed to interact with DnaK, ClpB and GroEL in *E. coli*^{14,21}. Due to the lack of further targets, Ap4A was also considered as a metabolic waste product^{8,38}.

Here we show that Ap4A interacts with and inhibits *BslIMPDH*. IMPDH was previously identified as a target of Ap4A in *E. coli*^{8,19} and in murine brain lysates¹⁹, but this interaction was considered physiologically irrelevant because Ap4A bound to *E. coli* IMPDH with only a 5-fold higher affinity than ATP, the cellular concentration of the latter being assumed to exceed that of Ap4A 5,000-fold⁸. Notably, IMPDHs from different organisms interact with different dinucleotides. The strength of these interactions and consequences on oligomerization state and activity vary considerably; for example, *PaIMPDH* binds Ap4A or ATP⁸ and exhibits an octameric topology irrespective of the activity-stimulating ligand ATP²⁵. The CBS of *A. gossypii* IMPDH possesses three nucleotide-binding sites, in contrast to two in most other IMPDHs^{32,39}. It binds ATP, GDP and Ap5G well, but Ap4A only with low affinity²⁶. An open octamer of *A. gossypii* IMPDH with higher enzymatic activity is induced by ATP, while GDP promotes a compacted octamer with diminished activity^{39,40}. Our analysis of *BslIMPDH* shows that adenosine dinucleotides (ApnA), and to a lesser extent also ATP, but not mixed adenosine/guanosine dinucleotides (ApnG) enforce formation of catalytically inactive octamers. Differences in IMPDH regulation seem compounded by the structural plasticity of their CBS domains⁴¹. This

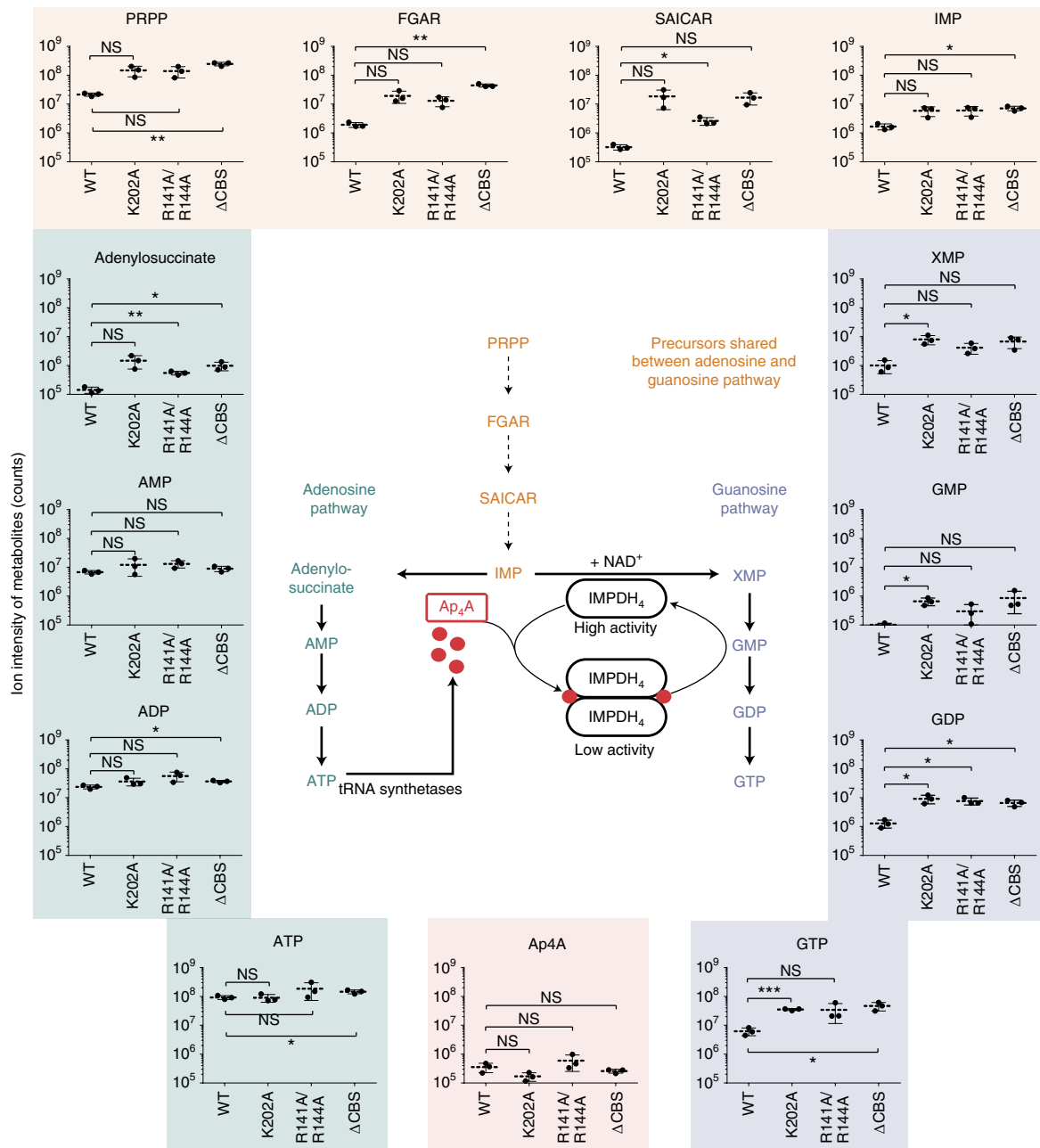


Fig. 4 | Mutations interfering with allosteric regulation of IMPDH activity perturb nucleotide metabolism of *B. subtilis*. In vivo quantification of purine nucleotide metabolism intermediates in wildtype (WT) *B. subtilis* 3610 and IMPDH mutant strains. Data represent mean \pm s.d. of $n = 3$ biological replicates. The abbreviations are: PRPP, phosphoribosylpyrophosphate; FGAR, phosphoribosyl-*N*-formylglycineamide; SAICAR, phosphoribosylaminoimidazolesuccinocarboxamide; IMP, inosine-5'-monophosphate; XMP, xanthosine-5'-monophosphate; GMP, guanosine-5'-mono-, di-, triphosphate; AMP, ADP, ATP, adenosine-5'-mono-, di-, triphosphate. The inset depicts a model of nucleotide metabolism and the regulation of *B. subtilis* IMPDH activity. Unpaired two-tailed *t*-tests were used to compare levels of metabolites for mutant strains versus WT. * $P \leq 0.05$, ** $P \leq 0.01$, *** $P \leq 0.001$; NS, not significant. Exact *P* values are, PRPP: 0.0653 (WT vs K202A), 0.0740 (WT vs R141A/R144A), 0.0079 (WT vs Δ CBS); FGAR: 0.0744 (WT vs K202A), 0.0587 (WT vs R141A/R144A), 0.0054 (WT vs Δ CBS); SAICAR: 0.1206 (WT vs K202A), 0.0360 (WT vs R141A/R144A), 0.0633 (WT vs Δ CBS); IMP: 0.0743 (WT vs K202A), 0.0706 (WT vs R141A/R144A), 0.0120 (WT vs Δ CBS); XMP: 0.0468 (WT vs K202A), 0.0748 (WT vs R141A/R144A), 0.0723 (WT vs Δ CBS); GMP: 0.0382 (WT vs K202A), 0.2521 (WT vs R141A/R144A), 0.1656 (WT vs Δ CBS); GDP: 0.0435 (WT vs K202A), 0.0286 (WT vs R141A/R144A), 0.0238 (WT vs Δ CBS); GTP: 0.0003 (WT vs K202A), 0.1658 (WT vs R141A/R144A), 0.0420 (WT vs Δ CBS); Adenylosuccinate: 0.0849 (WT vs K202A), 0.0061 (WT vs R141A/R144A), 0.0449 (WT vs Δ CBS); AMP: 0.3275 (WT vs K202A), 0.0895 (WT vs R141A/R144A), 0.1809 (WT vs Δ CBS); ADP: 0.1715 (WT vs K202A), 0.1095 (WT vs R141A/R144A), 0.0112 (WT vs Δ CBS); ATP: 0.8957 (WT vs K202A), 0.2897 (WT vs R141A/R144A), 0.0332 (WT vs Δ CBS); Ap₄A: 0.1116 (WT vs K202A), 0.3522 (WT vs R141A/R144A), 0.3207 (WT vs Δ CBS).

plasticity enables specific binding of different ligands, for example, mononucleotides, dinucleotides, S-adenosyl-methionine, or NAD, in different enzyme (sub)families⁴².

IMPDH functions at a step where the synthetic routes for adenosine and guanosine nucleotides branch at the conversion of IMP to XMP, which subsequently serves as substrate for guanosine

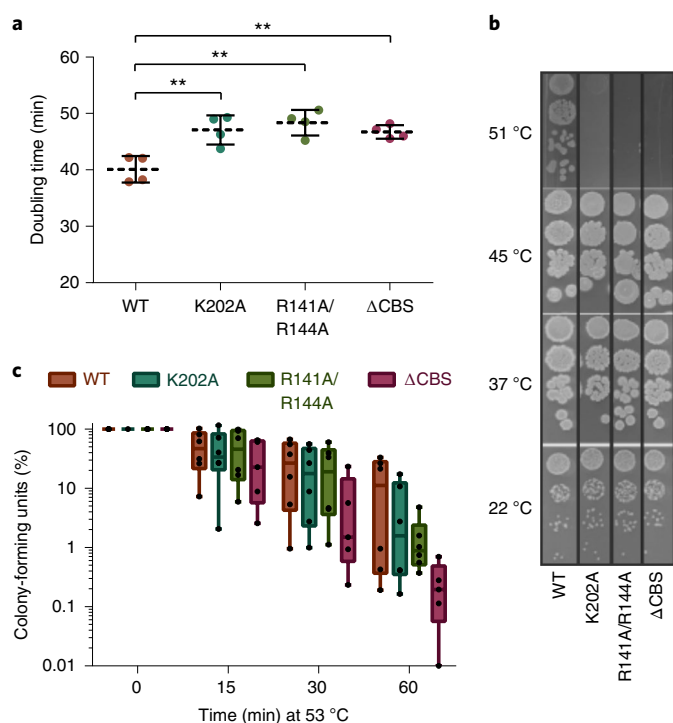


Fig. 5 | Allosteric regulation of IMPDH activity is critical for tolerance of *B. subtilis* to heat shock conditions.

a, Doubling times of wildtype *B. subtilis* and IMPDH mutant strains in liquid S7 minimal medium at 30 °C during the logarithmic growth phase. Data represent mean \pm s.d. of $n = 4$ biological replicates. Unpaired two-tailed *t*-tests were used to compare doubling times for mutant strains versus WT. ** $P \leq 0.01$. Exact *P* values are: 0.0073 (WT vs K202A), 0.0023 (WT vs R141A/R144A), 0.0054 (WT vs Δ CBS). **b, c**, Temperature-dependent growth of *B. subtilis* WT and IMPDH mutant strains. **b**, Serial dilutions of cultures from **a** were spotted on agar-containing S7 medium plates and incubated overnight at the indicated temperatures. One representative experiment is depicted. **c**, Cultures grown at 30 °C were diluted in pre-warmed liquid S7 medium to reach 53 °C after mixing. Colony-forming units were enumerated from aliquots withdrawn after indicated incubation times. In the boxplots, centre lines represent median values, boxes the 25th and 75th percentiles, and whiskers the minimum and maximum values. Individual data points from $n = 6$ ($n = 5$ for Δ CBS) biological replicates are displayed as individual points.

nucleotides (Fig. 4). Disrupting CBS-dependent inhibition of IMPDH activity in *B. subtilis* led to elevated GMP, GDP and GTP. GTP concentration can have a significant role in *B. subtilis* stress resistance⁴³, and GTP depletion downregulates transcription of ribosomal RNA⁴⁴. Thus, regulation of IMPDH activity might indirectly affect translation via GTP biosynthesis. Heat can induce protein unfolding/aggregation, requiring chaperones to facilitate protein refolding or removal. Therefore, slowing translation could prevent cells from overwhelming the molecular chaperones with both the heat-induced protein aggregation and the demand of nascent protein folding, thereby promoting cellular survival. On the other hand, downregulation of the guanosine nucleotides' de novo biosynthesis through CBS domain-dependent repression of IMPDH might favour the conversion of IMP to ATP, required for ATP-dependent chaperone and protein degradation systems.

Our data suggest that IMPDH regulation affects nucleotide metabolite homeostasis. Given the shared binding sites of ATP and Ap4A at the IMPDH CBS domains, we cannot rule out the possibility that ATP, either by itself or through competition with Ap4A, also interacts with IMPDH and that our mutations impeded this

potential ATP-dependent regulation. However, the K_d s of Ap4A and ATP for *Bs*IMPDH differ by 700-fold, and an intracellular Ap4A concentration of $\sim 24 \mu\text{M}$ would be sufficient to restrict *Bs*IMPDH activity in vivo in light of literature reports on cellular Ap4A levels and stress-dependent induction in some bacterial species: *E. coli* 0.2 μM (basal)⁸ or 2.4 μM (basal)⁴⁵ to 270 μM (104 $\mu\text{g ml}^{-1}$ cadmium sulfate after 160 min)⁴⁶ and 750 μM (shift from 37–50 °C after 120 min)⁴⁶; *S. typhimurium* <0.3 μM (basal) to 168 μM (180 $\mu\text{g ml}^{-1}$ diamide after 50 min) and 365 μM (110 $\mu\text{g ml}^{-1}$ cadmium chloride after 30 min)¹⁰; *S. typhimurium* 1 μM (basal) to 30 μM (shift from 28–50 °C after 50 min)¹¹. Notably, overexpression of a (p)ppGpp synthetase in *B. subtilis* increased Ap4A 4-fold, hinting at crosstalk between Ap4A and (p)ppGpp⁴⁷.

On the basis of our data, we hypothesize that the reduced fitness of *B. subtilis* strains with de-regulated IMPDH during heat shock (Fig. 5b,c), which is accompanied by an Ap4A increase, should be primarily linked to the dinucleotide and only to a lesser extent to ATP. While further research on the conserved nature of the Ap4A-dependent regulation of IMPDH is needed, we propose Ap4A as a central and conserved regulator in nucleotide metabolism.

Methods

Cloning of native and varied *Bs*IMPDH. The genes encoding full-length *Bs*IMPDH (*guaB*) or *Bs*IMPDH- Δ CBS were amplified by polymerase chain reaction (PCR) using chromosomal DNA of the *B. subtilis* NCIB3610 Δ comI strain¹⁸ as template. Primers are listed in Supplementary Table 2. PCR products for mutated *Bs*IMPDH were generated by overlapping PCR. PCR products were cloned into pET-24d(+) plasmid (Novagen) using standard cloning techniques. *B. subtilis* lysyl-tRNA synthetase (LysRS) was amplified by PCR from the same template and introduced into pET-24d(+) plasmid (Novagen) encoding for an N-terminal hexahistidine-tagged protein.

Synthesis of ³²P-labelled Ap4A. Radiolabelled Ap4A was synthesized with LysRS from *B. subtilis*. The protein was overexpressed in *E. coli* BL21(DE3) cells in lysogeny broth (LB) medium supplemented with 50 $\mu\text{g ml}^{-1}$ kanamycin and 0.5 mM isopropyl- β -D-thiogalactopyranoside (IPTG) (added at an optical density at a wavelength of 600 nm (OD_{600}) of approximately 0.5) at 20 °C for 16 h. The pelleted cells (3,500 \times g, 20 min, 4 °C) were resuspended in lysis buffer (20 mM HEPES-Na pH 8.0, 20 mM KCl, 20 mM MgCl₂, 250 mM NaCl, 20 mM imidazole) supplemented with protease inhibitors and DNaseI, and lysed by French Press. The lysate was run through a 1 ml HisTrap FF column (Cytiva) and eluted with a gradient of imidazole up to 500 mM. Fractions containing LysRS were dialysed into fresh lysis buffer supplemented with TEV protease (50 mM Tris-Cl pH 8.0, 1 mM dithiothreitol (DTT), 0.5 mM EDTA, 150 mM NaCl) and applied to a 1 ml HisTrap FF column (Cytiva) to obtain the cleaved protein, which was dialysed against SEC buffer (20 mM HEPES-Na pH 8.0, 20 mM KCl, 20 mM MgCl₂, 200 mM NaCl) overnight. LysRS was applied to a HiPrep 26/60 Sephacryl S-200 HR column (Cytiva) in SEC buffer to remove TEV. The protein was concentrated and stored in SEC buffer supplemented with 10% (v/v) glycerol.

To synthesize radiolabelled Ap4A, purified *B. subtilis* LysRS was incubated at a final concentration of 10 μM in 20 mM HEPES-Na pH 8.0, 20 mM KCl, 20 mM MgCl₂, 200 mM ZnCl₂, 1.7 U ml⁻¹ *E. coli* inorganic pyrophosphatase, 8 μCi ³²P- γ -ATP and 2 mM non-radiolabelled ATP. Lastly, 1 mM lysine was added to initiate the reaction. The reaction was incubated at 37 °C and after 5 h quenched by the addition of formic acid (0.33 M final). These conditions typically resulted in >70% conversion to Ap4A being a mix of labelled and unlabelled Ap4A. Ap4A was purified using a method adapted from Johnstone and Farr¹⁴ with AEX buffer A (50 mM NH₄HCO₃ pH 8.6) and AEX buffer B (700 mM NH₄HCO₃ pH 8.6). A 1 ml HiTrap QFF anion exchange chromatography column (Cytiva) was equilibrated with 10 column volumes (CV) of AEX buffer A and the Ap4A reaction, diluted 1:10 in AEX buffer A, loaded onto the column. The column was washed with 10 CV AEX buffer A, followed by a ramp of 0–20% B over 10 CV, 20–40% B over 15 CV, 40–55% B over 10 CV and 55–100% B over another 10 CV, all at 1 ml min⁻¹ flow rate. Elution fractions (1 ml) were analysed by thin-layer chromatography as described¹⁹ on PEI cellulose plates (Millipore) with 3 M (NH₄)₂SO₄ + 2% (w/v) EDTA as mobile phase. Plates were exposed to a phosphor screen and scanned on a Typhoon scanner. Pyrophosphate eluted upon wash with AEX buffer A, ATP eluted at the 20–40% B step and Ap4A eluted at the 40–55% B step. Fractions that contained at least 98% pure Ap4A were pooled and used for the DRaCALA screen. The final Ap4A probe solution had an estimated concentration of 0.66 mM.

DRaCALA. The *Bacillus anthracis* Gateway Clone set overexpression libraries with carbenicillin and gentamicin resistance cassettes were constructed and lysates with overexpressed proteins were obtained as described previously²³. Screening for binding targets of Ap4A was conducted by differential radial capillary action

of ligand assay (DRaCALA)²². ³²P-labelled Ap4A was diluted to 15 μ M total concentration in binding buffer (10 mM Tris-Cl pH 7.5, 100 mM NaCl, 5 mM MgCl₂), added to lysates at an equal volume, incubated for 10 min with shaking, and then spotted onto nitrocellulose paper. The spotted DRaCALA reactions were exposed to a phosphorescence and imaged with Typhoon scanner.

Expression and purification of BsIMPDPH. BsIMPDPH proteins were produced in *E. coli* BL21(DE3) in LB medium supplemented with 12.5 g l⁻¹ D(+)-lactose-mono-hydrate, 50 μ g ml⁻¹ kanamycin for 14 h at 30 °C. Cells were collected by centrifugation (3,500 \times g, 20 min, 4 °C), suspended in buffer A (20 mM HEPES-Na pH 8.0, 250 mM NaCl, 20 mM KCl, 20 mM MgCl₂ and 40 mM imidazole) and lysed through an LM10 microfluidizer (Microfluidics) at 12,000 psi. Lysate was treated for 1 h at room temperature with TURBO DNase (Thermo Fisher) and then centrifuged (47,850 \times g, 30 min, 4 °C). Supernatant was loaded onto a HisTrap HP 5 ml column (Cytiva) equilibrated with buffer A. After washing with 10 CV buffer A, BsIMPDPH was eluted with 4 CV buffer B (20 mM HEPES-Na pH 8.0, 250 mM NaCl, 20 mM KCl, 20 mM MgCl₂ and 250 mM imidazole). BsIMPDPH was concentrated (Amicon Ultracel-30K (Millipore)) to 1 ml and applied to SEC (HiLoad 26/600 Superdex 200 pg, Cytiva) equilibrated with 20 mM HEPES-Na pH 7.5, 200 mM NaCl, 20 mM KCl and 20 mM MgCl₂. BsIMPDPH-containing fractions were concentrated (Amicon Ultracel-30K (Millipore)) and snap-frozen in liquid nitrogen. BsIMPDPH concentration was quantified photometrically (NanoDrop Lite, Thermo Fisher), with extinction coefficients at 280 nm of 21,890 and 18,910 M⁻¹ cm⁻¹ for BsIMPDPH variants and BsIMPDPH- Δ CBS, respectively.

ITC. ITC experiments were performed at 25 °C with a MicroCal PEAQ-ITC instrument (Malvern Panalytical). The cell was filled with 25 μ M of purified BsIMPDPH and titrated with different concentrations of nucleotides to reach ligand saturation. Nucleotides were purchased from Jena Bioscience (purity of \geq 95%). BsIMPDPH and ligands were diluted in the same buffer: 20 mM HEPES-Na pH 7.5, 200 mM NaCl, 20 mM KCl and 20 mM MgCl₂. The titrations were performed with a first injection of 0.3 μ l or 0.4 μ l, which aimed to remove potential air bubbles in the syringe and was discarded from later analysis, followed by 18 injections of 2 μ l each for the Ap4A titration or 12 injections of 3 μ l each for all the other tested nucleotides. Data were processed with the MicroCal PEAQ-ITC Analysis software (Malvern Panalytical) and fitted with the 'single set of identical sites' model.

Assays for BsIMPDPH activity. All measurements were conducted with 100 nM BsIMPDPH in 100 mM Tris-Cl pH 8.0, 100 mM KCl and 2 mM DTT at 25 °C. All except one assay were conducted with NAD⁺ (Sigma Aldrich, \geq 95% by HPLC) concentration kept constant at 3 mM and IMP (Sigma Aldrich, \geq 99% by HPLC) employed in variable concentrations (25, 50, 100, 200, 400, 600, 800 and 1,000 μ M). In one assay (Fig. 1e), IMPDPH activity was quantified at constant IMP concentration (3 mM), and NAD⁺ employed in variable concentrations (25, 50, 100, 250, 500, 1,000, 2,500 and 5,000 μ M). Where denoted, nucleotides were supplemented with final concentrations of 1 μ M, 3 μ M, 10 μ M, 30 μ M and 100 μ M (Ap4A), 10 μ M (Ap3A, Ap5A, Ap6A, Ap3G, Ap4G and Ap5G), or 2 mM (AMP, ADP and ATP) as indicated in the figures.

Enzymatic reactions were started by the addition of BsIMPDPH, and the velocity of product formation was quantified by the increase in absorbance at 340 nm originating from the NADH product in a microplate reader (EPOCH2, BioTek). Analysis of BsIMPDPH enzyme kinetic parameters was performed with the GraphPad Prism version 6.0.1 software.

HDX-MS. Before HDX-MS, BsIMPDPH was mixed with Ap4A or ATP to reach final concentrations of 50 μ M and 5 mM, respectively. HDX-MS experiments were conducted and analysed as described previously, aided by a two-arm robotic autosampler (LEAP Technologies)⁴⁹. In brief, 7.5 μ l of BsIMPDPH solution were mixed with 67.5 μ l of D₂O-containing SEC buffer (20 mM HEPES-Na pH 7.5, 20 mM MgCl₂, 20 mM KCl, 200 mM NaCl) to start the exchange reaction. After 10, 30, 95, 1,000 or 10,000 s of incubation at 25 °C, samples of 55 μ l were taken from the reaction and mixed with an equal volume of quench buffer (400 mM KH₂PO₄/H₃PO₄, 2 M guanidine-HCl pH 2.2) kept cold at 1 °C. The resulting mixture (95 μ l) was injected into an ACQUITY UPLC M-Class System with HDX Technology (Waters)⁵⁰. Undeuterated samples were prepared similarly by 10-fold dilution in H₂O-containing SEC buffer. BsIMPDPH was digested online with immobilized porcine pepsin at 12 °C under a constant flow (100 μ l min⁻¹) of water + 0.1% (v/v) formic acid and the resulting peptic peptides collected on a trap column (2 mm \times 2 cm, kept at 0.5 °C) that was filled with POROS 20 R2 material (Thermo Fisher). After 3 min, the trap column was placed in line with an ACQUITY UPLC BEH C18 1.7 μ m 1.0 \times 100 mm column (Waters), and the peptides eluted at 0.5 °C using a gradient of water + 0.1% (v/v) formic acid (A) and acetonitrile + 0.1% (v/v) formic acid (B) at 30 μ l min⁻¹ flow rate as follows: 0–7 min/95–65% A, 7–8 min/65–15% A, 8–10 min/15% A. Peptides were ionized by electrospray ionization (capillary temperature 250 °C, spray voltage 3.0 kV) and mass spectra acquired from 50–2,000 *m/z* on a G2-Si HDMS mass spectrometer with ion mobility separation (Waters) in enhanced high-definition MS (HDMS^E) or high-definition MS (HDMS) mode for

undeuterated and deuterated samples, respectively^{51,52}. For lock mass correction, (Glu1)-Fibrinopeptide B standard (Waters) was employed. During each run, the pepsin column was washed three times with 80 μ l 4% (v/v) acetonitrile and 0.5 M guanidine hydrochloride, and blanks were performed between each sample. Three technical replicates (independent HDX reactions) were measured per incubation time.

Peptides were identified with ProteinLynx Global SERVER 3.0.1 (PLGS, Waters) from the non-deuterated samples acquired with HDMS^E by employing low energy, elevated energy and intensity thresholds of 300, 100 and 1,000 counts, respectively. Ions were matched to peptides with a database containing the amino acid sequences of BsIMPDPH, porcine pepsin and their reversed sequences, with the following search parameters: peptide tolerance, automatic; fragment tolerance, automatic; minimum fragment ion matches per peptide, 1; minimum fragment ion matches per protein, 7; minimum peptide matches per protein, 3; maximum hits to return, 20; maximum protein mass, 250,000; primary digest reagent, non-specific; missed cleavages, 0; and false discovery rate, 100. Deuterium incorporation into peptides was quantified with DynamX 3.0 software (Waters). Only peptides that were identified in all undeuterated samples and with a minimum intensity of 25,000 counts, a maximum length of 25 amino acids, a minimum number of two products with at least 0.1 product per amino acid, a maximum mass error of 25 ppm and retention time tolerance of 0.5 min were considered for analysis. All spectra were manually inspected and, if necessary, peptides omitted (for example, in case of low signal-to-noise ratio or presence of overlapping peptides). Parameters of the HDX-MS experiments are in Supplementary Table 1. Raw data are in Source Data (provided as Excel file).

Protein crystallization, X-ray diffraction and structure determination.

BsIMPDPH was crystallized at 20 °C by sitting drop vapour diffusion. For Ap4A-bound BsIMPDPH, 250 μ M of BsIMPDPH was incubated with 2 mM Ap4A for 10 min at 20 °C. For BsIMPDPH- Δ CBS, 250 μ M protein solution was employed. Crystallization screens were performed in SWISSCI MRC 2-well plates (Jena Bioscience) with a reservoir volume of 30 μ l by mixing 0.25 μ l of protein with an equal volume of precipitant solution. Crystals were obtained after 2 d. Optimization screens were carried out as hanging drop with a reservoir of 1 ml by adding 1 μ l precipitant solution to 1 μ l of protein solution. Ap4A-bound BsIMPDPH crystallized in 50 mM sodium acetate (pH 4.5) and 20% (v/v) 1,2-propanediol; BsIMPDPH- Δ CBS in 0.1 M sodium citrate pH 5.6, 0.2 M potassium/sodium tartrate and 2.0 M ammonium sulfate. Before data collection, crystals were flash-frozen in liquid nitrogen after addition of 20% (v/v) glycerol. Data were collected under cryogenic conditions at ID23-1 of the European Synchrotron Radiation Facility (ESRF) and at P14.2 beamline of BESSY II⁵³. Data were processed, reduced and merged with Mosflm⁵⁴ and AIMLESS⁵⁵. Structures of Ap4A-bound BsIMPDPH and BsIMPDPH- Δ CBS were solved by molecular replacement with PHASER⁵⁶ and the PaIMPDPH (PDB-ID: 4DQW⁵⁷) as search model. Structures were built in Coot⁵⁷, and refined with REFMAC5⁵⁸ and PHENIX refinement⁵⁹. Figures were generated with PYMOL⁶⁰ and ChimeraX⁶¹.

Mass photometry. Oligomerization of BsIMPDPH was determined by mass photometry³⁰ using the One MP mass photometer (Refeyn). Buffer composition in all measurements was: 100 mM Tris-Cl pH 8.0, 100 mM KCl and 2 mM DTT. To calibrate the instrument, native protein standards (Biorad) were diluted 50-fold in sample buffer at room temperature. Diluted calibration mixture (2 μ l) was mixed with 18 μ l of sample buffer in silicone wells on a cleaned microscope slide (170 \pm 5 μ m thickness, Marienfeld). We used the 66, 146, 480 and 1,048 kDa peaks of the standard proteins for a four-point calibration curve. For the measurements, 18 μ l buffer was pre-loaded into a silicone well, then 2 μ l of a 1,000 nM concentrated protein solution was mixed in before acquisition (100 nM BsIMPDPH final). NAD⁺ and IMP were used at 3 mM final concentrations. We collected 6,000 frames for each sample using default instrument parameters. Data were analysed with the DiscoverMP software provided by Refeyn, using default parameters with reflection and movement corrections for event extraction and fitting. Frames affected by strong vibration or aggregates moving across the image were manually excluded.

Bacterial growth conditions and strain construction. In vivo analyses were conducted using the non-domesticated *B. subtilis* NCBI3610 carrying the mutant *comI* Q12L⁴⁸ (3610, wild type). *B. subtilis* cultures were grown in S7 medium⁴⁷ at 30 °C. Mutant strains were constructed by the CRISPR/Cas9 method⁴² (Supplementary Table 2). Briefly, 5'- and 3'-ends of each repair template were amplified by PCR with one site-directed mutagenesis primer and one primer containing a unique BsaI cleavage site for Golden Gate assembly. The 5'- and 3'-ends were amplified by overlap-extension PCR, generating a mutant repair template flanked by two BsaI cleavage sites. Protospacers were designed and assembled as described⁴², and each was designed with two unique BsaI cleavage sites for Golden Gate assembly. *E. coli* TOP10 chemically competent cells were transformed with the Golden Gate reactions, the plasmids isolated and subsequently used for transformation of *E. coli* MC1061. Isolated plasmids from the latter were used for *B. subtilis* 3610 transformation⁶². Site-specific DNA sequencing confirmed mutants (Supplementary Table 3).

LC-MS quantification of metabolites. *B. subtilis* strains were grown in S7 medium supplemented with 20 amino acids (20 µg ml⁻¹ WY, 40 µg ml⁻¹ C, 50 µg ml⁻¹ ARNGQHILKMPSTVF, 500 µg ml⁻¹ DE) at 30 °C until an OD₆₀₀ of 0.6. For metabolite extraction, 5 ml of culture were filtered through a PTFE membrane (Sartorius). The membrane was submerged in 3 ml extraction solvent mix (50:50 (v/v) chloroform:water) kept on ice and mixed vigorously for 15 s. Extracts were centrifuged at 5,000 × g for 10 min at 4 °C, the aqueous phase removed and further centrifuged at 20,000 × g for 10 min at 4 °C. Samples were stored at -80 °C. Samples were run on an LC-MS/MS system (Q-exactive hybrid quadrupole-orbitrap mass spectrometer) equipped with an ACQUITY UPLC BEH C18 column (1.7 µm, 2.1 × 100 mm, Waters) in full-scan selected ion monitoring (MS-SIM) mode. MS parameters were: 70,000 resolution; automatic gain control of 10⁶; maximum injection time of 40 ms; and scan range of 90–1,000 m/z. Analytes were eluted with a gradient of 97:3 (v/v) water:methanol, 10 mM tributylamine pH 8 (solvent A) and acetonitrile (solvent B) at 0.2 ml min⁻¹ flow rate: 0–19 min/95–0% A, 19–24 min/0–95% A. Raw data were converted to mzXML format and quantification of metabolites was conducted using Metabolomics Analysis and Visualization Engine (MAVEN).

Normalized ion intensities of Ap4A were converted to intracellular concentrations as described⁴⁷ with $C_{Ap4A} = (V_{\text{extract}} \times IC_{Ap4A} / E_{LCMS}) / (V_{\text{culture}} \times OD \times F_{\text{cell}})$, where V_{extract} is the volume of the aqueous phase of the extract (1.5 ml); IC_{Ap4A} is the ion intensity of Ap4A in the sample; E_{LCMS} is the determined LC-MS detection efficiency of Ap4A (4.24 × 10⁷ counts per µM); V_{culture} is the volume of the collected culture; OD is the OD₆₀₀ of the collected culture; and F_{cell} is the approximate fraction of cell volume in a normalized culture (0.00052 ml per 1 ml culture per OD₆₀₀). F_{cell} was approximated on the basis of *B. subtilis* density of 2.2 × 10⁸ c.f.u. per ml per OD₆₀₀ unit and an intracellular volume of 2.38 fl (cell length of 4 µm and radius of 0.435 µm). Intracellular concentrations of Ap3A and Ap4G were determined using the same procedure. Intracellular concentrations of AMP, ADP and ATP were determined similarly but employed the LC-MS detection efficiency of ATP (2 × 10⁸ counts per µM).

Heat shock experiments. *B. subtilis* strains were inoculated into S7 media supplemented with 0.5% (w/v) casamino acids and grown at 30 °C until an OD₆₀₀ of 0.3–0.4. These cultures were inoculated into fresh media in a 96-well plate and grown in a plate reader (BioTek) at 30 °C with shaking for 16 h. For measurement of heat resistance, aliquots were withdrawn from cultures of each strain, and serial dilutions thereof employed to spot agar-containing S7 plates for incubation overnight at 22, 37, 45 or 51 °C. Plates were photographed to examine the growth at each temperature. For measurement of heat tolerance, 50 µl of the cultures were used to inoculate a tube containing 2 ml S7 medium supplemented with 0.5% (w/v) casamino acids pre-warmed to 53 °C. Samples for enumeration of colony-forming units were withdrawn before heat shock (0 min) or after 15, 30 or 60 min of incubation under vigorous agitation and incubated on LB agar plates at 30 °C until countable colonies were obtained.

Reporting summary. Further information on research design is available in the Nature Research Reporting Summary linked to this article.

Data availability

Structure factors and coordinates of X-ray crystallographic datasets have been deposited at the Protein Data Bank (www.rcsb.org) under the accession codes 7OJ1 and 7OJ2 for the Ap4A-bound BsIMPDPH and BsIMPDPH-ΔCBS, respectively. All other structural data employed in this manuscript (accession codes 3L2B, 3T5B, 4DQW, 4XTI, 4XWU, 5AHL, 5AHM, 5MCP, 6GJV, 6RPU) are publicly available in the Protein Data Bank. Source data for Figs. 1, 2, 4 and 5, and for Extended data Figs. 1, 2, 5, 6 and 8 are provided with this paper.

Received: 11 June 2021; Accepted: 29 June 2022;

Published online: 11 August 2022

References

- Steinchen, W. & Bange, G. The magic dance of the alarmones (p)ppGpp. *Mol. Microbiol.* **101**, 531–544 (2016).
- Hauryliuk, V., Atkinson, G. C., Murakami, K. S., Tenson, T. & Gerdes, K. Recent functional insights into the role of (p)ppGpp in bacterial physiology. *Nat. Rev. Microbiol.* **13**, 298–309 (2015).
- Hengge, R. High-specificity local and global c-di-GMP signaling. *Trends Microbiol.* **29**, 993–1003 (2021).
- Jenal, U., Reinders, A. & Lori, C. Cyclic di-GMP: second messenger extraordinaire. *Nat. Rev. Microbiol.* **15**, 271–284 (2017).
- Stülke, J. & Krüger, L. Cyclic di-AMP signaling in bacteria. *Annu. Rev. Microbiol.* **74**, 159–179 (2020).
- Zamecnik, P. G., Stephenson, M. L., Janeway, C. M. & Randerath, K. Enzymatic synthesis of diadenosine tetraphosphate and diadenosine triphosphate with a purified lysyl-sRNA synthetase. *Biochem. Biophys. Res. Commun.* **24**, 91–97 (1966).
- Ferguson, F., McLennan, A. G., Urbaniak, M. D., Jones, N. J. & Copeland, N. A. Re-evaluation of diadenosine tetraphosphate (Ap4A) from a stress metabolite to bona fide secondary messenger. *Front. Mol. Biosci.* **7**, 332 (2020).
- Despotović, D. et al. Diadenosine tetraphosphate (Ap4A) – an *E. coli* alarmone or a damage metabolite? *FEBS J.* **284**, 2194–2215 (2017).
- Charlier, J. & Sanchez, R. Lysyl-tRNA synthetase from *Escherichia coli* K12. Chromatographic heterogeneity and the lysU-gene product. *Biochemical J.* **248**, 43–51 (1987).
- Bochner, B. R., Lee, P. C., Wilson, S. W., Cutler, C. W. & Ames, B. N. AppppA and related adenylylated nucleotides are synthesized as a consequence of oxidation stress. *Cell* **37**, 225–232 (1984).
- Lee, P. C., Bochner, B. R. & Ames, B. N. AppppA, heat-shock stress, and cell oxidation. *Proc. Natl Acad. Sci. USA* **80**, 7496–7500 (1983).
- Nishimura, A. et al. Diadenosine 5',5'''-P1,P4-tetraphosphate (Ap4A) controls the timing of cell division in *Escherichia coli*. *Genes Cells* **2**, 401–413 (1997).
- Farr, S. B., Arnosti, D. N., Chamberlin, M. J. & Ames, B. N. An apaH mutation causes AppppA to accumulate and affects motility and catabolite repression in *Escherichia coli*. *Proc. Natl Acad. Sci. USA* **86**, 5010–5014 (1989).
- Johnstone, D. B. & Farr, S. B. AppppA binds to several proteins in *Escherichia coli*, including the heat shock and oxidative stress proteins DnaK, GroEL, E89, C45 and C40. *EMBO J.* **10**, 3897–3904 (1991).
- Ji, X. et al. Alarmone Ap4A is elevated by aminoglycoside antibiotics and enhances their bactericidal activity. *Proc. Natl Acad. Sci. USA* **116**, 9578–9585 (2019).
- Kimura, Y., Tanaka, C., Sasaki, K. & Sasaki, M. High concentrations of intracellular Ap4A and/or Ap5A in developing *Myxococcus xanthus* cells inhibit sporulation. *Microbiology* **163**, 86–93 (2017).
- Monds, R. D. et al. Di-adenosine tetraphosphate (Ap4A) metabolism impacts biofilm formation by *Pseudomonas fluorescens* via modulation of c-di-GMP-dependent pathways. *J. Bacteriol.* **192**, 3011–3023 (2010).
- Lundin, A. et al. The NudA protein in the gastric pathogen *Helicobacter pylori* is an ubiquitous and constitutively expressed dinucleoside polyphosphate hydrolase. *J. Biol. Chem.* **278**, 12574–12578 (2003).
- Guo, W. et al. Isolation and identification of diadenosine 5',5'''-P 1,P 4-tetraphosphate binding proteins using magnetic bio-panning. *Bioorg. Med. Chem. Lett.* **21**, 7175–7179 (2011).
- Azhar, M. A., Wright, M., Kamal, A., Nagy, J. & Miller, A. D. Biotin-c10-AppCH2ppA is an effective new chemical proteomics probe for diadenosine polyphosphate binding proteins. *Bioorg. Med. Chem. Lett.* **24**, 2928–2933 (2014).
- Fuge, E. K. & Farr, S. B. AppppA-binding protein E89 is the *Escherichia coli* heat shock protein ClpB. *J. Bacteriol.* **175**, 2321–2326 (1993).
- Roelofs, K. G., Wang, J., Sintim, H. O. & Lee, V. T. Differential radial capillary action of ligand assay for high-throughput detection of protein-metabolite interactions. *Proc. Natl Acad. Sci. USA* **108**, 15528–15533 (2011).
- Yang, J. et al. The nucleotide pGpp acts as a third alarmone in *Bacillus*, with functions distinct from those of (p) ppGpp. *Nat. Commun.* **11**, 5388 (2020).
- Hedstrom, L. IMP dehydrogenase: structure, mechanism, and inhibition. *Chem. Rev.* **109**, 2903–2928 (2009).
- Labesse, G. et al. MgATP regulates allostery and fiber formation in IMPDPHs. *Structure* **21**, 975–985 (2013).
- Fernández-Justel, D., Peláez, R., Revuelta, J. L. & Buey, R. M. The Bateman domain of IMP dehydrogenase is a binding target for dinucleoside polyphosphates. *J. Biol. Chem.* **294**, 14768–14775 (2019).
- Weis, D. D., Wales, T. E., Engen, J. R., Hotchko, M. & Ten Eyck, L. F. Identification and characterization of EX1 kinetics in H/D exchange mass spectrometry by peak width analysis. *J. Am. Soc. Mass Spectrom.* **17**, 1498–1509 (2006).
- Zhang, Z. & Smith, D. L. Determination of amide hydrogen exchange by mass spectrometry: a new tool for protein structure elucidation. *Protein Sci.* **2**, 522–531 (1993).
- Alexandre, T., Rayna, B. & Munier-Lehmann, H. Two classes of bacterial IMPDPHs according to their quaternary structures and catalytic properties. *PLoS ONE* **10**, e0116578 (2015).
- Young, G. et al. Quantitative mass imaging of single biological macromolecules. *Science* **360**, 423–427 (2018).
- Labesse, G., Alexandre, T., Gelin, M., Haouz, A. & Munier-Lehmann, H. Crystallographic studies of two variants of *Pseudomonas aeruginosa* IMPDPH with impaired allosteric regulation. *Acta Crystallogr. D* **71**, 1890–1899 (2015).
- Buey, R. M., Ledesma-Amaro, R., Balsara, M., de Pereda, J. M. & Revuelta, J. L. Increased riboflavin production by manipulation of inosine 5'-monophosphate dehydrogenase in *Ashbya gossypii*. *Appl. Microbiol. Biotechnol.* **99**, 9577–9589 (2015).
- Schäfer, H. et al. The alarmones (p)ppGpp are part of the heat shock response of *Bacillus subtilis*. *PLoS Genet.* **16**, e1008275 (2020).

34. Lee, Y.-N., Nechushtan, H., Figov, N. & Razin, E. The function of Lysyl-tRNA synthetase and Ap4A as signaling regulators of MITF Activity in Fc_γRI-activated mast cells. *Immunity* **20**, 145–151 (2004).
35. Yannay-Cohen, N. et al. LysRS serves as a key signaling molecule in the immune response by regulating gene expression. *Mol. Cell* **34**, 603–611 (2009).
36. Guerra, J. et al. Lysyl-tRNA synthetase produces diadenosine tetraphosphate to curb STING-dependent inflammation. *Sci. Adv.* **6**, eaax3333 (2020).
37. Luciano, D. J., Levenson-Palmer, R. & Belasco, J. G. Stresses that raise Np4A levels induce protective nucleoside tetraphosphate capping of bacterial RNA. *Mol. Cell* **75**, 957–966.e8 (2019).
38. Baltzinger, M., Ebel, J. P. & Remy, P. Accumulation of dinucleoside polyphosphates in *Saccharomyces cerevisiae* under stress conditions. High levels are associated with cell death. *Biochimie* **68**, 1231–1236 (1986).
39. Buey, R. M. et al. A nucleotide-controlled conformational switch modulates the activity of eukaryotic IMP dehydrogenases. *Sci. Rep.* **7**, 2648 (2017).
40. Buey, R. M. et al. Guanine nucleotide binding to the Bateman domain mediates the allosteric inhibition of eukaryotic IMP dehydrogenases. *Nat. Commun.* **6**, 8923 (2015).
41. Ereño-Orbea, J., Oyenarte, I. & Martínez-Cruz, L. A. CBS domains: ligand binding sites and conformational variability. *Arch. Biochem. Biophys.* **540**, 70–81 (2013).
42. Anashkin, V. A., Baykov, A. A. & Lahti, R. Enzymes regulated via cystathionine β-synthase domains. *Biochemistry* **82**, 1079–1087 (2017).
43. Kriel, A. et al. Direct regulation of GTP homeostasis by (p)ppGpp: a critical component of viability and stress resistance. *Mol. Cell* **48**, 231–241 (2012).
44. Krásný, L. & Gourse, R. L. An alternative strategy for bacterial ribosome synthesis: *Bacillus subtilis* rRNA transcription regulation. *EMBO J.* **23**, 4473–4483 (2004).
45. Plateau, P., Fromant, M., Kepes, F. & Blanquet, S. Intracellular 5',5'-dinucleoside polyphosphate levels remain constant during the *Escherichia coli* cell cycle. *J. Bacteriol.* **169**, 419–422 (1987).
46. Coste, H., Brevet, A., Plateau, P. & Blanquet, S. Non-adenylylated bis(5'-nucleosidyl) tetraphosphates occur in *Saccharomyces cerevisiae* and in *Escherichia coli* and accumulate upon temperature shift or exposure to cadmium. *J. Biol. Chem.* **262**, 12096–12103 (1987).
47. Fung, D. K., Yang, J., Stevenson, D. M., Amador-Noguez, D. & Wang, J. D. Small alarmone synthetase SasA expression leads to concomitant accumulation of pGpp, ppApp, and AppppA in *Bacillus subtilis*. *Front. Microbiol.* **11**, 2083 (2020).
48. Konkol, M. A., Blair, K. M. & Kearns, D. B. Plasmid-encoded ComI inhibits competence in the ancestral 3610 strain of *Bacillus subtilis*. *J. Bacteriol.* **195**, 4085–4093 (2013).
49. Osorio-Valeriano, M. et al. ParB-type DNA segregation proteins are CTP-dependent molecular switches. *Cell* **179**, 1512–1524.e15 (2019).
50. Wales, T. E., Fadgen, K. E., Gerhardt, G. C. & Engen, J. R. High-speed and high-resolution UPLC separation at zero degrees Celsius. *Anal. Chem.* **80**, 6815–6820 (2008).
51. Geromanos, S. J. et al. The detection, correlation, and comparison of peptide precursor and product ions from data independent LC-MS with data dependant LC-MS/MS. *Proteomics* **9**, 1683–1695 (2009).
52. Li, G.-Z. et al. Database searching and accounting of multiplexed precursor and product ion spectra from the data independent analysis of simple and complex peptide mixtures. *Proteomics* **9**, 1696–1719 (2009).
53. Mueller, U. et al. The macromolecular crystallography beamlines at BESSY II of the Helmholtz-Zentrum Berlin: current status and perspectives. *Eur. Phys. J.* **130**, 141 (2015).
54. Powell, H. R., Battye, T. G. G., Kontogiannis, L., Johnson, O. & Leslie, A. G. W. Integrating macromolecular X-ray diffraction data with the graphical user interface iMosflm. *Nat. Protoc.* **12**, 1310–1325 (2017).
55. Evans, P. R. & Murshudov, G. N. How good are my data and what is the resolution? *Acta Crystallogr. D* **69**, 1204–1214 (2013).
56. McCoy, A. J. Solving structures of protein complexes by molecular replacement with Phaser. *Acta Crystallogr. D* **63**, 32–41 (2007).
57. Emsley, P., Lohkamp, B., Scott, W. G. & Cowtan, K. Features and development of Coot. *Acta Crystallogr. D* **66**, 486–501 (2010).
58. Murshudov, G. N. et al. REFMAC5 for the refinement of macromolecular crystal structures. *Acta Crystallogr. D* **67**, 355–367 (2011).
59. Afonine, P. V. et al. Towards automated crystallographic structure refinement with phenix.refine. *Acta Crystallogr. D* **68**, 352–367 (2012).
60. The PyMOL Molecular Graphics System Version 1.8 (Schrödinger, 2015).
61. Pettersen, E. F. et al. UCSF ChimeraX: structure visualization for researchers, educators, and developers. *Protein Sci.* **30**, 70–82 (2021).
62. Burby, P. E. & Simmons, L. A. CRISPR/Cas9 editing of the *Bacillus subtilis* genome. *Bio Protoc.* **7**, e2272 (2017).
63. Tuominen, H. et al. Crystal structures of the CBS and DRTGG domains of the regulatory region of *Clostridium perfringens* pyrophosphatase complexed with the inhibitor, AMP, and activator, diadenosine tetraphosphate. *J. Mol. Biol.* **398**, 400–413 (2010).
64. Laskowski, R. A. & Swindells, M. B. LigPlot+: multiple ligand-protein interaction diagrams for drug discovery. *J. Chem. Inf. Model.* **51**, 2778–2786 (2011).
65. Makowska-Grzyska, M. et al. *Bacillus anthracis* inosine 5'-monophosphate dehydrogenase in action: the first bacterial series of structures of phosphate ion-, substrate-, and product-bound complexes. *Biochemistry* **51**, 6148–6163 (2012).
66. Alexandre, T. et al. First-in-class allosteric inhibitors of bacterial IMPDHs. *Eur. J. Med. Chem.* **167**, 124–132 (2019).

Acknowledgements

This work was supported by the priority programme of the Deutsche Forschungsgemeinschaft (DFG) SPP1879 – ‘Nucleotide second messenger signalling in bacteria’ (to G.B.), the USA National Institute of Health R35 GM127088 and the Howard Hughes Medical Institute Faculty Scholars Award (to J.D.W.), and the National Science Foundation (NSF) grant award no. 1715710 (to D.A.-N.). We thank the European Synchrotron Radiation Facility (Grenoble, France) and the Electron Storage Ring BESSY II (Berlin, Germany) for the excellent beamline support. We acknowledge support from the ‘DFG-core facility for interactions, dynamics and macromolecular assembly structure’ at the Philipps-University Marburg (to G.B.). G.H. acknowledges support from the Free-floater programme of the Max Planck Society.

Author contributions

J.D.W. and G.B. conceptualized the project. G.H. and D.A.-N. developed the methodology. P.I.G., M.K.M.Y., W.S., C.-N.M., J.Y. and A.P. conducted the experimental investigations. J.D.W. and G.B. acquired funding. J.D.W. and G.B. supervised the project. P.I.G., M.Y., W.S., J.D.W. and G.B. wrote the original draft. All authors read and commented on the manuscript.

Competing interests

The authors declare no competing interests.

Additional information

Extended data is available for this paper at <https://doi.org/10.1038/s41564-022-01193-x>.

Supplementary information The online version contains supplementary material available at <https://doi.org/10.1038/s41564-022-01193-x>.

Correspondence and requests for materials should be addressed to Jue D. Wang or Gert Bange.

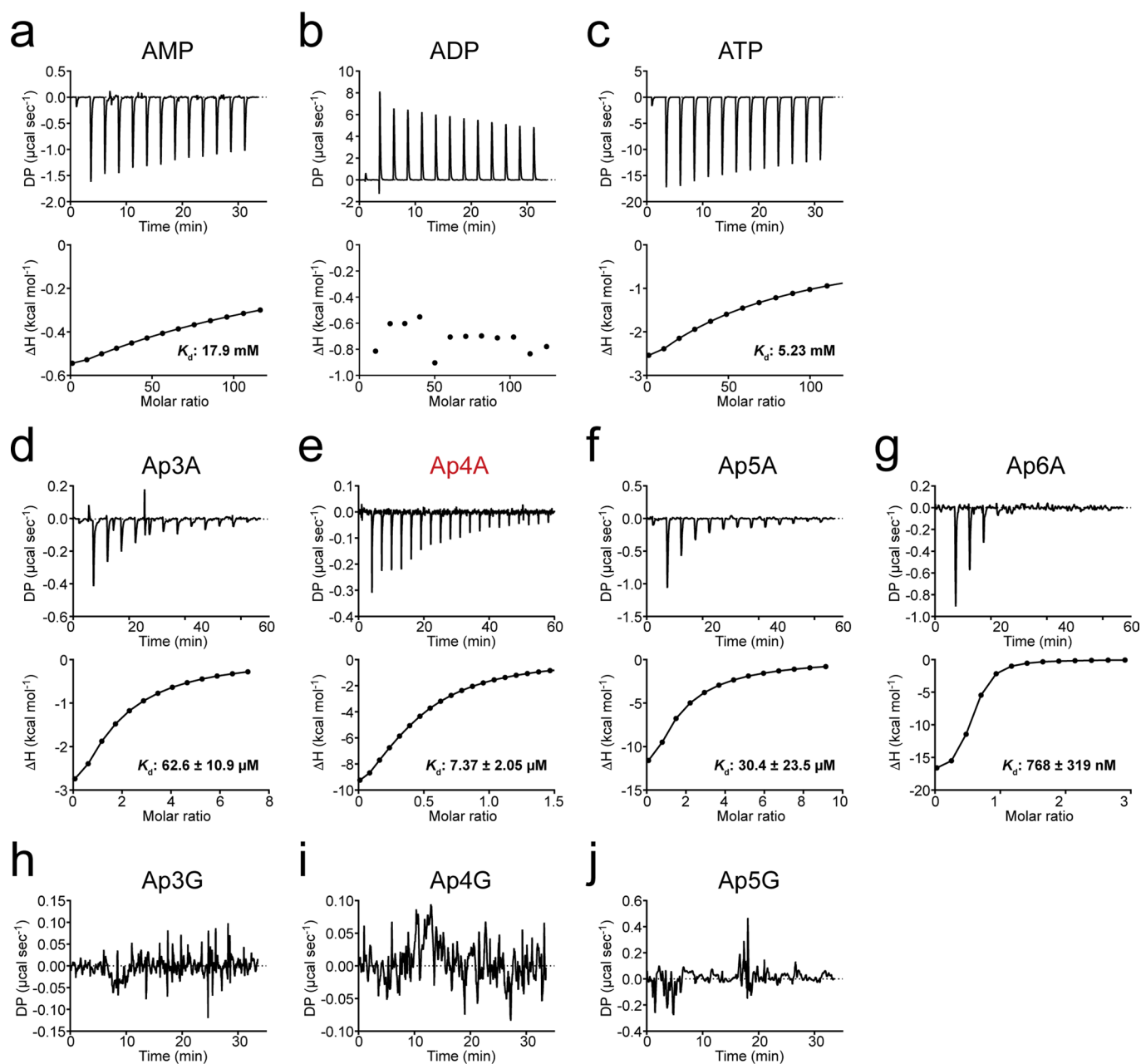
Peer review information *Nature Microbiology* thanks Natalia Tschowri and the other, anonymous, reviewer(s) for their contribution to the peer review of this work.

Reprints and permissions information is available at www.nature.com/reprints.

Publisher's note Springer Nature remains neutral with regard to jurisdictional claims in published maps and institutional affiliations.

Springer Nature or its licensor holds exclusive rights to this article under a publishing agreement with the author(s) or other rightsholder(s); author self-archiving of the accepted manuscript version of this article is solely governed by the terms of such publishing agreement and applicable law.

© The Author(s), under exclusive licence to Springer Nature Limited 2022



Extended Data Fig. 1 | Binding of nucleotides and dinucleotides to BsIMPDPH determined by isothermal titration calorimetry (ITC). a–j. A $25 \mu\text{M}$ concentrated solution of purified BsIMPDPH was titrated with **a.** AMP, **b.** ADP, **c.** ATP, **d.** Ap3A, **e.** Ap4A, **f.** Ap5A, **g.** Ap6A, **h.** Ap3G, **i.** Ap4G, or **j.** Ap5G. The differential power (DP, upper plot) for each injection of ligand was recorded and used to determine the dissociation constant K_d from a fitting of the calculated binding enthalpies (ΔH , lower plot).

a

	V_{\max} ($\mu\text{M min}^{-1}$)	K_m (μM)	K_i (μM)
No ligand	6.3 ± 0.2	63.2 ± 9.1	n.d.
Ap4A 1 μM	5.2 ± 0.2	58.3 ± 10.7	15.8 ± 1.8
Ap4A 3 μM	4.9 ± 0.2	47.0 ± 7.2	
Ap4A 10 μM	2.5 ± 0.2	41.4 ± 10.5	
Ap4A 30 μM	2.2 ± 0.2	35.0 ± 12.5	
Ap4A 100 μM	1.8 ± 0.1	41.0 ± 7.5	
AMP 2 mM	5.3 ± 0.2	71.2 ± 6.9	n.d.
ADP 2 mM	4.2 ± 0.2	62.4 ± 11.2	n.d.
ATP 2 mM	5.1 ± 0.2	94.7 ± 13.9	n.d.
Ap3A 10 μM	5.6 ± 0.3	58.8 ± 12.4	n.d.
Ap5A 10 μM	2.4 ± 0.2	23.7 ± 13.2	n.d.
Ap6A 10 μM	4.9 ± 0.1	46.5 ± 4.3	n.d.
Ap3G 10 μM	6.6 ± 0.2	47.5 ± 4.6	n.d.
Ap4G 10 μM	6.5 ± 0.2	71.9 ± 7.6	n.d.
Ap5G 10 μM	5.9 ± 0.3	59.6 ± 13.3	n.d.

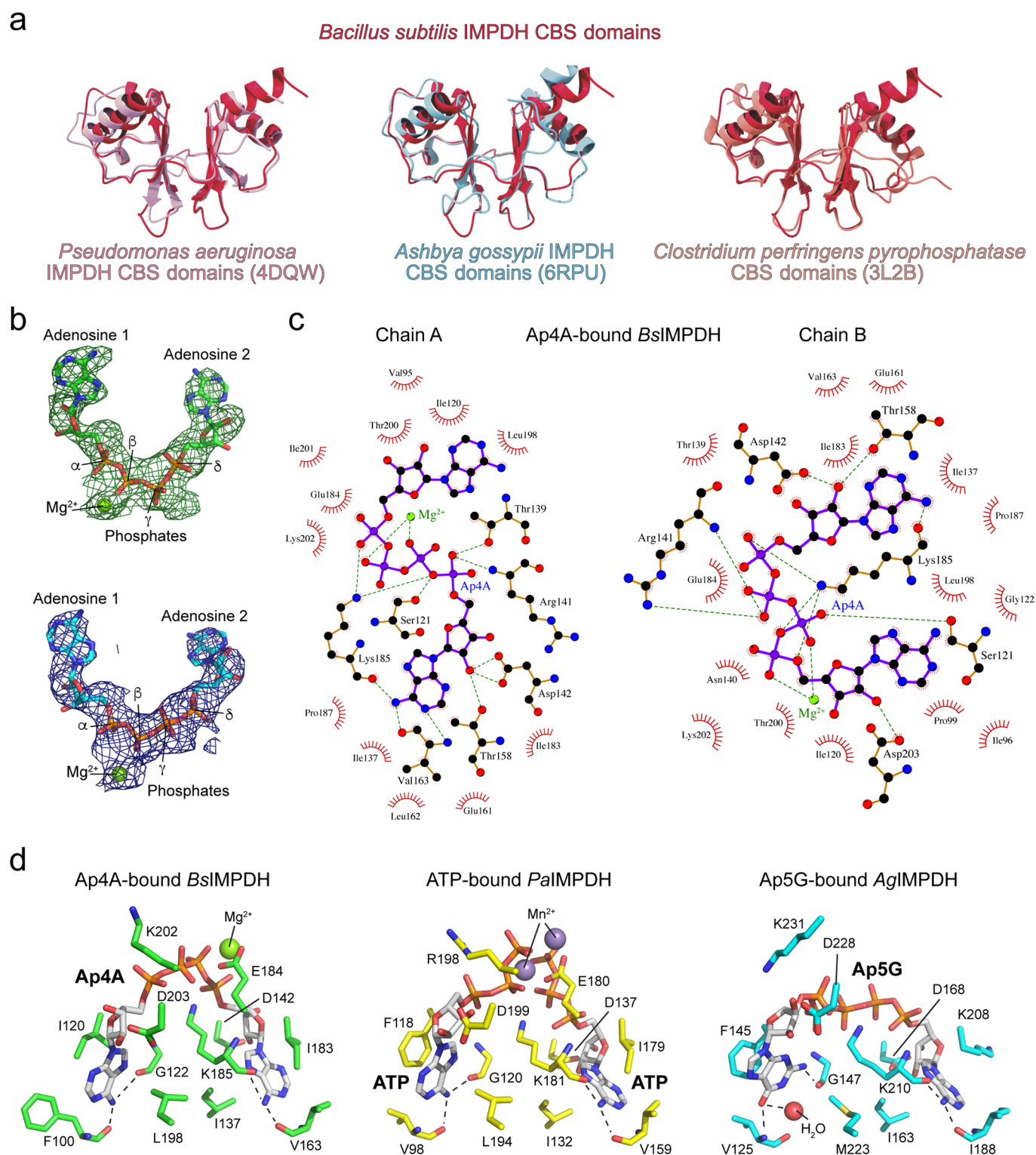
b

	V_{\max} ($\mu\text{M min}^{-1}$)	K_m (μM)	K_i (μM)
No ligand	8.1 ± 0.3	773 ± 81	n.a.
Ap4A 1 μM	5.9 ± 0.2	746 ± 77	25.7 ± 2.9
Ap4A 3 μM	5.9 ± 0.2	858 ± 82	
Ap4A 10 μM	4.2 ± 0.1	881 ± 66	
Ap4A 30 μM	3.3 ± 0.2	636 ± 73	
Ap4A 100 μM	2.0 ± 0.2	346 ± 97	

c

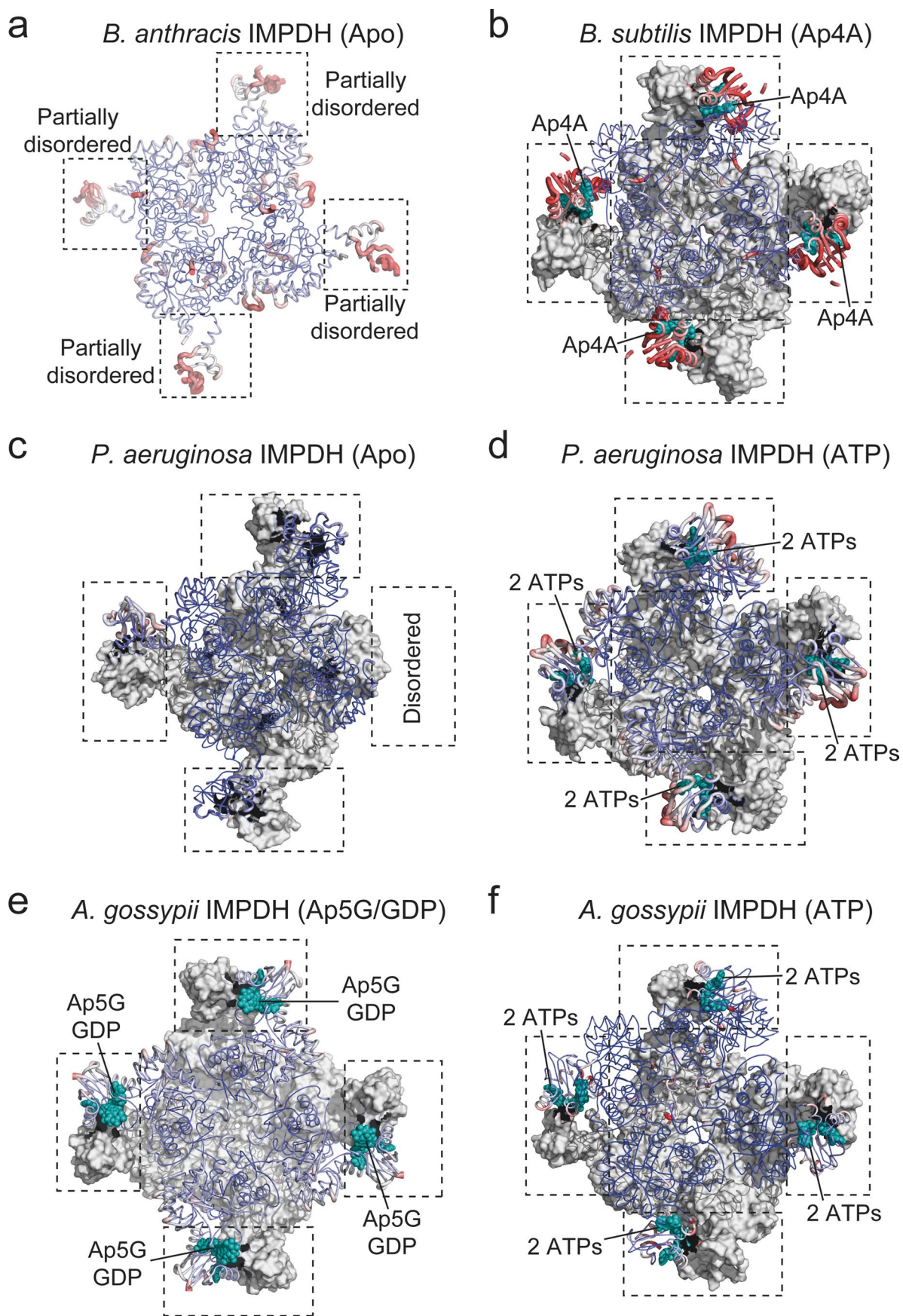
	No ligand		100 μM Ap4A		2 mM ATP	
	V_{\max} ($\mu\text{M min}^{-1}$)	K_m (μM)	V_{\max} ($\mu\text{M min}^{-1}$)	K_m (μM)	V_{\max} ($\mu\text{M min}^{-1}$)	K_m (μM)
BsIMPDPH						
WT	6.3 ± 0.2	63.2 ± 9.1	1.8 ± 0.1	41.0 ± 7.5	5.1 ± 0.2	94.7 ± 13.9
K202A	9.3 ± 0.3	27.8 ± 4.3	6.5 ± 0.2	35.6 ± 4.4	9.2 ± 0.2	32.4 ± 2.7
R141A/R144A	12.3 ± 0.2	25.2 ± 2.4	11.5 ± 0.3	31.4 ± 3.8	12.4 ± 0.3	30.2 ± 3.2
ΔCBS	10.6 ± 0.4	14.2 ± 4.5	11.7 ± 0.4	32.2 ± 5.4	11.3 ± 0.2	45.8 ± 4.4

Extended Data Fig. 2 | Enzyme kinetic parameters obtained for BsIMPDPH. a-c. The maximal velocity (V_{\max}) and Michaelis-Menten constant (K_m) of BsIMPDPH activity were determined in the presence of various ligands. For Ap4A, the inhibitory constant (K_i) was fitted from the change in V_{\max} in the presence of different Ap4A concentrations. The mean \pm SD of enzymological parameters was obtained with Graph Pad Prism from $n=2$ replicates. For assay results displayed in **a** (related to Fig. 1e-h) and **c** (related to Extended Data Fig. 6a), the concentration of NAD^+ was kept constant at 5 mM and the concentration of IMP variable between 25 and 1,000 μM . For the assay results displayed in **b** (related to Fig. 1e), the concentration of IMP was kept constant at 3 mM and the concentration of NAD^+ variable between 25 and 5,000 μM . n.d., not determined.



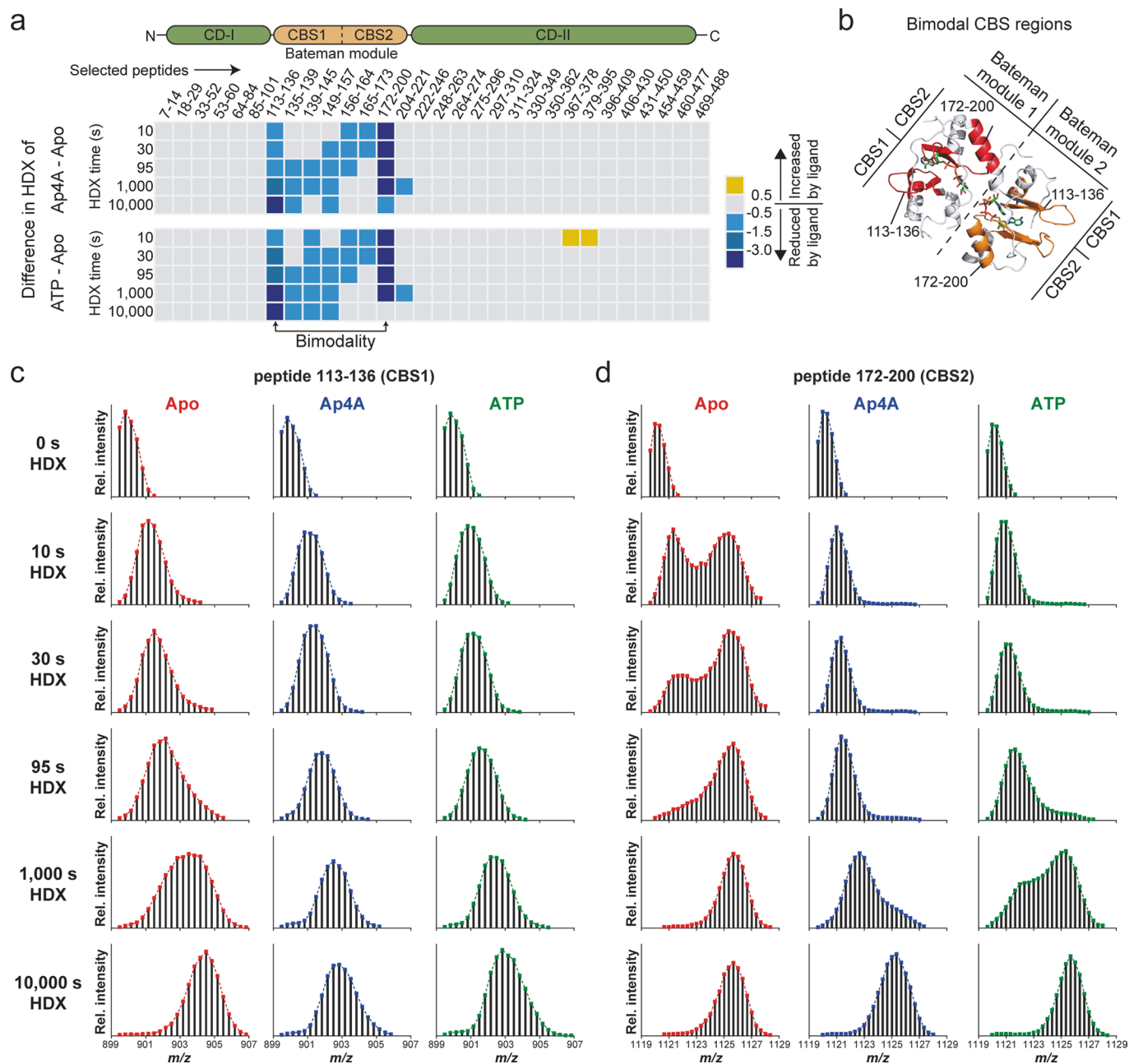
Extended Data Fig. 3 | See next page for caption.

Extended Data Fig. 3 | Coordination of Ap4A by the BslIMPDH CBS domains. **a.** The CBS domains of the *B. subtilis* IMPDH (red, this study) were aligned with the CBS domains of *P. aeruginosa* IMPDH (left; pink, PDB-ID: 4DQW²⁵), *A. gossypii* IMPDH (middle; light blue, PDB-ID: 6RPU²⁶), and *C. perfringens* pyrophosphatase (right; salmon, PDB-ID: 3L2B⁶³), revealing an overall similar topology. **b.** The unbiased $F_{\text{obs}} - F_{\text{calc}}$ difference electron density map (top) is coloured in green and red for positive and negative electron density, respectively, and contoured at 3.0σ . The Ap4A ligand was not present during the refinement. The $2F_{\text{obs}} - F_{\text{calc}}$ electron density map after final refinement (bottom), including the Ap4A ligand, is coloured in blue and contoured at 1.5σ . **c.** Coordination of Ap4A in chains A and B of the crystal structure of Ap4A-bound BslIMPDH. Atoms are displayed as spheres and coloured as follows: carbon, black; oxygen, red; nitrogen, blue; phosphorus, purple. Purple and orange solid lines illustrate ligand or non-ligand covalent bonds, and green dashed lines represent hydrogen bonds. Red semicircles denote hydrophobic interactions. The image was generated with LigPlot⁺⁶⁴. **d.** Coordination of ligands by the CBS domains of *B. subtilis* IMPDH with Ap4A (left), *P. aeruginosa* IMPDH with 2 ATP (middle, PDB-ID: 4DQW²⁵), and *A. gossypii* IMPDH with Ap5G (right, PDB-ID: 6RPU²⁶). Ligands and amino acid residues lining the ligand-binding sites are shown as sticks and coloured by element (carbon, green/yellow/cyan; oxygen, red; nitrogen, blue; phosphorus, orange). Green and purple spheres represent magnesium and manganese ions, respectively. Dashed lines denote hydrogen bonding interactions between the main chain carbonyl/amide groups and the adenine and guanine nucleobases. *A. gossypii* IMPDH does not require a divalent metal ion to coordinate the GDP ligand, whereas metal ion coordination in the prokaryotic *B. subtilis* and *P. aeruginosa* IMPDHs is achieved by E184 and E180 residues, respectively⁴⁰.

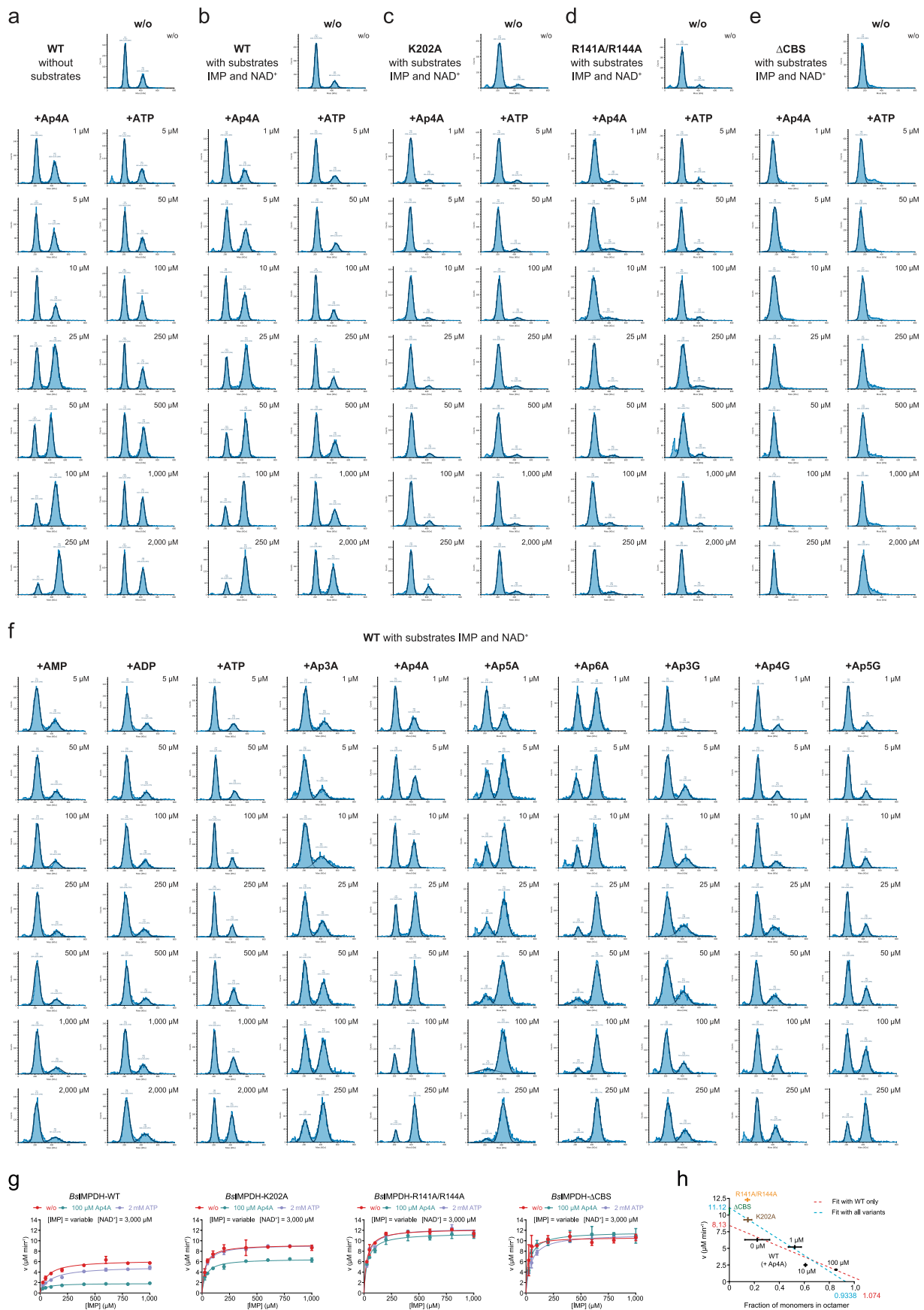


Extended Data Fig. 4 | See next page for caption.

Extended Data Fig. 4 | Conformational flexibility of CBS domains in crystal structures of selected IMPDH proteins. a-f. The crystal structures of IMPDH proteins from **a.** *B. anthracis* in apo-state (PDB-ID: 3TSB⁶⁵), **b.** *B. subtilis* bound to Ap4A (this study), **c.** *P. aeruginosa* in apo-state (PDB-ID: 6GJV⁶⁶), **d.** *P. aeruginosa* bound to ATP (PDB-ID: 4DQW²⁵), **e.** *A. gossypii* bound to Ap5G and GDP (PDB-ID: 6RPU²⁶), and **f.** *A. gossypii* bound to ATP (PDB-ID: 5MCP³⁹) are shown as ribbon and colored to their B factors from 20 (blue) to 150 Å² (red). For octameric biological assemblies, the bottom tetrameric ring is shown in grey surface. CBS domains are indicated by black dashed rectangles, and teal spheres denote the nucleotide ligands coordinates within the CBS domains.

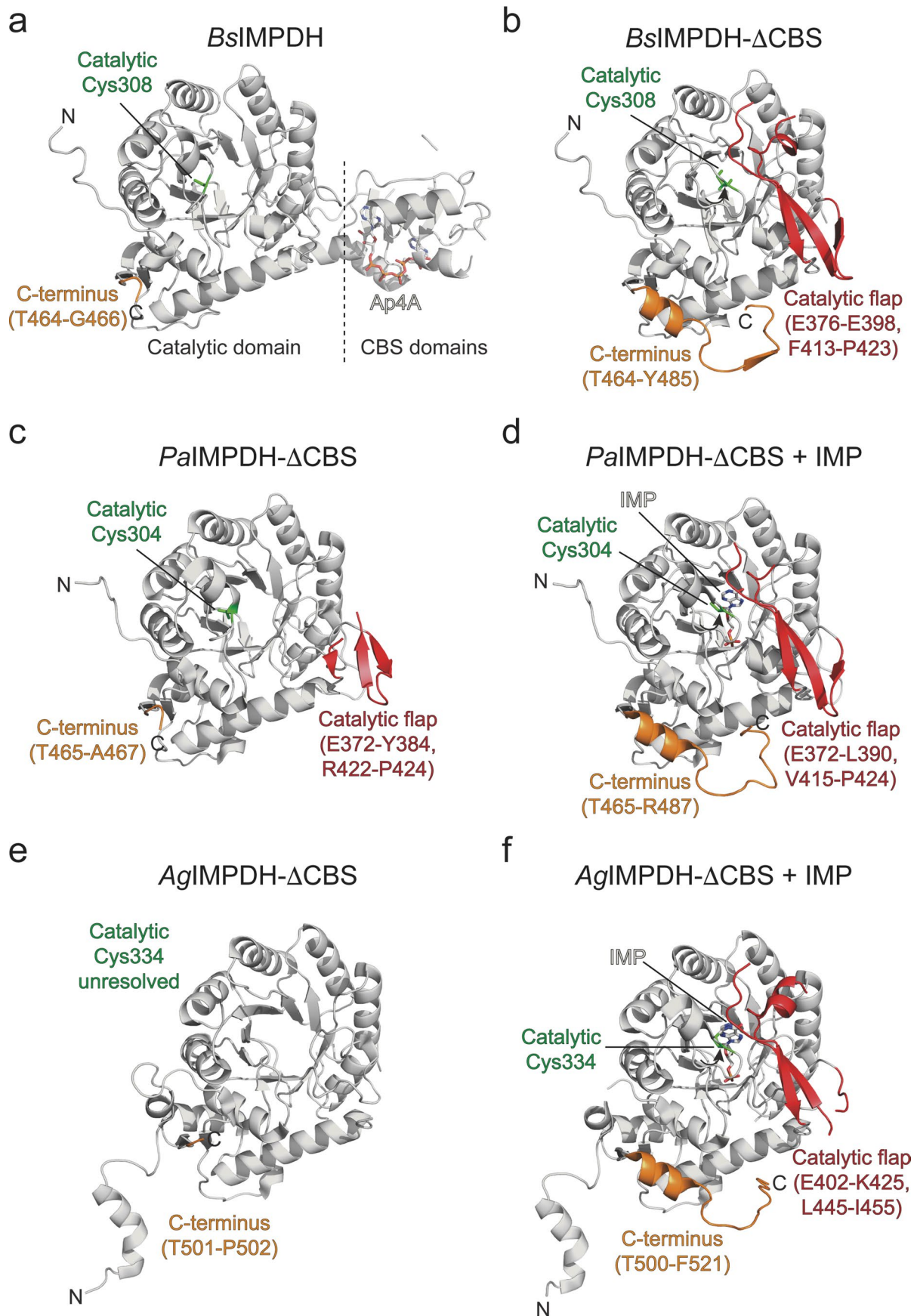


Extended Data Fig. 5 | Influence of Ap4A and ATP on conformational flexibility of BsIMPDH CBS domains by hydrogen/deuterium exchange mass spectrometry. a. Difference in hydrogen/deuterium exchange (HDX) of representative peptides in the presence of Ap4A (top) or ATP (bottom), expressed as the difference in HDX of ligand-bound BsIMPDH versus its apo-state. **b.** Location of selected peptides exhibiting bimodality in HDX (EX1 kinetics) displayed on the adjacent CBS domains of two monomers of Ap4A-bound BsIMPDH. **c-d.** Mass spectra of two selected BsIMPDH peptides exhibiting EX1 kinetics for hydrogen/deuterium exchange, that is, **c.** the peptides containing residues 113-136, and **d.** residues 172-200 of BsIMPDH. The occurrence of a fast-exchanging population in the apo-state (red) is indicative for unfolding of secondary structures, which is restricted in samples of Ap4A-bound (blue) and ATP-bound (green) BsIMPDH.



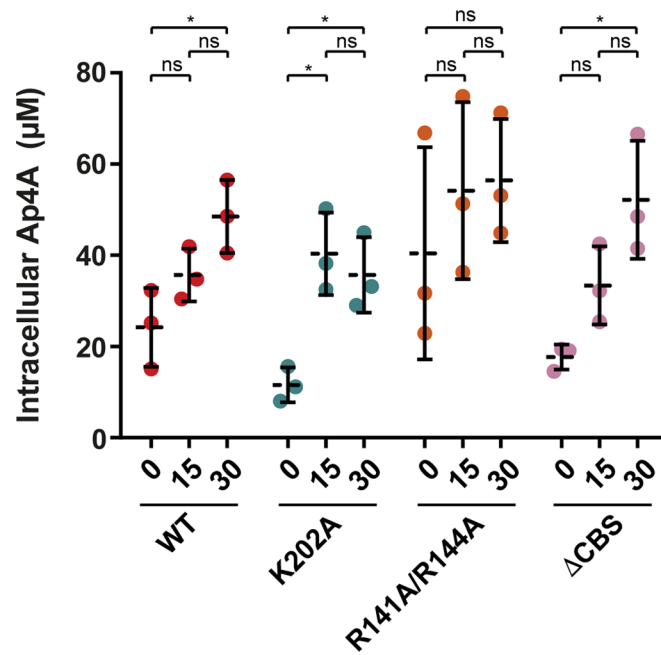
Extended Data Fig. 6 | See next page for caption.

Extended Data Fig. 6 | Enzymatic activity and oligomeric state of *Bs*IMPDPH-WT and CBS domain variants. **a.** Representative distributions of tetrameric and octameric *Bs*IMPDPH species for *Bs*IMPDPH-WT in the absence of IMP and NAD⁺ substrates and in dependence of Ap4A or ATP concentration. **b-e.** Representative distributions of tetrameric and octameric *Bs*IMPDPH species of **b.** *Bs*IMPDPH-WT, **c.** *Bs*IMPDPH-K202A, **d.** *Bs*IMPDPH-R141A/R144A, and **e.** *Bs*IMPDPH- Δ CBS, all in the presence of IMP and NAD⁺ substrates and in dependence of Ap4A or ATP concentration. **f.** Representative distributions of tetrameric and octameric *Bs*IMPDPH species for *Bs*IMPDPH-WT in the presence of IMP and NAD⁺ substrates and in dependence of the indicated adenosine nucleotides or *Apn*A and *Apn*G dinucleotides added. In **a-f**, the numbers in the diagrams reflect the molecular weight of the observed oligomeric species (mean and SD), the number of observed molecules for either species and their percentage of all observed molecules in the sample. **g.** Effect of 10 μ M Ap4A or 2 mM ATP on the enzyme-kinetic behavior of *Bs*IMPDPH-WT and CBS domain variants K202A, R141A/R144A and Δ CBS for conversion of the IMP substrate into XMP. Individual data points of $n=2$ replicates are shown, and parameters of the fits are given in Extended Data Fig. 2c. **h.** Correlation between observed fraction of IMPDPH monomers in oligomeric state and the apparent V_{\max} of IMPDPH activity. Linear regression was performed either with values for *Bs*IMPDPH WT only (red trace) or all depicted values including WT and variants (blue trace). Red and blue numbers denote values for the fraction and V_{\max} at the intersects with the x-axis and y-axis, respectively.



Extended Data Fig. 7 | See next page for caption.

Extended Data Fig. 7 | Different conformations of catalytic flap and C-termini regions in crystal structures of IMPDH enzymes. a-f. Cartoon representations of the crystal structures of **a.** Ap4A-bound full-length *B. subtilis* (*Bs*) IMPDH, **b.** *B. subtilis* (*Bs*) IMPDH- Δ CBS, **c.** *P. aeruginosa* (*Pa*) IMPDH- Δ CBS (PDB-ID: 5AHL³¹), **d.** *P. aeruginosa* (*Pa*) IMPDH- Δ CBS with substrate IMP in the active site (PDB-ID: 5AHM³¹), **e.** *A. gossypii* (*Ag*) IMPDH- Δ CBS (PDB-ID: 4XWU³²), and **f.** *A. gossypii* (*Ag*) IMPDH- Δ CBS with substrate IMP in the active site (PDB-ID: 4XTI³²). The catalytic cysteine (green), catalytic flap (red) and C-termini (orange) were colored and denoted where possible.



Extended Data Fig. 8 | Quantification of rising intracellular Ap4A concentrations in *B. subtilis* after non-lethal heat shock. *In vivo* quantification of Ap4A in wildtype (WT) *B. subtilis* 3610 and IMPDH mutant strains. Data represent mean \pm SD of $n = 3$ biological replicates. Unpaired two-tailed t-tests were used to compare Ap4A levels for WT and IMPDH mutant strains of heat-shocked conditions (15 min, 30 min) versus the untreated control (0 min). Asterisks indicate p -values: * $p \leq 0.05$; ns, not significant. Exact p -values are, WT: 0.1382 (15 vs. 0 min), 0.0943 (30 vs. 15 min), 0.0235 (30 vs. 0 min); K202A: 0.0191 (15 vs. 0 min), 0.5491 (30 vs. 15 min), 0.0223 (30 vs. 0 min); R141A/R144A: 0.4789 (15 vs. 0 min), 0.8778 (30 vs. 15 min), 0.3756 (30 vs. 0 min); Δ CBS: 0.0753 (15 vs. 0 min), 0.1146 (30 vs. 15 min), 0.0390 (30 vs. 0 min).

Reporting Summary

Nature Research wishes to improve the reproducibility of the work that we publish. This form provides structure for consistency and transparency in reporting. For further information on Nature Research policies, see our [Editorial Policies](#) and the [Editorial Policy Checklist](#).

Statistics

For all statistical analyses, confirm that the following items are present in the figure legend, table legend, main text, or Methods section.

n/a Confirmed

- The exact sample size (n) for each experimental group/condition, given as a discrete number and unit of measurement
- A statement on whether measurements were taken from distinct samples or whether the same sample was measured repeatedly
- The statistical test(s) used AND whether they are one- or two-sided
Only common tests should be described solely by name; describe more complex techniques in the Methods section.
- A description of all covariates tested
- A description of any assumptions or corrections, such as tests of normality and adjustment for multiple comparisons
- A full description of the statistical parameters including central tendency (e.g. means) or other basic estimates (e.g. regression coefficient) AND variation (e.g. standard deviation) or associated estimates of uncertainty (e.g. confidence intervals)
- For null hypothesis testing, the test statistic (e.g. F , t , r) with confidence intervals, effect sizes, degrees of freedom and P value noted
Give P values as exact values whenever suitable.
- For Bayesian analysis, information on the choice of priors and Markov chain Monte Carlo settings
- For hierarchical and complex designs, identification of the appropriate level for tests and full reporting of outcomes
- Estimates of effect sizes (e.g. Cohen's d , Pearson's r), indicating how they were calculated

Our web collection on [statistics for biologists](#) contains articles on many of the points above.

Software and code

Policy information about [availability of computer code](#)

Data collection	Äkta system: UNICORN 7 (Cytiva); X-Ray Data Collection: MxCube3, MxCube2 (https://github.com/mxcube); MicroCal PEAQ-ITC Control Software version 1.2.2 (Malvern); AcquireMP software version 2.4 (Refeyn); SWIFT II version 2.06 (Biochrom Ltd); MassLynx MS version 4.1 (Waters); Benchling (biological Software, 2021, https://benchling.com) was used to design CRISPR guide RNAs. Other software for data collection were part of experimental instruments.
Data analysis	Microsoft Office suite 2019 for Windows; Microsoft Excel (version 2.105) was used to perform Student's t-test on metabolomics data; GraphPad Prism 6 for Windows; LigPlot+ version 2.2 (https://www.ebi.ac.uk/thornton-srv/software/LigPlus/); Pymol version 1.8.2.0 (Schroedinger); Coot versions 0.8.9.2 and 0.9.4.1 (doi:10.1107/S0907444910007493); iMosflm version 7.4 (https://www.mrc-lmb.cam.ac.uk/harry/imosflm/ver740/); REFMAC version 5.0.32 (https://www.ccp4.ac.uk/html/refmac5/); Phenix versions 1.17.1-3660 and 1.19 (https://doi.org/10.1107/S2059798319011471); AIMLESS version 0.7.6; Chimera version 1.13.1, ChimeraX version 1.1, CCP4 suite version 7.1; MicroCal PEAQ-ITC Analysis Software version 1.2.2 (Malvern); DynamX version 3.0 software (Waters); ProteinLynx Global SERVER version 3.0.1 (PLGS, Waters); DiscoverMP software version 2.4 (Refeyn); MAVEN (Metabolomics Analysis and Visualization Engine, version 2011.6.17, http://genomics-pubs.princeton.edu/mzroll/index.php) was used for LC-MS data quantification and analysis; ImageJ (version 1.52a, https://imagej.nih.gov/ij/) was used for analysis of DRaCALA.

For manuscripts utilizing custom algorithms or software that are central to the research but not yet described in published literature, software must be made available to editors and reviewers. We strongly encourage code deposition in a community repository (e.g. GitHub). See the Nature Research [guidelines for submitting code & software](#) for further information.

Data

Policy information about [availability of data](#)

All manuscripts must include a [data availability statement](#). This statement should provide the following information, where applicable:

- Accession codes, unique identifiers, or web links for publicly available datasets
- A list of figures that have associated raw data
- A description of any restrictions on data availability

Structure factors and coordinates of X-ray crystallographic datasets have been deposited at the Protein Data Bank (www.rcsb.org) under the accession codes 7OJ1 and 7OJ2 for the Ap4A-bound BsIMPDPH and BsIMPDPH-ΔCBS, respectively. All other structural data employed in this manuscript (accession codes 3L2B, 3TSB, 4DQW, 4XTI, 4XWU, 5AHL, 5AHM, 5MCP, 6GJV, 6RPU) are publicly available in the Protein Data Bank. Source data are provided with this paper for figures 1, 2, 4, and 5, and for Extended data figures 1, 2, 5, 6, and 8.

Field-specific reporting

Please select the one below that is the best fit for your research. If you are not sure, read the appropriate sections before making your selection.

Life sciences Behavioural & social sciences Ecological, evolutionary & environmental sciences

For a reference copy of the document with all sections, see nature.com/documents/nr-reporting-summary-flat.pdf

Life sciences study design

All studies must disclose on these points even when the disclosure is negative.

Sample size	Biochemical experiments (e.g. enzyme activity, mass photometry) were performed in duplicate with different enzyme preparations thus eliminating any bias from disparate enzyme activities originating from the preparation procedure. Experiments on bacterial strains (e.g. metabolomics) were conducted on biological triplicates. Statistical analyses were performed where possible and appropriate to judge the statistical significance of the data.
Data exclusions	We did not exclude any data from consideration.
Replication	Controls verifying specific enzyme activities between different enzyme preparations were conducted routinely. Biochemical experiments (e.g. enzyme activity, mass photometry) were performed in duplicate with different enzyme preparations. Experiments on bacterial strains (e.g. metabolomics) were performed at least in biological triplicates. The exact number of experiments or repeats is given in the figure legends. All attempts at replicating our results were successful.
Randomization	This is not relevant to the study as we did not perform sampling. Microorganisms used in this study were selected and divided randomly in the different conditions, and no criteria of selection were applied.
Blinding	Blinding was not performed in the study. All collected data relied on quantitative outputs, which as such were not open to any subjective bias in the analysis and/or interpretation of the results.

Reporting for specific materials, systems and methods

We require information from authors about some types of materials, experimental systems and methods used in many studies. Here, indicate whether each material, system or method listed is relevant to your study. If you are not sure if a list item applies to your research, read the appropriate section before selecting a response.

Materials & experimental systems

n/a	Involvement in the study
<input checked="" type="checkbox"/>	<input type="checkbox"/> Antibodies
<input checked="" type="checkbox"/>	<input type="checkbox"/> Eukaryotic cell lines
<input checked="" type="checkbox"/>	<input type="checkbox"/> Palaeontology and archaeology
<input checked="" type="checkbox"/>	<input type="checkbox"/> Animals and other organisms
<input checked="" type="checkbox"/>	<input type="checkbox"/> Human research participants
<input checked="" type="checkbox"/>	<input type="checkbox"/> Clinical data
<input checked="" type="checkbox"/>	<input type="checkbox"/> Dual use research of concern

Methods

n/a	Involvement in the study
<input checked="" type="checkbox"/>	<input type="checkbox"/> ChIP-seq
<input checked="" type="checkbox"/>	<input type="checkbox"/> Flow cytometry
<input checked="" type="checkbox"/>	<input type="checkbox"/> MRI-based neuroimaging

Publication #2

Title: Inhibition of SRP-dependent protein secretion by the bacterial alarmone (p)ppGpp









Authors: Laura Czech, Christopher-Nils Mais, Hanna Kratzat, Pinku Sar-
mah, Pietro Giammarinaro, Sven-Andreas Freibert, Hanna Folke Esser, Jo-
anna Musial, Otto Berninghausen, Wieland Steinchen, Roland Beckmann,
Hans-Georg Koch & Gert Bange.

Journal: Nature Communications

Year: 2022

Contributions: Conceptualization: G.B., L.C.; Investigation: C.N.M.,
H.F.E., H.G.K., H.K., J.M., L.C., O.B., P.G., P.S., W.S.; Visualization:
C.N.M., G.B., H.F.E., H.K., L.C.; Funding acquisition: G.B., H.G.K., R.B.;
Supervision: G.B., L.C., H.G.K., R.B.; Writing: G.B., H.G.K., H.K., L.C.,
R.B.; All authors have read and commented on the manuscript.

Inhibition of SRP-dependent protein secretion by the bacterial alarmone (p)ppGpp

Laura Czech ^{1,8}✉, Christopher-Nils Mais ^{1,8}, Hanna Kratzat ², Pinku Sarmah^{3,4}, Pietro Giammarinaro¹, Sven-Andreas Freibert ^{5,6}, Hanna Folke Esser², Joanna Musial², Otto Berninghausen ², Wieland Steinchen¹, Roland Beckmann ², Hans-Georg Koch ³ & Gert Bange ^{1,7}✉

The stringent response enables bacteria to respond to nutrient limitation and other stress conditions through production of the nucleotide-based second messengers ppGpp and pppGpp, collectively known as (p)ppGpp. Here, we report that (p)ppGpp inhibits the signal recognition particle (SRP)-dependent protein targeting pathway, which is essential for membrane protein biogenesis and protein secretion. More specifically, (p)ppGpp binds to the SRP GTPases Ffh and FtsY, and inhibits the formation of the SRP receptor-targeting complex, which is central for the coordinated binding of the translating ribosome to the SecYEG translocon. Cryo-EM analysis of SRP bound to translating ribosomes suggests that (p)ppGpp may induce a distinct conformational stabilization of the NG domain of Ffh and FtsY in *Bacillus subtilis* but not in *E. coli*.

¹Center for Synthetic Microbiology (SYNMIKRO) and Department of Chemistry Philipps-Universität Marburg, Marburg, Germany. ²Gene Center Munich, Department of Biochemistry, Ludwig-Maximilians-Universität, LMU, Munich, Germany. ³Institute of Biochemistry and Molecular Biology, Faculty of Medicine, Albert-Ludwigs-Universität Freiburg, Freiburg, Germany. ⁴Faculty of Biology, Albert-Ludwigs-Universität Freiburg, Freiburg, Germany. ⁵Institut für Zytobiologie, Philipps-Universität Marburg, Marburg, Germany. ⁶Core Facility “Protein Biochemistry and Spectroscopy”, Philipps-Universität Marburg, Marburg, Germany. ⁷Max-Planck Institute for terrestrial Microbiology, Marburg, Germany. ⁸These authors contributed equally: Laura Czech, Christopher-Nils Mais. ✉email: laura.czech@staff.uni-marburg.de; gert.bange@synmikro.uni-marburg.de

Central to the bacterial response to starvation and stress are the guanosine-based second messengers ppGpp and pppGpp (also: (p)ppGpp or “alarmones”)^{1,2}. Biosynthesis and degradation of (p)ppGpp relies on RelA/SpoT homology (RSH)-type proteins^{3,4}. Most prominent and conserved are the RelA/Rel proteins, which sense amino acid starvation during the stringent response by detecting ribosomes blocked by cognate, uncharged tRNAs at their A-site^{5–9}. The (p)ppGpp synthetase activity of these enzymes is stimulated upon binding to stalled ribosomes by a molecular mechanism conserved in Gram-negative and -positive bacteria^{9–12}. Besides the Rel/RelA enzymes, many bacterial species contain further RSH-enzymes commonly referred to as small alarmone synthetases and hydrolases (summarized in ref. 4).

As the most prominent consequence of elevated alarmone levels, protein biosynthesis is downregulated through direct inhibition of translational GTPases (recently summarized in refs. 2,13). Yet, alarmones effect a wide range of physiological and metabolic processes by their specific interactions with numerous proteins and also RNA targets (recently summarized in refs. 14,15). A recent affinity-based screening approach for (p)ppGpp targets in *Escherichia coli* supported this idea by identifying over 50 potential targets¹⁶. Notably, the bacterial signal recognition particle (SRP) GTPases Ffh and FtsY were also identified in this screen, suggesting that (p)ppGpp may potentially also regulate the essential SRP-dependent pathway of membrane protein insertion. This appears plausible, since in bacteria the biogenesis of a large portion of transmembrane and some secreted proteins relies on the SRP machinery (reviewed in refs. 17–20). However, this idea has never been challenged and thus a mechanistic understanding of how (p)ppGpp could modulate the SRP pathway is not available to date.

SRP is a conserved ribonucleoprotein particle consisting of the GTPase Ffh and the SRP-RNA^{20–22} and its mode of operation is well understood^{23–26}. Briefly, SRP recognizes hydrophobic signal sequences in the context of translating ribosomes, and SRP bound to ribosome-nascent chain complexes (RNCs) in turn interacts in a GTP-dependent manner with its receptor FtsY, also a GTPase, which localizes at the cytoplasmic membrane periphery of bacteria via a membrane-targeting sequence^{27,28}. Consequently, the RNC is transferred onto the SecYEG translocon followed by dissociation of the SRP-FtsY complex after hydrolysis of GTP enabling the initiation of a new round of SRP-mediated protein targeting. Ffh and FtsY are multi-domain proteins, which share the highly homologous NG domain (reviewed in ref. 20). The NG domain consists of a bundle of four α -helices followed by a GTPase (G) domain common to small G proteins, such as Ras^{29,30}. When bound to GTP, the NG domains of Ffh and FtsY form the heterodimeric targeting complex, which regulates the transfer of a RNC to a vacant and membrane-embedded translocon through a series of conformational rearrangements (summarized in ref. 21). Within the targeting complex, both GTPases share a composite active site in which two GTPs reciprocally align, such that the 3'-OH group of the ribose of one GTP interacts with the γ -phosphate of the other, and vice versa^{31–33}. This unique nucleotide arrangement is essential for productive formation of the SRP-FtsY complex³¹, and the reciprocal stimulation of both GTPase activities in the context of the SRP-RNA³⁴, which finally enables productive transfer of the RNC onto the translocon. However, a widely unaddressed question is whether the SRP-mediated protein-targeting pathway is subject to regulation in response to stress conditions, e.g., amino acid starvation.

Here, we show that the alarmones (p)ppGpp specifically bind to the GTPase domains of SRP and its receptor FtsY resulting in an inhibition of targeting complex formation. This in turn restricts the SRP-dependent pathway of membrane protein insertion and secretion during stressful times.

Results

In vitro inhibition of SRP-dependent post-translational membrane protein targeting and insertion by (p)ppGpp. To investigate whether and how the alarmones (p)ppGpp would interfere with the SRP-dependent targeting process, we analyzed the influence of ppGpp and pppGpp on the SRP-dependent insertion of membrane proteins. As a first model, we chose the single-spanning membrane protein YohP from *E. coli*, which was recently shown to be strictly dependent on SRP/FtsY for membrane insertion^{18,35}. A major advantage of using YohP is that SRP acts post-translationally during YohP insertion and thus the (p)ppGpp effect on SRP/FtsY-dependent insertion can be analyzed without impairing the GTP-dependent steps of translation, which are also known targets of (p)ppGpp (recently summarized in refs. 2,14,15).

YohP was in vitro synthesized and ³⁵S-labeled using an *E. coli* coupled transcription/translation system³⁶. Translation was subsequently terminated by the addition of chloramphenicol and ribosomes were removed by ultracentrifugation. In vitro synthesized YohP was then incubated with *E. coli* inverted inner membrane vesicles (INV) and membrane insertion was determined by proteinase K (prot. K) resistance. In the presence of INV, almost 70% of the in vitro synthesized YohP were prot. K resistant, indicating that insertion into the *E. coli* membrane had occurred (Fig. 1a, b). In contrast, basically all YohP was degraded in the absence of INV. When YohP was incubated with INV in the presence of increasing ppGpp or pppGpp levels, a concentration-dependent decrease of YohP insertion was observed for both ppGpp and pppGpp (Fig. 1a, b), with a complete block of insertion at 0.6 mM (p)ppGpp. These data demonstrate that both ppGpp and pppGpp inhibit membrane insertion of the SRP-dependent membrane protein YohP.

The assays described above do not require the addition of purified SRP/FtsY, because sufficient amounts of both proteins are bound to INV³⁶. This, however, makes it difficult to assign the observed inhibition of YohP insertion by (p)ppGpp to impaired SRP/FtsY activity. Therefore, we assayed the effect of (p)ppGpp on YohP insertion in a highly purified assay system, which consisted of reconstituted SecYEG-proteoliposomes, and purified SRP and FtsY. When in vitro synthesized YohP was incubated with liposomes or SecYEG-proteoliposomes without adding SRP/FtsY, no significant prot. K resistance was observed (Fig. 1c, d). However, in the presence of SRP/FtsY and SecYEG-proteoliposomes about 70% of the in vitro synthesized YohP was resistant against prot. K treatment, indicative for membrane insertion (Fig. 1c, d). No prot. K protection of YohP was observed when SRP/FtsY were added to liposomes or in the presence of just SRP/FtsY (Supplementary Fig. 1). Adding ppGpp or pppGpp together with SRP/FtsY reduced YohP insertion into SecYEG proteoliposomes drastically, further validating that ppGpp and pppGpp inhibit SRP and FtsY and thus block YohP insertion. The (p)ppGpp concentrations required for inhibiting YohP insertion into SecYEG-proteoliposomes were much lower than the concentrations required for inhibition in the INV system (Fig. 1c, d). This likely reflects the fact that in addition to SRP and FtsY, additional GTP-binding proteins are present in INV, which may also bind (p)ppGpp. Taken together, these experiments clearly show that (p)ppGpp efficiently inhibits the SRP-dependent membrane insertion of membrane proteins via the SecYEG translocon.

In vitro inhibition of SRP-dependent co-translational membrane protein targeting and insertion by (p)ppGpp. Since SRP-dependent targeting of YohP occurs post-translationally and thus deviates from the canonical co-translational SRP-dependent targeting, we also tested the influence of (p)ppGpp on co-translational

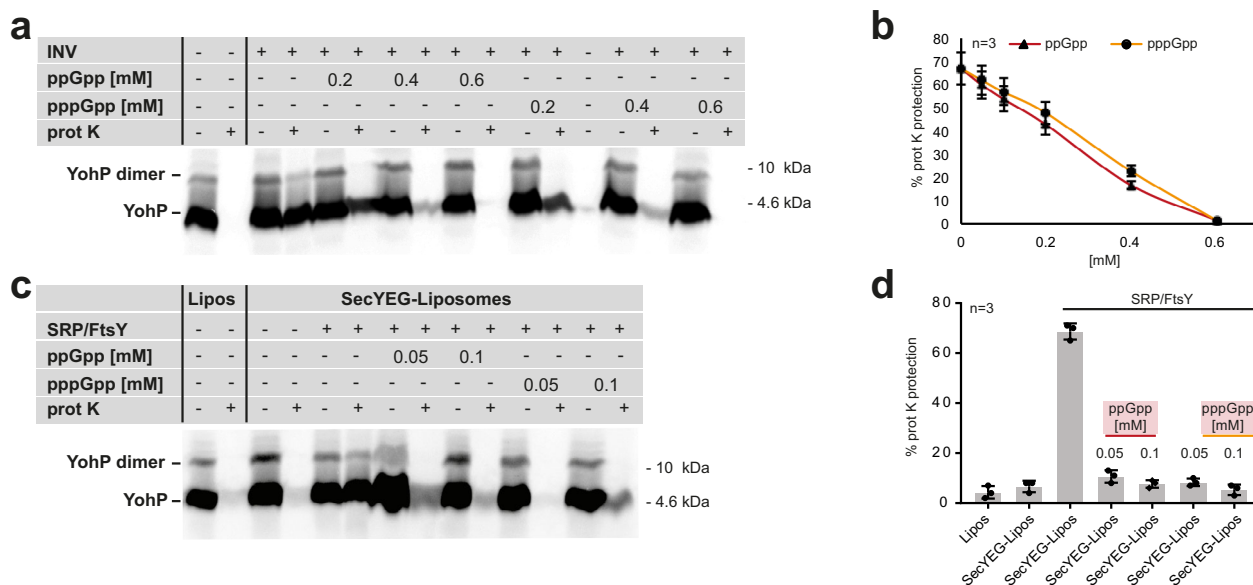


Fig. 1 Post-translational targeting of SRP substrate YohP is inhibited by (p)ppGpp. **a** YohP was in vitro synthesized using a purified coupled transcription/translation system (CTF system) and translation was terminated by the addition of chloramphenicol (35 mg mL⁻¹). Samples were then centrifuged for removing ribosomes and aggregates and the supernatant was incubated with INV (inner membrane vesicles) or INV-buffer for 10 min in the presence of 10 μM GTP. Where indicated, ppGpp or pppGpp were added together with INV. Subsequently, one half of the sample was directly TCA precipitated, while the other half was first treated with proteinase K (prot K) before TCA precipitation. Samples were then separated by SDS-PAGE and analyzed by autoradiography. **b** Quantification of three independent experiments as described in **a** and the mean values (±SD) are shown. **c** As in **a**, but insertion was analyzed in the presence of liposomes of reconstituted SecYEG-proteoliposomes. Liposomes were generated from *E. coli* phospholipids and contained 70% PE, 25% PG and 5% CL, and proteoliposomes contained 100 ng μL⁻¹ SecYEG complex. When indicated, insertion was performed in the presence of absence of purified SRP/FtsY (20 ng μL⁻¹, each) and at the indicated (p)ppGpp concentrations. Uncropped images are shown in the Supplementary Material (Supplementary Fig. 2). Samples were further processed as described in **a**. **d** Quantification of three independent experiments as described in **c** and the mean values (±SD) are shown.

membrane targeting of LepB- and FtsQ-RNCs, which are classical SRP substrates^{18,37,38}. LepB- and FtsQ-RNCs were in vitro synthesized and incubated with INV or SecYEG-proteoliposomes in the presence or absence of SRP/FtsY and (p)ppGpp. Efficient membrane targeting of these RNCs was then analyzed by floatation analyses, which separates membrane-bound RNCs from non-bound RNCs³⁹. In the presence of INV, both RNCs were almost exclusively found in the membrane fraction (MF) but remained in the soluble fraction in the absence of INV or in the presence of liposomes (Fig. 2a, b). When membrane binding of LepB- and FtsQ-RNCs to SecYEG-proteoliposomes was analyzed, both RNCs were found in the membrane fraction when purified SRP and FtsY were present but were recovered from the soluble fraction in their absence (Fig. 2a, b). This demonstrates that the assay reliably reports co-translational targeting of RNCs to the SecYEG-translocon by SRP and its receptor FtsY. Importantly, the addition of either ppGpp or pppGpp completely blocked membrane targeting of LepB- and FtsQ-RNCs (Fig. 2a, b). Quantification of several ($n \geq 3$) independent experiments confirmed the inhibitory effect of (p)ppGpp on SRP-dependent targeting of RNCs to the SecYEG-translocon (Fig. 2c). In summary, these data demonstrate that (p)ppGpp inhibit also co-translational membrane targeting by the SRP pathway.

(p)ppGpp reduces GTPase activities of SRP and its receptor. SRP/FtsY complex formation followed by the subsequent GTPase activities of Ffh and FtsY is required for the successful delivery of target proteins to the SecYEG translocon^{18,35}. Therefore, we tested whether GTP hydrolysis would be impaired in the presence of (p)ppGpp. Hence, full-length (*Ec*)Ffh and the NG domain of

(*Ec*)FtsY (Fig. 3a) were tested for their GTP hydrolysis activity in the presence of 4.5S RNA (i.e., the SRP-RNA), the well characterized ΔEspP signal peptide and the signal peptide mimicking detergent C₁₂E₈ (nonionic detergent octaethyleneglycol dodecylether), which all have been shown to stimulate the GTPase activity of the targeting complex (Fig. 3b)⁴⁰. The assays were conducted using 1 mM GTP and increasing amounts of ppGpp (Fig. 3c) and pppGpp (Fig. 3d) ranging from 0 to 10 mM. While the GTPase activities of full-length (*Ec*)Ffh and (*Ec*)FtsY-NG alone were very low, GTP hydrolysis was stimulated when both proteins were present (Fig. 3c, d)⁴¹. The GTPase activities were further stimulated in the presence of 4.5S RNA^{41,42}, and through the addition of the ΔEspP signal peptide or the signal peptide mimic C₁₂E₈ (Fig. 3c, d)⁴⁰. In each of the tested conditions, addition of (p)ppGpp resulted in a reduction of GTP hydrolysis when the alarmones were supplemented at concentrations equimolar to the GTP substrate (1 mM) or higher consistent with a competitive mode of inhibition, whereby ppGpp appeared to be a slightly more potent inhibitor than pppGpp (Fig. 3c, d). Taken together, our data show that the alarmones (p)ppGpp inhibit the GTPase activity observed when SRP and its receptor are present, irrespective of the presence or absence of the SRP-RNA, the signal peptide or its mimicry. It is well established that (p)ppGpp levels rise approximately three times above the GTP levels under stringent conditions in the model organisms *E. coli*^{43–45} and *B. subtilis*^{46–48}, further supporting the physiological relevance of the (p)ppGpp action on the SRP machinery.

Binding of (p)ppGpp to the NG domains of Ffh and its receptor FtsY. Our data suggested that (p)ppGpp directly interferes with the

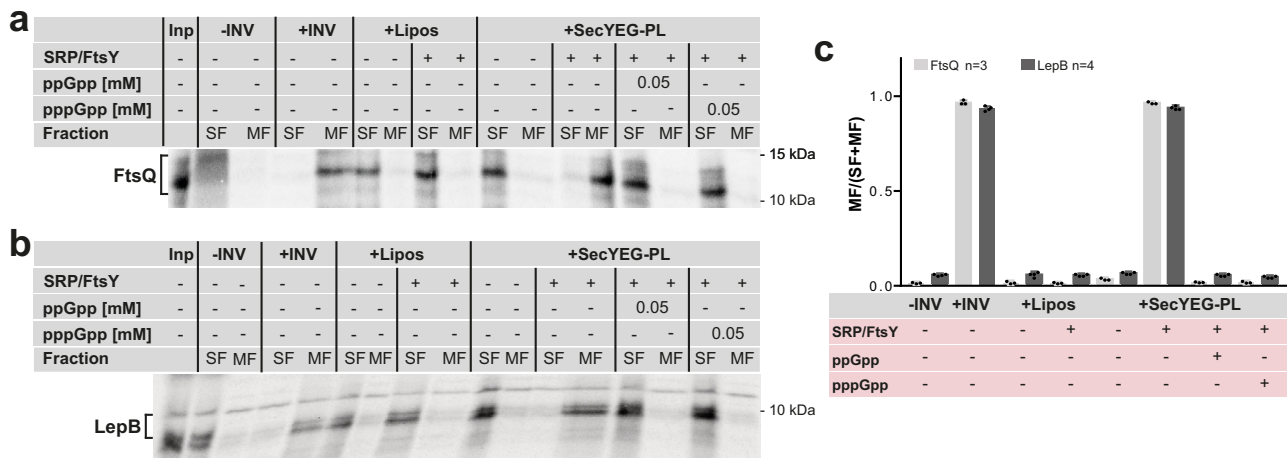


Fig. 2 Co-translational membrane targeting of ribosome-nascent chains (RNCs) is inhibited by (p)ppGpp. a and b RNCs of the SRP substrates FtsQ (**a**) or LepB (**b**) were in vitro synthesized (input, Inp) and incubated with INV (inner membrane vesicles) or reconstituted SecYEG proteoliposomes (SecYEG-PL; 100 ng SecYEG μL^{-1}). INV buffer and liposomes (lipos) served as a control. When indicated, purified SRP and FtsY (20 ng μL^{-1} each) and ppGpp or pppGpp (50 μM final concentration) were present during incubation. Samples were then subjected to floatation gradient centrifugation and the membrane fraction (MF) and soluble fraction (SF) were separated and analyzed by SDS-PAGE and autoradiography. Uncropped images are shown in the Supplementary Material (Supplementary Fig. 2) **c** Quantification of membrane targeting of FtsQ-RNCs ($n=3$, biologically independent experiments) and LepB-RNCs ($n=4$, biologically independent experiments) in the presence of (p)ppGpp. Radioactively labeled bands in the MF and SF were quantified using the *ImageQuant* software and are displayed as MF/(SF + MF). Error bars indicate the SEM values, which were determined using GraphPad Prism.

GTPases of SRP and its receptor FtsY (Fig. 3a–d). To understand the action of (p)ppGpp on Ffh and FtsY GTPases further mechanistically, we next employed the GTPase-containing NG domains of *E. coli* (*Ec*) Ffh and FtsY (Ffh-NG and FtsY-NG, respectively; Fig. 3a) and probed their binding affinity for ppGpp and pppGpp by isothermal titration calorimetry (ITC). Determination of the dissociation constants (K_D) of (*Ec*)Ffh-NG revealed an affinity of $7.9 \pm 1.9 \mu\text{M}$ for ppGpp-binding while its counterpart GDP exhibited an affinity of $2.2 \pm 0.6 \mu\text{M}$ (Fig. 3e; Supplementary Figs. 3 and 4). For the NG domain of the SRP-receptor (*Ec*)FtsY a K_D of $21.7 \pm 5.4 \mu\text{M}$ for ppGpp and $9.8 \pm 1.1 \mu\text{M}$ for GDP were obtained (Fig. 3e and Supplementary Figs. 3 and 4). These K_D values show that ppGpp exhibits similar binding affinities as its GDP counterpart for the SRP-GTPases Ffh and FtsY.

Next, we wanted to probe the affinities of the Ffh and FtsY-NG-domains for GTP and its counterpart pppGpp. Determination of K_D by ITC of (*Ec*)Ffh-NG revealed an affinity of $13.9 \pm 7.1 \mu\text{M}$ for pppGpp-binding while its counterpart GTP exhibited an affinity of $0.7 \pm 0.5 \mu\text{M}$ (Fig. 3e; Supplementary Figs. 3 and 4). For the (*Ec*)FtsY-NG, we were unable to determine a reliable K_D -value by ITC, because of protein aggregation in the presence of either of the two nucleotides during the ITC runs. It might be that the exposure of FtsY-NG to either GTP or pppGpp leads to an expelling of the amphipathic membrane-targeting sequence (MTS)^{27,28}, thus causing the observed aggregation under the relatively high protein concentrations (i.e., 50 μM) used for the ITC experiments. Thus, we decided to recapitulate the K_D 's of (*Ec*)Ffh-NG and (*Ec*)FtsY-NG for ppGpp and pppGpp by microscale thermophoresis (MST), which requires much less protein concentration. Our MST experiments show that the alarmones pppGpp and ppGpp bind with similar K_D 's as their GTP and GDP counterparts, respectively, to either (*Ec*)Ffh-NG and (*Ec*)FtsY-NG (Fig. 3e and Supplementary Fig. 4). We would like to note that the K_D -values for GTP and pppGpp measured by MST are somewhat higher than those obtainable by ITC (Fig. 3e) and other methods (e.g., refs. 41,49). The reason for this observation is likely due to required labeling of the analyzed proteins with the fluorescent dye at lysine residues, which might weaken the binding of nucleotides. Despite of this, (*Ec*)Ffh-NG

and (*Ec*)FtsY-NG show similar K_D -values for GTP and pppGpp when measured by MST (Fig. 3e; Supplementary Figs. 3 and 4). This strongly suggests that pppGpp exhibits similar binding affinities as its GTP counterpart for the SRP-GTPases Ffh and FtsY. Overall, these observations indicate that the alarmones can act as competitive inhibitors of GDP/GTP by occupying the same binding sites in FtsY and Ffh. Our data might also suggest that SRP-GTPases slightly favor the binding of ppGpp over pppGpp.

Disruption of Ffh-FtsY complex formation in the presence of (p)ppGpp.

If (p)ppGpp can indeed act as a competitive inhibitor of the GTPases SRP/FtsY, we asked whether they would directly interfere with the strictly GTP-dependent formation of the SRP/FtsY-targeting complex (Fig. 3f). Thus, we incubated equal amounts of (*Ec*)Ffh-NG and (*Ec*)FtsY-NG in the presence of the non-hydrolysable GTP analog guanosine-5'-[(β,γ) -imido]triphosphate (GMPPNP), which enabled trapping of the *E. coli* Ffh/FtsY heterodimer stabilized by two GTP-mimicking GMPPNP molecules, followed by quantitative analysis of the complex formation by SEC (Fig. 3f, g). We next analyzed to which extent the presence of either ppGpp or pppGpp affects GMPPNP-dependent Ffh/FtsY complex formation (Fig. 3g–i). Thus, we added increasing amounts of each of the two alarmones and analyzed the complex formation in the presence of either 0.25, 0.5 or 1 mM GMPPNP. These experiments show that complex formation was half-inhibited at equal (p)ppGpp/GMPPNP ratios and roughly abolished when the (p)ppGpp concentrations exceeded those of GMPPNP by two-fold (Fig. 3h, i for ppGpp and pppGpp, respectively). These data further consolidate the idea that (p)ppGpp acts as competitive inhibitor of GTP, because formation of the Ffh/FtsY-targeting complex requires two GTP (or GMPPNP) molecules.

Crystallographic analysis of alarmone binding. To gain a molecular understanding of the (p)ppGpp inhibition of the GTP-dependent SRP/FtsY-targeting complex formation, we decided to structurally analyze the (p)ppGpp-bound states of Ffh and FtsY. We determined the crystal structures of the pppGpp-bound NG

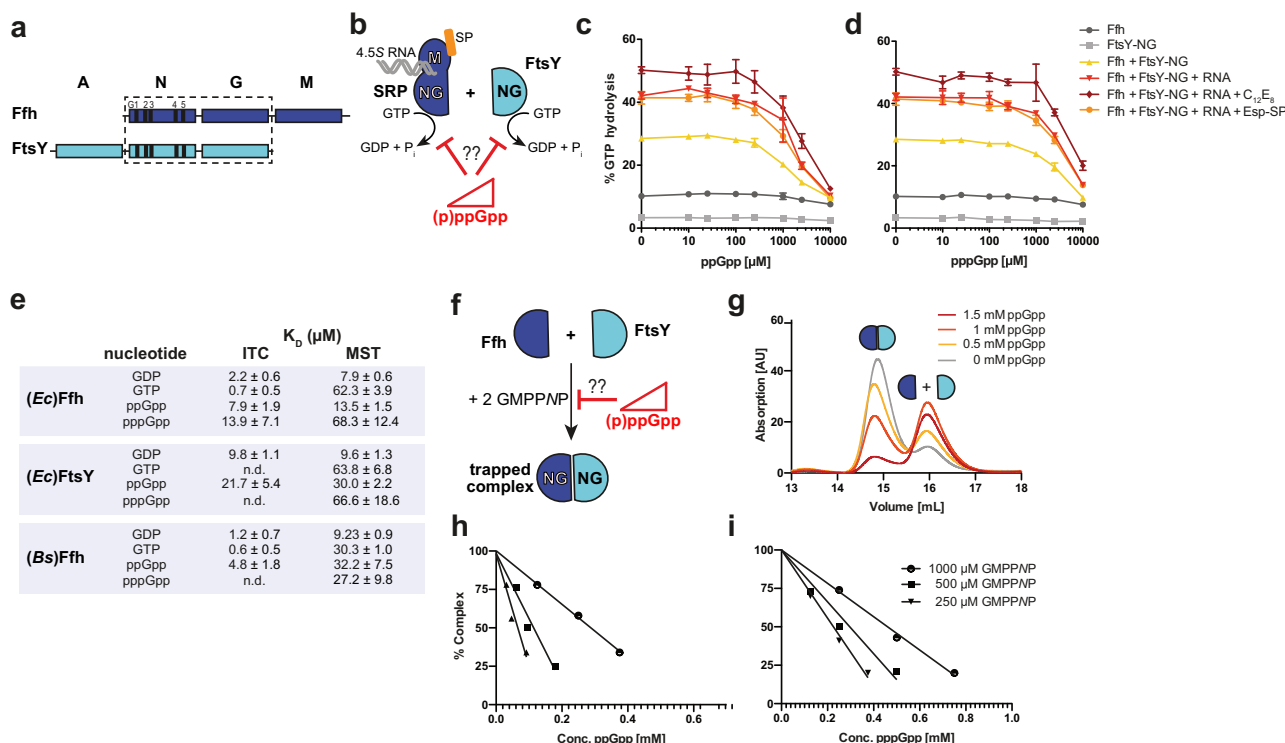


Fig. 3 (p)ppGpp reduces GTPase activity and complex formation of SRP and FtsY. **a** Domain architecture of the bacterial SRP-GTPases Ffh (blue) and FtsY (cyan), both sharing the conserved GTPase-containing NG domain. The G-elements G1-G5 as well as the A and M domains specific to FtsY and Ffh, respectively, are shown. **b** Scheme of the experimental setup for analyzing the impact of increasing concentrations of (p)ppGpp on the GTPase activities of SRP and FtsY. Orange sphere depicts the signal peptide (SP), and gray strands the SRP RNA. **c** and **d** GTPase activity of full-length Ffh and FtsY-NG was assayed in the presence of increasing amounts of the competitors ppGpp (**c**) and pppGpp (**d**). Where indicated, 5 μM (Ec)FtsY-NG, 6 μM of 4.5S RNA, 5 μM Esp-signal peptide and 100 μM C₁₂E₈ (signal peptide mimic) were added to the reaction including 5 μM full-length (Ec)Ffh and 1 mM GTP. The data represent mean values (\pm SD) of $n = 3$ replicates. **e** The table lists the K_D values obtained for the binding of GDP, GTP, ppGpp and pppGpp to (Ec)Ffh, (Ec)FtsY- and (Bs)Ffh-NG domains determined either by isothermal titration calorimetry (ITC) or microscale thermophoresis (MST). **f** Scheme of the experimental setup for analyzing the impact of increasing concentrations of (p)ppGpp on the GTP-dependent formation of the Ffh/FtsY-NG domain complex. **g** Analytical size-exclusion chromatography (SEC) monitoring the complex formation and dissociation of Ffh-NG and FtsY-NG (100 μM each) incubated with 1 mM GMPPNP and in the absence or presence of increasing ppGpp concentrations (0, 0.5, 1, and 1.5 mM). **h** and **i** Percentage of formed Ffh-NG/FtsY-NG complexes (50 μM each) in the presence of different GMPPNP concentrations (250, 500, and 1,000 μM) analyzed in the presence of increasing ppGpp (**h**) and pppGpp (**i**) concentrations, respectively.

domains of (Ec)Ffh and (Ec)FtsY at resolutions of 2.5 and 2.4 Å, respectively (Fig. 4a–d; Supplementary Fig. 5 and Supplementary Table 1), as well as the crystal structures of (Bs)Ffh and (Ec)Ffh in complex with ppGpp and Mg²⁺ at resolutions of 2.5 and 2.8 Å, respectively (Supplementary Table 1; Supplementary Figs. 5 and 6). Each of the alarmones could be unambiguously identified by and placed into the available densities (Supplementary Fig. 5). The ppGpp or pppGpp molecules are bound to the G domains of Ffh and FtsY and occupy the canonical guanosine nucleotide-binding site (Fig. 4a–d and Supplementary Fig. 6). In detail, the guanine moiety of (p)ppGpp is recognized by the well-described aspartate of the G4 element responsible for the discrimination of guanosine nucleotides by P-loop type GTPases (Fig. 4b, d and Supplementary Fig. 6b, d). The α -, β -, and γ -phosphates of (p)ppGpp are coordinated by the G1-element (P-loop), and by residues originating from the switch I and II regions including the G2 and G3 elements, respectively. The δ - and ϵ -phosphate, which are covalently bound to the 3'-OH group of the ribose moiety and discriminate (p)ppGpp from its GDP/GTP counterparts, point away from the active sites of both GTPases (Fig. 4b, d). Both phosphates are not coordinated or form any obvious contacts to the GTPases of Ffh and FtsY (Fig. 4b, d). The missing coordination leads to a high flexibility of the δ - and ϵ -phosphate, as observed in the crystals of (Ec)Ffh with

pppGpp (Supplementary Fig. 5e, f). We conclude that ppGpp and pppGpp interact with the SRP-GTPases Ffh and FtsY in the same way as its counterparts GDP and GTP, respectively, also providing the structural explanation for their comparable K_D values (see above; Fig. 3e).

Previous structural analysis showed that the essential targeting complex forms through a strictly GTP-dependent, pseudo-symmetric heterodimer of the NG domains of Ffh and FtsY (Fig. 4e)^{31,32,50,51}. In this complex, the G domains of Ffh and FtsY form a shared catalytic center into which each GTPase provides one GTP molecule (Fig. 4f). These two GTP molecules reciprocally interact with each other in a way that the 3'-OH group of the ribose moiety of one GTP interacts with the γ -phosphate moiety of the other, and vice versa (Fig. 4f). The tight and reciprocal arrangement of both GTPs via their 3'-OH groups is essential for complex association, reciprocal GTPase activation and catalysis³¹. Our structural analysis of (p)ppGpp-bound Ffh or FtsY now shows that this reciprocal nucleotide arrangement is no longer possible, when the δ -, ϵ -pyrophosphate moieties at the 3'-OH group of the alarmones prevent the formation of the crucial hydrogen bond, and by introducing electrostatic repulsion by the negatively charged phosphates (Fig. 4g). This structural view explains our biochemical observation that (p)ppGpp efficiently hinders formation of the Ffh/FtsY complex, and all subsequently

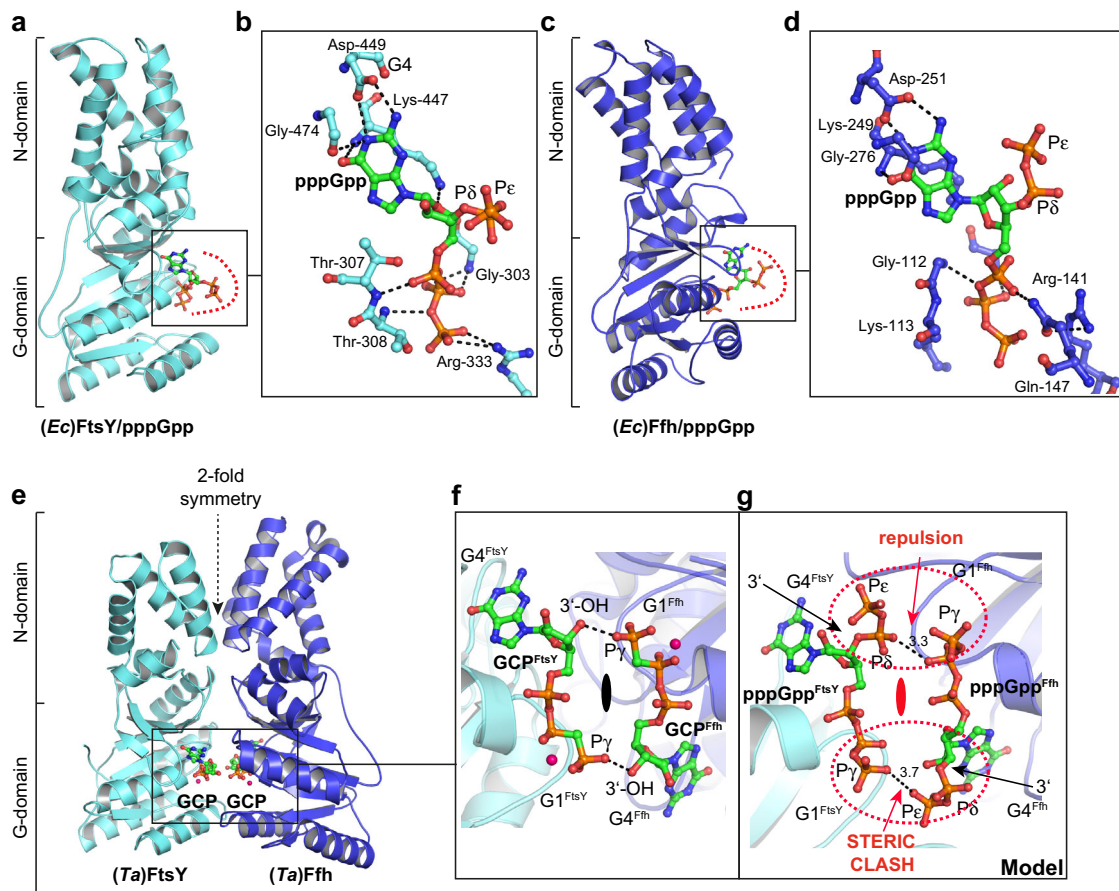


Fig. 4 (p)ppGpp binds in the nucleotide-binding pocket of the Ffh and FtsY-NG domains. **a** Overall topology of (Ec)FtsY-NG in complex with pppGpp. **b** Zoom into the active site of (Ec)FtsY-NG bound to pppGpp highlighting the residues involved in ligand binding. **c** Overall topology of (Ec)Ffh-NG in complex with pppGpp. **d** Detailed view of the active site and the residues involved in binding of pppGpp. **e** Overall topology of the Ffh/FtsY-NG domain heterodimer from *Thermus aquaticus* (Ta) bound to two GCP (GppCp, a non-hydrolysable GTP-analog) molecules mimicking the binding of GTP in the twinned nucleotide-binding site (PDB-ID: 1OKK)³². **f** Zoom into the nucleotide-binding pocket shared between the NG domains of Ffh and FtsY. The 3'-OH of one GCP molecule interacts with the γ -phosphate of the opposing GCP molecule and vice versa. **g** Overlay of the Ffh/FtsY heterodimer with the pppGpp-bound structures of (Ec)Ffh and (Ec)FtsY (this study). Close up of the shared nucleotide-binding site shows that the δ - and ϵ -phosphates at the 3'-OH position of the ribose moiety of (p)ppGpp will lead to charge repulsion, where the hydrogen bond is formed in the heterodimer. Reciprocal arrangement of the two GTP nucleotides in the shared catalytic side of the Ffh/FtsY heterodimer would thereby be prevented.

associated steps such as the reciprocal stimulation of Ffh and FtsY GTPase activity during interaction with the SecYEG complex.

pppGpp affects the conformational flexibility of SRP-bound to RNCs in the Gram-positive model organism *B. subtilis*. So far, we could show that (p)ppGpp hinders SRP-mediated protein targeting at the level of the GTP-dependent SRP-FtsY-targeting complex formation. However, this does not exclude that pppGpp may already affect the RNC-bound SRP through its binding to the Ffh-NG domain. The (*Bs*)Ffh-NG domain also bound ppGpp and pppGpp with similar affinities as their GDP and GTP counterparts, respectively (Fig. 3e; Supplementary Figs. 3 and 4). Next, we analyzed SRP bound to (*Bs*)MifM-stalled RNCs, and (*Ec*)TnaC-stalled RNCs bearing the FtsQ transmembrane segment (TM) in the NC in the presence of either pppGpp or GMPPNP by cryo-EM. Using a *B. subtilis* cell-free system we translated the MifM-stalling mRNA, which contains the MifM leader peptide with shortened C-terminus, a defined ribosome stalling site, the MifM N-terminal TM and a cleavable His-tag⁵². Stalled RNCs were isolated via affinity purification and sucrose density gradient centrifugation. Subsequently, the RNCs were reconstituted with recombinant (*Bs*)SRP (Ffh and 6S RNA), in the presence of either pppGpp or GMPPNP. Cryo-EM analysis revealed stalled 70S

ribosomes with a P-site tRNA and a nascent chain in the peptide exit tunnel as observed before⁵². The GMPPNP and pppGpp datasets contained stably bound SRP in 24% and 38% of the particles, respectively (Supplementary Fig. 7 and Supplementary Table 2), which overall resembled the previously observed RNC-SRP complex⁵³. However, in the previously observed (*Bs*)RNC-SRP reconstruction in the absence of nucleotides⁵³, but also in the new RNC-SRP-GMPPNP reconstructions (*this study*, Supplementary Fig. 7), the Ffh-NG domain of SRP was largely delocalized. In contrast, the pppGpp dataset revealed the Ffh-NG domain in a stable conformation for the majority (57%) of the SRP-containing particles (Supplementary Fig. 7). This final class was then refined to an average resolution of 3.3 Å with local resolution ranging from below 3.0 Å in the ribosomal core to 8–10 Å for SRP and the periphery of the ribosome (Fig. 5a, b and Supplementary Fig. 8a, b). Structural analysis of the SRP M domain showed an open conformation (Fig. 5c) with a rod-like density representing the signal sequence bound in a position very similar to previously observed structures^{53–57}. The M domain contacted the 23S rRNA H24 via helix3 (Arg-399) and helix4 (Asn-414, Gln-411) and is additionally positioned by multiple interactions with the 6S RNA, which in turn interacts with H100 of the 23S rRNA (Fig. 5c).

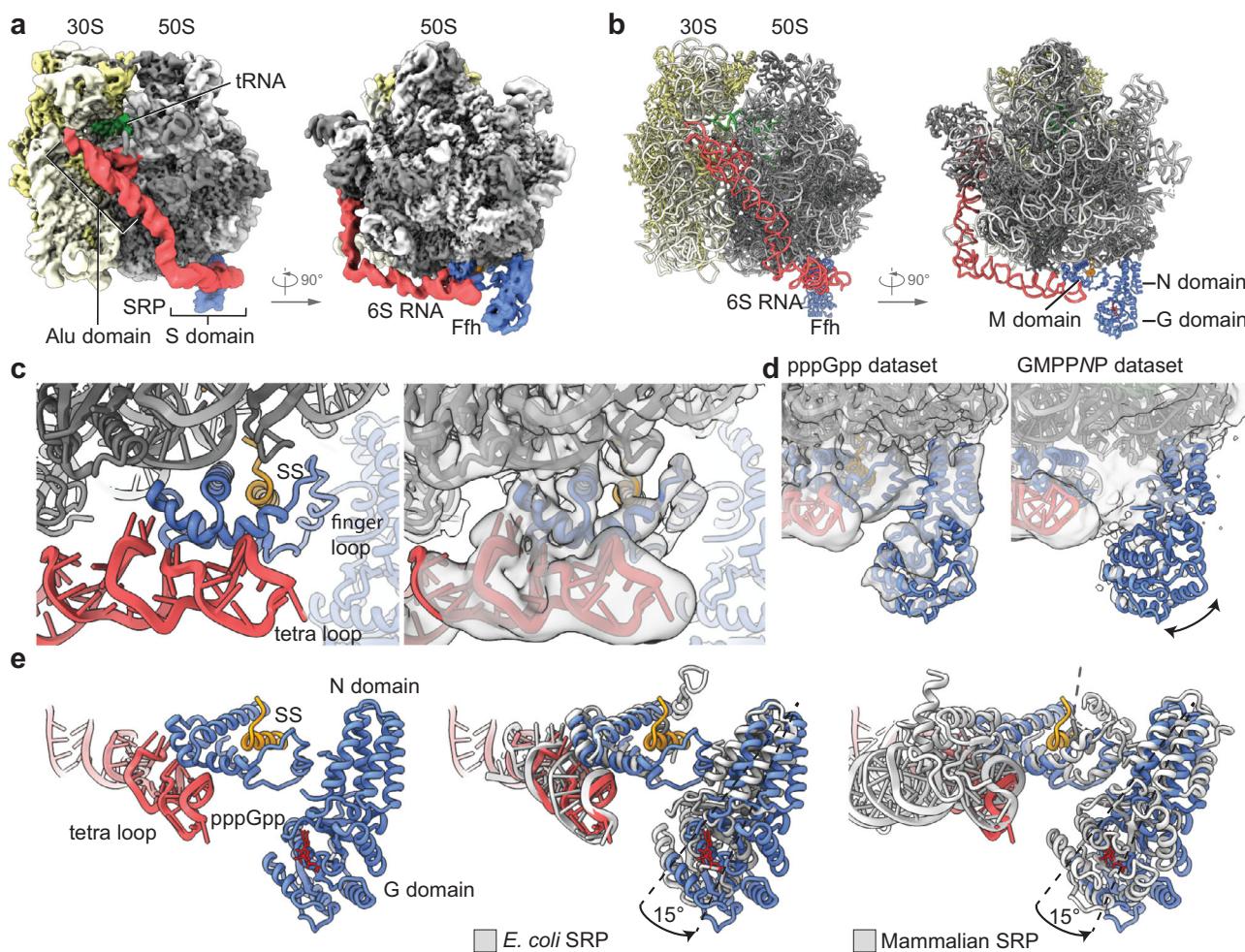


Fig. 5 Cryo-EM structures of SRP-RNC complexes. **a** pppGpp dataset cryo-EM map of (*Bs*)SRP-bound MifM-stalled RNCs filtered at local resolution, small 30S subunit in yellow and large 50S subunit in gray, SRP 6S RNA in red and Ffh in blue. SRP consists of two functional domains: the signal sequence recognition domain (S domain) and the translational elongation arrest domain (Alu domain). The S domain of the SRP is homologous to the domains II–IV of the eukaryotic 7S RNA and carries the Ffh subunit whereas the Alu domain resembles the domain I of the 7S RNA and binds to the GTPase center of the ribosome²¹. **b** Molecular model of (*Bs*)SRP-bound MifM-stalled RNCs. **c** Zoomed view of the Ffh-M domain with signal sequence (SS) bound and transparent cryo-EM density in gray (right). **d** Comparison of Ffh-NG domain cryo-EM density for the pppGpp and GMPPNP dataset. **e** Zoomed view of the S domain of SRP and position of nucleotide-binding site in the Ffh-NG domain (left); comparison with previously found positions of the NG domain in bacteria (PDB 5GAF, *E. coli*) and eukaryotes (PDB 3JAJ, *Oryctolagus cuniculus*) (right). Structures are aligned on the large ribosomal subunit.

In the GMPPNP dataset, a final SRP-containing class was refined to an average resolution of 3.0 Å (Supplementary Fig. 8c, d). Here, no distinct conformational sub-states could be resolved for the Ffh-NG domain and all attempts to sub-classify the data with a mask around the S domain did not reveal any distinct NG domain density (Supplementary Fig. 7). These observations were similar as before for the (*Bs*)RNC-SRP apo complex in the absence of any nucleotides⁵³. In both structures, the apo and the GMPPNP-bound one, flexibility of the NG domain coincided with a higher degree of flexibility also of the Ffh-M domain, which in contrast to the pppGpp structure lacked clear density for the signal sequence (SS), the flexible finger loop and the GM linker connecting M and NG domains. Taken together, the presence of pppGpp results in a stabilization of the NG domain conformation of Ffh on the *B. subtilis* RNC after signal sequence recognition, which might already provide a steric problem for the initial phase of heterodimer formation (Fig. 5d).

pppGpp seems not to affect the conformational flexibility of SRP-bound to RNCs in the Gram-negative model organism *E. coli*. In contrast to the Gram-positive bacterium *B. subtilis*, the

Gram-negative model bacterium *E. coli* contains an SRP with an approximately 200 bases shorter SRP-RNA, while the Ffh protein is highly conserved between both model organisms. Thus, we also investigated whether pppGpp would induce a similar stabilization of the Ffh-NG domain with *E. coli* RNCs as we observed for the *B. subtilis* system (see previous chapter). *E. coli* RNCs were prepared by in vivo translation using a construct containing a N-terminal cleavable His-tag, the FtsQ-TM and the TnaC-stalling sequence^{58,59}. As for the *B. subtilis* samples, the RNCs were isolated via affinity purification, sucrose density gradient centrifugation, and reconstituted with recombinant (*Ec*)SRP (Ffh and 4.5S RNA) in the presence of either pppGpp or GMPPNP. Cryo-EM analysis revealed stalled 70S ribosomes with a P-site tRNA and a nascent chain in the peptide exit tunnel. Both datasets were classified for the presence of SRP and NG domain. However, no difference in the conformation of the NG domain between the pppGpp and GMPPNP treated samples could be observed (Supplementary Fig. 9). As a second approach to facilitate an unbiased comparison, the GMPPNP and pppGpp datasets were combined and sorted for the presence of SRP together

(Supplementary Fig. 10). After this joined classification, SRP-containing particles (Supplementary Fig. 10 and Supplementary Table 3) were segregated again into the GMPPNP and pppGpp datasets, and refined to an average resolution of 3.2 and 3.1 Å, respectively. Local resolution for SRP ranges between 5 and 12 Å with the lowest resolution in the NG domain region indicating flexibility (Supplementary Fig. 11). Also, by using this strategy and in contrast to the *B. subtilis* system, no significant difference in the overall SRP binding as well as in the somewhat flexible NG domain position could be observed. Overall, both structures and the position of the NG domain were in agreement with previously observed *E. coli* SRP-bound ribosome cryo-EM structures⁵⁴. Thus, it appears that pppGpp does not affect the conformation of the SRP bound to RNCs in *E. coli*.

In *B. subtilis*, the presence of pppGpp results in stabilization of the Ffh-NG domain conformation on the RNC after signal sequence recognition, which might already provide a steric problem for the initial phase of heterodimer formation (Fig. 5d). In contrast to (Bs)SRP, the NG domains of Ffh or SRP54 in RNC-bound *E. coli* or mammalian SRP, respectively, display a less flexible binding to the ribosome independent of nucleotides. While the (Bs)SRP N domain contacted the ribosomal protein uL29 through NG loops 1 and 2 similar to *E. coli* and mammalian SRP^{54–57}, the position of the G domain has changed by ~13 Å as a result of a rotation of the entire NG domain by about 15 degrees (Fig. 5e). Yet, comparison of the position of (Bs)SRP with these structures showed a different binding mode, in case of the pppGpp-bound state (Bs)SRP rotated away from the 6S RNA tetra-loop and the Ffh-M domain (Fig. 5e).

Discussion

Adaptation to stress conditions requires adjustable regulatory networks and signaling mechanisms that enable bacterial cells to survive threatening nutrient limitations and other environmental extremes. In this study, we shed light on an additional regulatory role of the stress signaling alarmone (p)ppGpp. We link the bacterial stress and starvation triggered (p)ppGpp response to the negative regulation of the SRP machinery required for the insertion into and the secretion of proteins across the cytoplasmic membrane. Our study unravels the molecular mechanism by which the alarmone (p)ppGpp can restrict the insertion of membrane proteins through the SRP-mediated co- and post-translational-targeting pathways (Fig. 6).

Mechanism of (p)ppGpp-dependent inhibition of the SRP-system. The alarmones ppGpp and pppGpp bind to the GTPases of Ffh and FtsY with binding affinities in the low μM range, closely reflecting the affinities of their counterparts GDP and GTP, respectively (Fig. 3e; Supplementary Figs. 3 and 4). Consequently, both alarmones can act as competitive inhibitors of GDP and especially GTP, which is critically required to enable interaction of SRP with its receptor. Both interact via their NG domains, which form a composite active site in which two GTP molecules reciprocally align, such that the 3'-OH group of one GTP interacts with the γ -phosphate of the other, and vice versa^{31–33}. However, when either Ffh or FtsY or both are bound to (p)ppGpp, this reciprocal arrangement of the two GTPs within the Ffh-FtsY heterodimer is no longer possible. The δ -, ϵ -pyrophosphate moieties at the 3'-OH groups of ppGpp and pppGpp prevent the formation of this crucial nucleotide arrangement³¹, and additionally introduce an electrostatic repulsion through the negatively charged phosphates (Fig. 4g). Consequently, SRP-receptor formation and the subsequent stimulation of both GTPases are impaired, as shown in this study.

We also investigated whether the pppGpp would already impact SRP at a RNC presenting a signal sequence, prior to the interaction

of SRP with the receptor. We analyzed the SRP particles of *B. subtilis* and *E. coli*, both of which strongly differ in the length of the SRP RNA, in the context of their cognate RNCs. To our surprise, we found that in *B. subtilis*—but not in *E. coli*—SRP is stabilized by pppGpp on the RNC in an unusual and rather rigid conformation with the NG domain more distant from the SRP RNA compared to other RNC-SRP complexes. This restricted mobility suggests that in *B. subtilis* pppGpp may already inhibit the earliest step in the targeting process that immediately follows recognition of the signal sequence. During this step, facilitated by the conserved tetra-loop of the SRP RNA, FtsY would usually engage in the first SRP-NG domain interaction to initiate productive heterodimer formation. The restricted mobility of the pppGpp-bound NG domain of SRP could possibly prevent this productive early interaction with FtsY, thereby potentially adding a second layer of inhibition of the secretory pathway. However, these observations require further investigation. Moreover, we did not observe a similar pppGpp-dependent stabilization of the RNC-bound SRP in the *E. coli* model system. While we cannot explain the structural differences between *B. subtilis* and *E. coli* due to limited local resolution of our reconstructions, this potential extra layer of inhibition might not exist in *E. coli*. Why that is so requires further clarification.

Physiological considerations. Intracellular (p)ppGpp concentrations can raise from low basal levels (appr. 10–40 μM) during logarithmic growth^{43,44} up to 800 μM when cells enter stationary phase⁶⁰. Moreover, in circumstances of acute amino acid starvation intracellular alarmone levels peak at appr. 1 mM^{43,47,61,62}. Hence, different targets (with varying affinities) are regulated over a gradient of (p)ppGpp concentrations during the growth of a bacterial population, while very high concentrations of (p)ppGpp (appr. 1 mM) result in growth arrest^{63–65}. A detailed view on (p)ppGpp targets shows that the binding affinities vary between low μM range, e.g., for RNA polymerase, and many ribosome biogenesis factors (Era, ObgE, or RbgA) up to a few hundred μM in the case of the DNA primase DnaG or proteins involved in carbon metabolism (overview in ref. 15). Such a gradual system allows the cells to fine tune metabolic processes and balance fluxes in response to changes in nutrient availability and other stressful conditions. Importantly for targets that are bound competitively by (p)ppGpp and GTP, the intracellular concentration of GTP impairs the fraction of (p)ppGpp-bound proteins. While the intracellular GTP concentration in *E. coli* during normal, unstressed growth conditions varies between 1–5 mM, it is highly reduced during stringent conditions caused by the inhibition of GTP anabolism through increasing (p)ppGpp concentrations^{43–45}. This negative correlation has also been described in *B. subtilis*^{46–48}. Consequently, inhibition of GTPases is also dependent on the GTP to (p)ppGpp ratio. This relation is e.g., reflected in the inhibition of the GTPase RbgA involved in ribosome biogenesis, where an inhibitor constant K_i of 300 μM (ppGpp) and 500 μM (pppGpp) has been determined⁶⁶. The major (p)ppGpp synthetases Rel (in *B. subtilis*) and RelA (in *E. coli*) require the binding of deacetylated amino acids and N-terminal association to the ribosome to enable full activation of (p)ppGpp production^{9,12,67}. Hence, (p)ppGpp regulation may not only be dependent on global pools, but also on local pools present in proximity of the ribosome-Rel complex. This local production of (p)ppGpp will inevitably influence the GTPases of the SRP/FtsY-targeting machinery. During harsh environmental conditions bacterial cells may use the shutdown of essential pathways such as transcription (RNA pol)⁶⁸, ribosome biogenesis (Era, ObgE, or RbgA)^{66,69–71}, translation^{60,72} and also SRP-dependent membrane targeting through the stringent response alarmone as a pausing mechanism. It allows microorganisms to slow down their

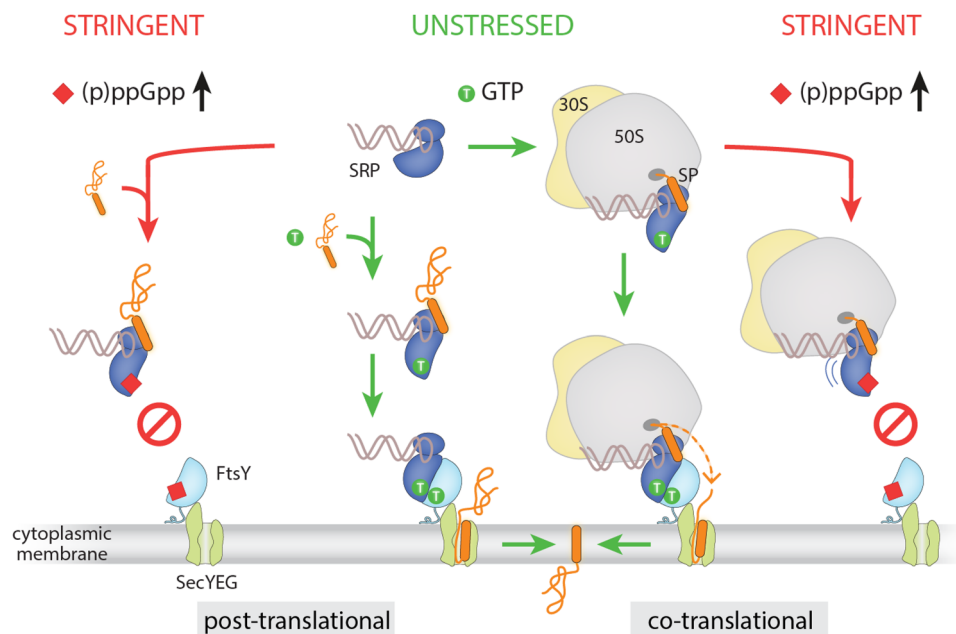


Fig. 6 Schematic summary of the bimodal interference of the alarmone (p)ppGpp with the post- and co-translational SRP-dependent membrane-targeting pathway. In unstressed cells, SRP (Ffh in blue and SRP RNA in gray) usually recognizes a signal peptide (SP, orange) at the ribosomal exit tunnel (co-translational) but can recognize some proteins also after they have been released from the ribosome (post-translational). Binding of a GTP (green) to both SRP and the SRP receptor FtsY (light blue) then allows the formation of the SRP-FtsY-targeting complex, which leads to stimulation of GTP hydrolysis and transfer of the RNC to the SecYEG translocon (light green). In contrast, under stringent stress conditions, (p)ppGpp (red) binds to SRP and prevents formation of the SRP-FtsY-targeting complex through steric hindrance both during post- and co-translation membrane targeting.

cellular processes and metabolisms, rather entering a persistence-like state to preserve the ability to recover when conditions are favorable again. Hence, inhibition of the SRP pathway might be an additional layer of cellular control and adaptive pausing to survive during stressful times.

Methods

In vitro synthesis of 4.5S and 6S RNA. For in vitro synthesis of 4.5S RNA, pT7/T3 α 19, carrying the 4.5S RNA coding sequence⁷³ was linearized using BamHI. In vitro transcription was performed using the AmpliScribe T7-Flash Transcription kit (Epicentre Biotechnologies, Madison, USA). The 4.5S RNA was purified using the RNA purification Kit (Qiagen, Hilden Germany) and stored at -80°C . For in vitro synthesis of 6S RNA, the plasmid pUC19 coding for (*Bs*) 6S RNA⁵³ was linearized using restriction enzyme HindIII HF (NEB). Two micrograms of DNA and in house-prepared T7 polymerase were incubated in 5 mM DTT, 8 mM ATP, CTP, GTP, UTP, 10x T7 buffer (400 mM Tris pH 7.9, 25 mM spermidine 260 mM MgCl_2 , 0.1% (v/v) Triton X-100) at 37°C for 3 h. After in vitro transcription, the RNA was precipitated using phenol/chloroform, resuspended in water, and stored at -80°C .

Plasmid construction and protein purification. Protein purification of full-length constructs originating from *E. coli* followed previously described protocols for SecYEG⁷⁴, full-length (*Ec*)Ffh⁷⁴ and (*Ec*)FtsY⁷⁵. In brief, for (*Ec*)Ffh and (*Ec*)FtsY purification, expression was induced by adding 1 mM IPTG and cells were broken using a French Pressure cell (Thermo Fisher Scientific, Schwerte, Germany). Proteins were purified via their His-tags using an Äkta chromatography system using a HisTrap FF nickel column (GE Healthcare, Waukesha, WI, USA). SecYEG was purified after arabinose induction (0.5%) from *E. coli* cells carrying pBAD-SecY_{His}G. Membranes were isolated, solubilized with 1% dodecyl maltoside and purified via Talon resin (Takara, St. Germaine-en-Laye, France). For over-expression and purification of the (*Ec*)Ffh- and (*Ec*)FtsY-NG domains, the coding gene fragments from *E. coli* were amplified by polymerase chain reaction (PCR) and cloned into pET24d (Novagen) via the NcoI/XhoI (FtsY) or NcoI/HindIII (Ffh) restriction sites (primers are listed in Supplementary Table 4). This resulted in the plasmids pNM103 and pNM101, respectively. Both proteins contained a C-terminal hexa-histidine (His_6) tag. The gene fragment encoding the Ffh-NG domain from *B. subtilis* was amplified by polymerase chain reaction (PCR) and cloned into a pET24d (Novagen) vector modified for modular cloning via BsaI restriction sites (primers are listed in Supplementary Table 4). This resulted in the plasmids pLC163. (*Bs*)Ffh-NG also contained a N-terminal hexa-histidine (His_6) tag. Proteins derived from *E. coli* were produced in *E. coli* BL21 (DE3) (Novagen).

Four liters of LB medium containing ($50\ \mu\text{g mL}^{-1}$ kanamycin) and 1% (w/v) lactose for autoinduction of the P_{lac} promoter driving the T7 polymerase required for recombinant gene expression were incubated in an aerial shaker for 18 h at 30°C overnight. Proteins derived from *B. subtilis* were produced in *E. coli* Rosetta pLysS (Novagen). 4 liters of LB medium containing ($50\ \mu\text{g mL}^{-1}$ kanamycin) were inoculated with an overnight culture to an OD_{578} of 0.08 and incubated at 37°C in an aerial shaker (180 rpm). When cultures reached OD_{578} of 0.5 overproduction of the recombinant proteins was induced by the addition of 1 mM IPTG and the cultures were further incubated for 3 h. After harvesting, cells were lysed by a Microfluidizer (M110-L, Microfluidics). The lysis buffer contained 20 mM HEPES-Na (pH 8.0), 250 mM NaCl, 20 mM KCl, and 50 mM imidazole. Cell debris was then removed by high-speed centrifugation for 20 min at $48,000 \times g$. All proteins were initially purified by Ni-ion affinity chromatography, eluting in lysis buffer containing 250 mM imidazole. 30 mM (final concentration) ethylenediaminetetraacetic acid (EDTA) was subsequently added and incubated for 10 min at room temperature. Anion-exchange chromatography (MonoQ 5/50 GL, GE Healthcare) was conducted utilizing a linear gradient of buffer A (20 mM HEPES-Na (pH 7.5), 20 mM EDTA, 100 mM NaCl and buffer B (buffer A containing 1 M NaCl) over 20 column volumes (CV). The eluted proteins were concentrated (10 kDa MWCO) and further polished by size-exclusion chromatography on a S200 XK26 column or a S200 XK16 column (GE Healthcare) with SEC buffer consisting of 20 mM HEPES-Na (pH 7.5), 200 mM NaCl, 20 mM KCl, and 20 mM MgCl_2 . Purified proteins were analyzed for the presence of remaining bound nucleotides using a standard nucleotide HPLC method as described below.

The plasmid pET46 coding for full-length (*Bs*)Ffh with N-terminal 6xHis-tag and HRV 3C cleavage site was transformed in *E. coli* strain BL21(DE3). Cells were grown in LB medium to mid-log phase ($\text{OD}_{600} = 0.6$) at 37°C and induced with 1 mM IPTG at 16°C for 20 h. Cells were harvested by centrifugation at $5471 \times g$ and 4°C for 8 min, washed with buffer A (25 mM HEPES/KOH pH 7.5, 500 mM KCl, 10 mM imidazole, 1 mM DTT, 0.1 mM EDTA, 0.1 mM PMSF, 1:1000 protease inhibitor (pill mL^{-1}), 10% (v/v) glycerol) and frozen in liquid nitrogen. Frozen cells were ground using a Spex SamplePrep Freezer Mill and the powder stored at -80°C until further use. After 15 g of cell powder was thawed in 100 mL buffer A, cell debris was removed by centrifugation at $30,597 \times g$ for 20 min. The cleared lysate was then incubated with 6 mL of prewashed TALON metal affinity resin for 2 h. Afterwards the beads were washed with 15 (CVs) buffer A, 7 CVs buffer B (25 mM HEPES/KOH pH 7.5, 1,000 mM KCl, 10 mM imidazole, 1 mM DTT, 0.1 mM PMSF, 1:1000 protease inhibitor (pill mL^{-1}), 10% (v/v) glycerol) and 3 CVs buffer A without protease inhibitor. The beads were then incubated with $0.22\ \text{mg mL}^{-1}$ 3 C protease in buffer C (25 mM HEPES/KOH pH 7.5, 500 mM KCl, 1 mM DTT, 10% (v/v) glycerol) overnight on a wheel. The elution was diluted 1:10 in buffer D (25 mM HEPES/KOH pH 7.5, 100 mM KCl, 1 mM DTT, 10% (v/v) glycerol) and loaded with $1\ \text{mL min}^{-1}$ flow rate on a HiTrap SP HP cation-

exchange chromatography column. The column was washed with 5 CVs buffer D and elute over a 4 CVs gradient from 0–100% buffer E (buffer D with 1000 mM KCl). 1 mL fractions were collected and analyzed by sodium dodecyl sulfate–polyacrylamide gel electrophoresis (SDS-PAGE). Ffh-containing fractions were pooled and concentrated to 1 mL using an Amicon 30k MWCO and subjected to size-exclusion chromatography using a Superdex 200. Again, Ffh-containing fractions were pooled, concentrated, and used for reconstitution of SRP.

In vitro protein synthesis, protein purification, and generation of proteoliposomes. For protein transport assay, YohP cloned in pET19b was synthesized in vitro using a purified transcription/translation system composed of cytosolic translation factors (CTF) and high salt-washed ribosomes^{35,36}. The ³⁵S-Methionine/³⁵S-Cysteine labeling mix was obtained from Perkin Elmer (Wiesbaden, Germany). INV's of *E. coli* cells were prepared by sucrose gradient centrifugation of cell extracts as described⁷⁶ and resuspended in INV buffer (50 mM triethanolamine acetate, pH 7.5, 200 mM sucrose, 1 mM DTT). After in vitro synthesis, samples were incubated for 10 min at 37 °C with 35 µg mL⁻¹ chloramphenicol for inhibiting translation and then centrifuged for 30 min at 186,000 × g in a Beckmann TLA55 rotor for removing ribosomes. The supernatant containing YohP was then incubated with INV, liposomes or SecYEG-proteoliposomes for 10 min at 37 °C in the presence of 10 µM GTP. When indicated, (p)ppGpp dissolved in 50 mM triethanolamine acetate, pH 7.5 was added during the incubation step. After incubation, one half of the reaction was directly precipitated with 10% (w/v) trichloroacetic acid (TCA), while the other half was first treated with 0.5 mg mL⁻¹ proteinase K for 15 min at 25 °C and only then precipitated with TCA. Proteinase K was inactivated in 10% (w/v) TCA by incubation for 10 min at 56 °C. Next, the samples were denatured at 56 °C for 10 min in 35 µL of TCA loading dye (prepared by mixing one part of solution III (1 M dithiothreitol) with 4 parts of solution II (6.33% (w/v) SDS, 0.083 M Tris, 30% (v/v) glycerol and 0.053% (w/v) bromophenol blue) and 5 parts of solution I (0.2 M Tris, 0.02 M EDTA pH 8)) and analyzed after separation on a modified SDS-PAGE³⁵ by phosphor imaging. For quantification of YohP insertion, autoradiography samples were analyzed by using the *ImageQuant* (GE Healthcare) software. All experiments were performed three times as independent biological replicates and representative images are shown. Mean values and SEM values were determined by using either Excel (Microsoft Corp.) or GraphPad Prism (GraphPad Prism Corp. San Diego). (*Ec*)Ffh (full-length) was concentrated on a 10 kDa centrifugal filter (Amicon Ultra, Witten, Germany) and re-buffered in HT buffer containing 50% (v/v) glycerol (50 mM HEPES, pH 7.6, 100 mM KOAc, pH 7.5, 10 mM Mg(OAc)₂, 1 mM DTT) using a PD-10 column (GE Healthcare, Munich Germany). The protein was stored at –20 °C. (*Ec*)FtsY (full-length) was re-buffered in HT buffer using a PD-10 Column (GE Healthcare, Munich, Germany) and stored at –80 °C. SRP was reconstituted by incubating 1.5 µM (*Ec*)Ffh with 0.1 mg mL⁻¹ 4.5S RNA (see above) for 15 min at 25 °C in HT buffer. *E. coli* phospholipids were purchased from Avanti polar lipids, Inc (Alabaster, USA) and liposomes were generated as described⁷⁷, representing a phospholipid composition of 70% phosphatidylethanolamine (PE), 25% phosphatidylglycerol (PG) and 5% cardiolipin (CL). SecYEG-proteoliposomes were created as described^{74,78}. In brief, 200 µg of liposomes and 14–16 µg of purified (*Ec*)SecYEG were prepared in 150 µL buffer (50 mM triethanolamine acetate (TeaOAc), pH 7.5, 1 mM DTT, and 1.5% octyl-β-glycoside). The samples were dialyzed with PL-buffer (50 mM TeaOAc, pH 7.5, 1 mM DTT), pelleted and resuspended in PL-buffer to a final protein concentration of 100 ng µL⁻¹ and stored at –80 °C. Before each use, proteoliposomes were briefly sonicated. In in vitro protein transport assays, 1 µL liposomes or proteoliposomes were used per in vitro reaction.

Floation analyses of FtsQ and LepB ribosome-associated nascent chains (RNCs). For in vitro synthesizing FtsQ- and LepB-RNCs, the T7-dependent expression vectors pKSM-FtsQ and pKSM-LepB were used^{37,79}. In brief, the first 102 amino acids of LepB, and the first 120 amino acids of FtsQ were fused to the SecM stalling sequence and cloned into the pET19b vector. In vitro synthesis was performed in a coupled transcription/translation system as described for YohP. After in vitro synthesis, the RNCs were incubated with INV's (1 µL), liposomes (2 µL), or SecYEG-proteoliposomes (2 µL; 100 ng SecYEG µL⁻¹) in floation buffer (50 mM triethanolamine acetate, pH 8.0; 10 µM GTP, 10 mM magnesium acetate, 70 mM potassium acetate; 250 mM sucrose and 1 mM DTT) for 15 min at 25 °C. When indicated, SRP/FtsY (20 ng µL⁻¹ each) and ppGpp or pppGpp (50 µM final concentration) was present during incubation. Membrane binding of RNCs was assayed by floation analyses³⁹. The reaction mixture was adjusted to 1.6 M sucrose (final volume 100 µL) and overlaid with 200 µL of 1.25 M sucrose and 100 µL 0.25 M sucrose, each prepared in floation buffer. Following centrifugation in a TLA 100.2 rotor (Beckmann-Coulter) at 43,490 × g for 90 min, the upper 200 µL of the gradient, containing the membrane fraction (MF) were withdrawn and precipitated with 10% (w/v) TCA (final concentration). The pelleted (non-bound soluble fraction, SF) RNCs were resuspended in the remaining 200 µL of the gradient and TCA precipitated. Samples were subsequently analyzed by 15% SDS-PAGE and autoradiography. RNC binding to membranes was quantified by using the *ImageQuant* (GE Healthcare, München, Germany) software. The experiments were performed at least three times as independent experiments and representative images are shown. Mean values and SEM values were determined by using either Excel (Microsoft Corp.) or GraphPad Prism (GraphPad Prism Corp. San Diego).

Analytical size-exclusion chromatography (SEC). For the analytical SEC, purified NG domains of (*Ec*)FtsY and (*Ec*)Ffh were diluted in a buffer containing 20 mM HEPES (pH 7.5), 200 mM NaCl, 20 mM MgCl₂ and 20 mM KCl to a final concentration of 100 µM (Fig. 3g) and 50 µM (Fig. 3h, i) each. Indicated amounts of nucleotides were added simultaneously, and the solution was incubated for 30 min at room temperature. 100 µL were then injected at 4 °C on a pre-equilibrated S200 300/10 GL analytical size-exclusion column (GE Healthcare, München, Germany) on an Äkta system (UNICORN 7.6; Cytiva). Data has been plotted using GraphPad Prism (GraphPad Prism Corp. San Diego).

Isothermal titration calorimetry (ITC). Ligands and proteins (purified NG domains of (*Ec*)Ffh, (*Ec*)FtsY and (*Bs*)Ffh) were diluted with a buffer containing 20 mM HEPES-Na (pH 7.5), 200 mM NaCl, 20 mM MgCl₂ and 20 mM KCl. The NG domains of (*Ec*)Ffh, (*Ec*)FtsY and (*Bs*)Ffh were titrated in the sample-cell at a nominal concentration of 25 µM each. The nucleotides GDP, GTP, ppGpp and pppGpp (Jena Bioscience, Germany) were placed in the syringe and their concentrations were predetermined by absorbance at 252 nm to saturate the protein samples during the titrations. All the measurements were performed at 25 °C with the instrument MicroCal PEAQ-ITC (©Malvern Panalytical) with a method consisting of 13 injections (first 0.4 µL, and the rest 3 µL each) and 150 s of spacing. The raw data (see source) were processed with the MicroCal PEAQ-ITC Analysis Software (©Malvern Panalytical) using the “one set of sites” models.

Microscale thermophoresis. Ligand binding assays with purified NG domains of (*Ec*)Ffh, (*Ec*)FtsY and (*Bs*)Ffh proteins were carried out by microscale thermophoresis (MST)⁸⁰. All experiments were performed on a Monolith NT.115 (NanoTemper Technologies GmbH, Munich, Germany; software: NanoTemper Control Version 2.0.2.29) at 21 °C (red LED power was set to 50–100% and infrared laser power to 75%). After labeling of primary amines within (*Ec*)Ffh, (*Ec*)FtsY, and (*Bs*)Ffh (50 µM each) with the dye NT 647 (according to the manufacturers protocol), the proteins were re-buffered in SEC buffer containing 20 mM HEPES-Na, 20 mM KCl, 20 mM MgCl₂, 200 mM NaCl (final pH 7.5), 10 mg mL⁻¹ BSA and 0.007% Tween. Two-hundred nanomolar of (*Ec*)Ffh, (*Ec*)FtsY, and (*Bs*)Ffh were titrated with GDP, GTP, ppGpp, and pppGpp starting from a concentration ranging between 0.75 and 3 mM, respectively. At least six independent MST experiments per ligand and protein were recorded at 680 nm and analyzed using NanoTemper Analysis version 1.5.37 and 1.2.009, and Origin8G software suits.

Determination of GTPase activity. GTPase activity of full-length (*Ec*)Ffh and the NG domain of (*Ec*)FtsY was assayed in a buffer containing 25 mM HEPES-K pH 7.5, 10 mM Mg(OAc)₂, 300 mM K(OAc), 1 mM DTT, and 2.5% (v/v) glycerol. The samples contained 5 µM (*Ec*)Ffh, 5 µM (*Ec*)FtsY-NG, 6 µM 4.5S RNA, 5 µM ΔEspP (EspP signal peptide sequence: MKK HKR ILA LCF LGL LQS SYS WAK KKK, custom synthesized from Genosphere Biotechnologies (France)⁴⁰, and 100 µM C₁₂E₈ (octaethylglykol-monododecylether, Sigma Aldrich)⁴⁰ as indicated in figures. Alarmones ppGpp (Jena Bioscience, ≥95% purity) or pppGpp (Jena Bioscience, ≥85% purity) were supplemented in concentrations of 10, 25, 100, 250, 1000, 2500, or 10,000 µM as indicated in the figures. The enzymatic reactions were initiated by the addition of 1 mM GTP (Jena Bioscience, ≥99% purity) and allowed to proceed for 60 min at 37 °C, after which 40 µL double-distilled water were added immediately followed by 150 µL of chloroform. The reaction tubes were then vigorously agitated for 5 s, heated up at 95 °C for 15 s and snap-frozen in liquid nitrogen. The tubes were thawed and, after centrifugation (17,300 × g, 10 min, 4 °C), an aliquot of the aqueous phase was withdrawn for analysis. The nucleotide content was determined by high-performance liquid chromatography (HPLC) on an Agilent 1260 Infinity system (software: ChemStation Rev. B04.03-SP1) equipped with a Metrosep A Supp 5–150/4.0 column (Metrohm). Ten microliters of sample were injected and nucleotides eluted isocratically at 0.6 mL min⁻¹ flow rate of 100 mM (NH₄)₂CO₃ pH 9.25 and detected at 260 nm wavelength. Commercial GDP and GTP solutions served as standards for the identification of the nucleotides based on their retention time. Data has been plotted using Microsoft Excel (version 14.6.8) and GraphPad Prism (GraphPad Prism Corp. San Diego).

Crystallization and structure determination. Crystallization was performed by the sitting-drop method at 20 °C in 250-nL drops consisting of equal parts of protein and precipitation solutions. Protein solutions of 2.5–3 mM were incubated with 10 mM (final concentration) pppGpp or ppGpp, respectively, for 10 min at room temperature. Crystallization conditions were: (*Ec*)Ffh-NG with ppGpp and Mg²⁺ (0.2 M ammonium acetate, 20% (w/v) PEG 3350); (*Ec*)Ffh-NG with pppGpp (0.2 M sodium chloride, 0.1 M CHES pH 9.5, 50% (v/v) PEG 400); (*Ec*)FtsY-NG with pppGpp (8.5% (v/v) isopropanol, 0.085 M HEPES pH 7.5, 17% (w/v) PEG 4000, 15% (v/v) glycerol); (*Bs*)Ffh-NG with ppGpp and Mg²⁺ (0.1 M CHES pH 9.5, 30% (v/v) PEG 400). Prior to data collection, crystals were flash-frozen in liquid nitrogen using a cryo-solution that consisted of mother-liquor supplemented with 20% (v/v) glycerol. Data were collected under cryogenic conditions at the European Synchrotron Radiation Facility (Grenoble, France⁸¹) and at Deutsches Elektronen-Synchrotron (Hamburg, Germany). MxCube2 and MxCube3 were used for data collection (<https://github.com/mxcube>). Data were processed with XDS (version January 31, 2020) and scaled with XSCALE⁸². All structures were determined by

molecular replacement with PHASER⁸³, manually built in COOT⁸⁴ (Coot Version 0.9.4.1), and refined with PHENIX⁸⁵ (Phenix Version 1.17.1-3660 and 1.19). The search model for the Ffh structures was the *Thermus aquaticus* Ffh (PDB-ID: 3NGI⁸⁶ <https://www.rcsb.org/structure/3NGI>). A structure of *E. coli* FtsY was already known and has been used as a model for molecular replacement (PDB-ID: 2YHS²⁷ <https://www.rcsb.org/structure/2YHS>). Figures were prepared with Pymol (www.pymol.org)^{87,88}.

Reconstitution of (Ec)SRP and (Bs)SRP. For SRP reconstitution, the 6S SRP RNA was heated to 65 °C and then cooled down to 4 °C to allow proper folding. The 6S RNA and a tenfold molar excess of purified full-length (Bs)Ffh were then incubated together and loaded on a Superdex 200 using buffer F (25 mM HEPES/KOH pH 7.5, 300 mM KOAc, 10 mM Mg(OAc)₂, 1 mM DTT, 2% glycerol). One milliliter fractions were collected and analyzed by SDS-PAGE and agarose gel. SRP-containing fractions were combined, concentrated and stored at -80 °C until further use.

***B. subtilis* in vitro translation and reconstitution of SRP-bound RNCs.** The MifM-encoding mRNA, which contains the MifM leader peptide with shortened C-terminus, a defined stalling site, the MifM N-terminal transmembrane segment (TM), a V5-tag and a cleavable His-tag, was prepared as described before by PCR amplification, DNA purification, in vitro transcription and phenol/chloroform precipitation⁵². The translation extract was prepared from the *B. subtilis* strain 168 Δ hpf Δ ssrA Δ yjbM Δ ywaC⁸⁹. Cells were grown in LB medium supplemented with 1% (w/v) glucose, harvested at an OD₆₀₀ between 0.6 and 0.8 and pelleted by centrifugation at 5471 × g and room temperature for 5 min. Afterwards, cells were resuspended in PBS (137 mM NaCl, 2.7 mM KCl, 10 mM Na₂HPO₄, 2 mM KH₂PO₄, pH 7.4), pelleted again by centrifugation at 5471 × g and 4 °C for 15 min and resuspended in lysis buffer (10 mM HEPES pH 8.2, 60 mM K-glutamate, 14 mM Mg(OAc)₂). Cell lysis was performed using a microfluidizer (Microfluidics M-110L) and cell debris was removed by centrifugation at 30,597 × g and 4 °C for 20 min. The extract was aliquoted and frozen in liquid nitrogen. Activity of the extract as well as Mg buffer concentration was determined using the Luciferase Assay System (Promega).

The in vitro translation reaction was performed in 4 × 500 μL reaction volume. In all, 640 μL cell extract were mixed with energy buffer (final concentration in 2 mL: 2% (w/v) PEG 8000, 50 mM HEPES/KOH pH 8.2, 10 mM NH₄OAc, 130 mM KOAc, 30 mM Na-pyruvate, 4 mM Na-oxalate, 50 μg mL⁻¹ tRNA (from *E. coli*; Sigma 10109541 001), 0.2 mg mL⁻¹ folinic acid, 0.1 μg mL⁻¹ creatine kinase, 20 mM creatine phosphate, 4 mM ATP, 3 mM GTP, 0.1 mM amino acid mix, 1 mM DTT, 0.08 U SUPERase[•]In™ RNase Inhibitor (Invitrogen), 15 mM Mg(OAc)₂). After heating the mixture to 32 °C for 2 min, 50 μg of mRNA were added to each aliquot and the in vitro translation was incubated at 32 °C for 40 min while shaking at 900 rpm. For affinity purification of ribosome-nascent chain complexes, the in vitro translation was incubated with 400 μL of prewashed TALON metal affinity resin for 45 min on a wheel. The flow-through was collected, beads were washed with 5 CVs buffer A (30 mM HEPES pH 7.5/KOH, 250 mM KOAc, 25 mM Mg(OAc)₂, 20 mM imidazole, 0.1% DDM) and eluted by incubation for 2 h with 1 CV buffer B (30 mM HEPES pH 7.5/KOH, 250 mM KOAc, 25 mM Mg(OAc)₂, 0.1% (w/v) DDM, 1.1 mg mL⁻¹ 3C protease). The sample was loaded on a 10–40% sucrose gradient (30 mM HEPES pH 7.5/KOH, 250 mM KOAc, 25 mM Mg(OAc)₂, 0.1% (w/v) DDM, 10–40% (w/v) sucrose) and spun in a SW 40 Ti rotor (Beckman Coulter) at 54,322 × g for 16 h at 4 °C. The gradient was fractionated at a BioComp Gradient Station *ip* using a Triax Flow Cell for UV measurement. The 70S peak fractions were combined and RNCs were pelleted by centrifugation in a TLA110 rotor (Beckman Coulter) at 434,513 × g for 2 h at 4 °C. The pellet was resuspended in buffer C (25 mM HEPES pH 7.5/KOH, 150 mM KOAc, 10 mM Mg(OAc)₂, 2 mM DTT), frozen in liquid nitrogen and stored at -80 °C. For reconstitution, RNCs and SRP were thawed on ice. SRP was incubated with either GMPPNP or pppGpp for 10 min at room temperature and with tenfold molar excess mixed with MifM-stalled RNCs. The final complex was incubated for 10 min at room temperature and subsequently analyzed by cryo-EM.

***E. coli* translation in vivo and reconstitution of SRP-bound RNCs.** The TnaC-stalled RNCs were prepared as previously described using the *E. coli* KC6 Δ ssrA Δ smpB strain^{58,59,90}. Cells were grown at 37 °C to an OD₆₀₀ of 0.5 and expression of the of the RNC construct was induced with 0.2% arabinose. After 1 h, cells were harvested and resuspended in buffer A (50 mM HEPES pH 7.5/KOH, 250 mM KOAc, 25 mM Mg(OAc)₂, 1 mM tryptophan, 0.1% (w/v) DDM, 250 μg mL⁻¹ chloramphenicol and 0.1% EDTA-free complete proteinase inhibitors). Cells were lysed using a microfluidizer (Microfluidics M-110L) and centrifuged (5471 × g, 4 °C, 20 min). The cleared lysate was loaded on a sucrose cushion (buffer A + 750 mM sucrose) and spun in a Type 45 Ti Rotor (Beckman Coulter) for 20 h at 72,465 g and 4 °C. The pellet was resuspended in buffer B (50 mM HEPES pH 7.5/KOH, 250 mM KOAc, 25 mM Mg(OAc)₂, 250 mM sucrose, 1 mM tryptophan, 0.1% (w/v) DDM, 250 μg mL⁻¹ chloramphenicol and 0.1% EDTA-free complete proteinase inhibitors) and RNCs were isolated by incubation for 1 h with prewashed TALON metal affinity resin. The nascent chain consists of an N-terminal His-tag, an HRV 3C protease cleavage site and the transmembrane segment of FtsQ (residues 4–51) followed by the stalling sequence of the tryptophanase leader peptide (TnaC). The amino acid sequence of the nascent chain is MGHHHHHHHH DYDIPTTLEVF LQFGPGTAAL

NTRNSEEVS SRRNNGTRLA GILFLLVCTV TVLVSGWVVL GWMEDYPPYDV PDYAGPNLH ISVTSKWFNI DNKIVDHRP*. The beads were washed with buffer C (50 mM HEPES pH 7.5/KOH, 500 mM KOAc, 25 mM Mg(OAc)₂, 250 mM sucrose, 1 mM tryptophan, 0.1% (w/v) DDM, 250 μg mL⁻¹ chloramphenicol and 0.1% EDTA-free complete proteinase inhibitors) and buffer D (50 mM HEPES pH 7.5/KOH, 250 mM KOAc, 25 mM Mg(OAc)₂, 0.1% (w/v) DDM, 250 μg mL⁻¹ chloramphenicol). Elution was performed with buffer D + 150 mM imidazole. The eluate was loaded on a sucrose gradient (buffer D + 10–40% (w/v) sucrose) and spun in a SW 40 Ti rotor (Beckman Coulter) at 54,322 × g for 16 h at 4 °C. The 70S peak was harvested and pelleted again in a TLA110 rotor (Beckman Coulter) at 434,513 × g for 2 h at 4 °C and resuspended in buffer D + 1 mM tryptophane. Purified RNCs were reconstituted with SRP, which was pre-incubated with either GMPPNP or pppGpp for 10 min at room temperature. A 10-fold molar excess of SRP was mixed with TnaC-stalled RNCs, incubated again for 10 min at room temperature and subsequently analyzed by cryo-EM.

Cryo-EM sample preparation, data collection, and processing. A volume of 3.5 μL of the reconstituted SRP-RNC complex was applied to 2 nm pre-coated Quantifoil R3/3 holey carbon support grids and vitrified in liquid ethane using a Vitrobot mark IV (FEI Company, Netherlands) (wait time 45 s, blotting time 2 s). For the *B. subtilis* samples, 9976 and 9508 movies were collected on a Titan Krios at 300 kV for the pppGpp sample and the GMPPNP sample, respectively. The collection was recorded on a K2 Summit direct electron detector with an electron dose of approx. 1.06 e⁻/Å² per frame for 10 frames (defocus range of 0.5 to 5 μm). The magnified pixel size was 1.059 Å/pixel. All frames were gain corrected and subsequently aligned and summed using MotionCorr⁹¹ and CTF parameters were determined using CTFIND⁹² (version 4.1.13). After visual inspection of the micrographs, particles were picked using Gautomatch⁹³ (version v0.56; <http://www.mrc-lmb.cam.ac.uk/kzhang/>). The particles were extracted and processed following the standard workflow in RELION 3.1⁹⁴. For both datasets, the 2D classification was used to remove non-ribosomal particles and in the following 3D classification programmed 70S were selected. These were further sub-classified using spherical masks around the SRP Alu domain and the SRP S domain (Supplementary Fig. 7). SRP-bound RNCs were then refined and CTF-corrected. The particles were imported to Cryosparc v3.2.0⁹⁵ and refined to a final resolution of 3.33 Å (pppGpp sample) and 2.96 Å (GMPPNP sample) (Supplementary Fig. 8).

For the *E. coli* samples, 14,285 and 15,042 movies were collected on a Titan Krios at 300 kV for the pppGpp sample and the GMPPNP sample, respectively. The collection was recorded on a Falcon II direct electron detector. The electron dose was approx. 2.5 e⁻/Å² per frame for 16 frames (defocus range of 0.5 to 5 μm) and the magnified pixel size was 1.09 Å/pixel. All frames were corrected and aligned as described above. After visual inspection of the micrographs, crYOLO⁹⁶ (version 1.7.6) was used for particle picking. For both datasets, the particles were extracted and processed following the standard workflow in RELION 3.1⁹⁴. The 2D classification was used to remove non-ribosomal particles and in the following 3D classification programmed 70S were selected. First, a focused classification with a mask around SRP was used to enrich SRP-bound RNCs. Second, a focused classification with a mask around the NG domain of Ffh was used to classify for different conformations. No differences between the final classes of the two datasets could be observed (Supplementary Fig. 9). Therefore, in an alternative classification attempt, particles of both datasets were combined and sub-classified using spherical masks around SRP (Supplementary Fig. 10). The class containing the best density for the NG domain was selected and particles were separated according to the nucleotide dataset. SRP-bound RNCs were then refined and CTF-corrected to a final resolution of 3.1 Å (pppGpp sample) and 3.2 Å (GMPPNP sample) again without revealing differences for the NG domain conformation (Supplementary Fig. 11).

Model building and refinement of cryo-EM data. Chimera version 1.13.1⁹⁷ and ChimeraX version 1.1⁹⁸ were used for rigid body fits and figures. The structures of *B. subtilis* ErmDL-stalled ribosome complex (rRNA and r-proteins; PDB 6HA1 <https://www.rcsb.org/structure/6HA1>)⁹⁹, the *B. subtilis* MifM-stalled ribosome complex (mRNA, tRNA, nascent chain; PDB 3J9W <https://www.rcsb.org/structure/3J9W>)⁵² and of the *B. subtilis* signal recognition particle (SRP RNA, Ffh-M domain, signal sequence; PDB 4UE4 <https://www.rcsb.org/structure/4UE4>)⁵³ were fitted into the cryo-EM map, side chains of proteins and rRNA were adjusted using Coot (version 0.8.9.2)⁸⁴ and all models were real space refined using Phenix (version 1.19)⁸⁵. The structure of the *B. subtilis* Ffh-NG domain bound to pppGpp (this study) was fitted into the cryo-EM-map and combined with the refined structure (Supplementary Table 2). The structure of the *E. coli* RNC in complex with SRP (PDB 5GAF <https://www.rcsb.org/structure/5GAF>)⁵⁴ was fitted into the obtained cryo-EM maps for interpretation and visualization. No further modeling of the *E. coli* RNCs with SRP was performed.

Reporting summary. Further information on research design is available in the Nature Research Reporting Summary linked to this article.

Data availability

Coordinates and structure factors of the crystal structures and coordinates of the cryo-EM structure have been deposited at the Protein Data Bank with the accession codes:

709F, 709G, 709H, 709I, 705B. Cryo-EM maps have been deposited at the EMDB with the accession codes: 12734, 12735, 13839, 13840. All other data generated in this study are provided in the Supplementary Information and Source Data file, or are available from the corresponding authors upon request. Already published datasets used in this study are: 1OKK, 3NG1, 2YHS, 6HA1, 3J9W, 4UE4, 5GAF. Source data are provided with this paper.

Received: 7 May 2021; Accepted: 7 February 2022;
Published online: 25 February 2022

References

1. Haurlyuk, V., Atkinson, G. C., Murakami, K. S., Tenson, T. & Gerdes, K. Recent functional insights into the role of (p)ppGpp in bacterial physiology. *Nat. Rev. Microbiol.* **13**, 298–309 (2015).
2. Bange, G., Brodersen, D. E., Liuzzi, A. & Steinchen, W. Two P or Not Two P: understanding regulation by the bacterial second messengers (p)ppGpp. *Annu. Rev. Microbiol.* **75**, 383–406 (2021).
3. Atkinson, G. C., Tenson, T. & Haurlyuk, V. The RelA/SpoT Homolog (RSH) superfamily: distribution and functional evolution of ppGpp synthetases and hydrolases across the tree of life. *PLoS ONE* **6**, e23479 (2011).
4. Steinchen, W. & Bange, G. The magic dance of the alarmones (p)ppGpp. *Mol. Microbiol.* **101**, 531–544 (2016).
5. Arenz, S. et al. The stringent factor RelA adopts an open conformation on the ribosome to stimulate ppGpp synthesis. *Nucleic Acids Res.* **44**, 6471–6481 (2016).
6. Wendrich, T. M., Blaha, G., Wilson, D. N., Marahiel, M. A. & Nierhaus, K. H. Dissection of the mechanism for the stringent factor RelA. *Mol. Cell* **10**, 779–788 (2002).
7. Loveland, A. B. et al. Ribosome.RelA structures reveal the mechanism of stringent response activation. *eLife* **5**, e17029 (2016).
8. Brown, A., Fernández, I. S., Gordiyenko, Y. & Ramakrishnan, V. Ribosome-dependent activation of stringent control. *Nature* **534**, 277–280 (2016).
9. Pausch, P. et al. Structural basis for regulation of the opposing (p)ppGpp synthetase and hydrolase within the stringent response orchestrator Rel. *Cell Rep.* **32**, 108157 (2020).
10. Hogg, T., Mechold, U., Malke, H., Cashel, M. & Hilgenfeld, R. Conformational antagonism between opposing active sites in a bifunctional RelA/SpoT homolog modulates (p)ppGpp metabolism during the stringent response. *Cell* **117**, 57–68 (2004).
11. Tamman, H. et al. A nucleotide-switch mechanism mediates opposing catalytic activities of Rel enzymes. *Nat. Chem. Biol.* **16**, 834–840 (2020).
12. Roghanian, M. et al. (p)ppGpp controls stringent factors by exploiting antagonistic allosteric coupling between catalytic domains. *Mol. Cell* **81**, 3310–3322.e6 (2021).
13. Bennison, D. J., Irving, S. E. & Corrigan, R. M. The impact of the stringent response on TRAFAC GTPases and prokaryotic ribosome assembly. *Cells* **8**, 1313 (2019).
14. Irving, S. E., Choudhury, N. R. & Corrigan, R. M. The stringent response and physiological roles of (pp)ppGpp in bacteria. *Nat. Rev. Microbiol.* <https://doi.org/10.1038/s41579-020-00470-y> (2020).
15. Steinchen, W., Zegarra, V. & Bange, G. (p)ppGpp: magic modulators of bacterial physiology and metabolism. *Front. Microbiol.* **11**, 2072 (2020).
16. Wang, B. et al. Affinity-based capture and identification of protein effectors of the growth regulator ppGpp. *Nat. Chem. Biol.* **15**, 141–150 (2019).
17. Kuhn, A., Koch, H.-G. & Dalbey, R. E. Targeting and insertion of membrane proteins. *EcoSal Plus* **7**, <https://doi.org/10.1128/ecosalplus.ESP-0012-2016> (2017).
18. Steinberg, R., Knüpfner, L., Origi, A., Asti, R. & Koch, H. G. Co-translational protein targeting in bacteria. *FEMS Microbiol. Lett.* **365**, 1–15 (2018).
19. Shan, S. & Walter, P. Co-translational protein targeting by the signal recognition particle. *FEBS Lett.* **579**, 921–926 (2005).
20. Grudnik, P., Bange, G. & Sinning, I. Protein targeting by the signal recognition particle. *Biol. Chem.* **390**, 775–782 (2009).
21. Akopian, D., Shen, K., Zhang, X. & Shan, S. Signal recognition particle: An essential protein-targeting machine. *Annu. Rev. Biochem.* **82**, 693–721 (2013).
22. Wild, K., Becker, M. M. M., Kempf, G. & Sinning, I. Structure, dynamics, and interactions of large SRP variants. *Biol. Chem.* **401**, 63–80 (2019).
23. Saraogi, I., Akopian, D. & Shan, S. O. A tale of two GTPases in cotranslational protein targeting. *Protein Sci.* **20**, 1790–1795 (2011).
24. Zhang, X. & Shan, S. O. Fidelity of cotranslational protein targeting by the signal recognition particle. *Annu. Rev. Biophys.* **43**, 381–408 (2014).
25. Shan, S. ATPase and GTPase tangos drive intracellular protein transport. *Trends Biochem. Sci.* **41**, 1050–1060 (2016).
26. Bange, G. & Sinning, I. SIMIBI twins in protein targeting and localization. *Nat. Struct. Mol. Biol.* **20**, 776–780 (2013).
27. Stjepanovic, G. et al. Lipids trigger a conformational switch that regulates Signal Recognition Particle (SRP)-mediated protein targeting. *J. Biol. Chem.* **286**, 23489–23497 (2011).
28. Parltitz, R. et al. *Escherichia coli* signal recognition particle receptor FtsY contains an essential and autonomous membrane-binding amphipathic helix. *J. Biol. Chem.* **282**, 32176–32184 (2007).
29. Freymann, D. M., Keenan, R. J., Stroud, R. M. & Walter, P. Structure of the conserved GTPase domain of the signal recognition particle. *Nature* **385**, 361–364 (1997).
30. Montoya, G., Svensson, C., Lührink, J. & Sinning, I. Crystal structure of the NG domain from the signal-recognition particle receptor FtsY. *Nature* **385**, 365–368 (1997).
31. Egea, P. F. et al. Substrate twinning activates the signal recognition particle and its receptor. *Nature* **427**, 215–221 (2004).
32. Focia, P. J., Shepotinovskaya, I. V., Seidler, J. A. & Freymann, D. M. Heterodimeric GTPase core of the SRP targeting complex. *Science* **303**, 373–377 (2004).
33. Wild, K. et al. Structural basis for conserved regulation and adaptation of the signal recognition particle targeting complex. *J. Mol. Biol.* **428**, 2880–2897 (2016).
34. Powers, T. & Walter, P. Reciprocal stimulation of GTP hydrolysis by two directly interacting GTPases. *Science* **269**, 1422–1424 (1995).
35. Steinberg, R. et al. Posttranslational insertion of small membrane proteins by the bacterial signal recognition particle. *PLoS Biol.* **18**, e3000874 (2020).
36. Koch, H. G. et al. In vitro studies with purified components reveal signal recognition particle (SRP) and SecA/SecB as constituents of two independent protein-targeting pathways of *Escherichia coli*. *Mol. Biol. Cell* **10**, 2163–2173 (1999).
37. Denks, K. et al. The signal recognition particle contacts uL23 and scans substrate translation inside the ribosomal tunnel. *Nat. Microbiol.* **2**, 16265 (2017).
38. Steinberg, R. & Koch, H. G. The largely unexplored biology of small proteins in pro- and eukaryotes. *FEBS J.* <https://doi.org/10.1111/febs.15845> (2021).
39. Neumann-Haefelin, C., Schäfer, U., Müller, M. & Koch, H. G. SRP-dependent co-translational targeting and SecA-dependent translocation analyzed as individual steps in the export of a bacterial protein. *EMBO J.* **19**, 6419–6426 (2000).
40. Bradshaw, N., Neher, S. B., Booth, D. S. & Walter, P. Signal sequences activate the catalytic switch of SRP RNA. *Science* **323**, 127–130 (2009).
41. Peluso, P., Shan, S. O., Nock, S., Herschlag, D. & Walter, P. Role of SRP RNA in the GTPase cycles of Ffh and FtsY. *Biochemistry* **40**, 15224–15233 (2001).
42. Peluso, P. et al. Role of 4.5 S RNA in assembly of the bacterial Signal Recognition Particle with its receptor. *Science* **288**, 1640–1643 (2000).
43. Varik, V., Oliveira, S. R. A., Haurlyuk, V. & Tenson, T. HPLC-based quantification of bacterial housekeeping nucleotides and alarmone messengers ppGpp and pppGpp. *Sci. Rep.* **7**, 1–12 (2017).
44. Zborníková, E., Knejzlík, Z., Haurlyuk, V., Krásný, L. & Rejman, D. Analysis of nucleotide pools in bacteria using HPLC-MS in HILIC mode. *Talanta* **205**, 120161 (2019).
45. Liu, K. et al. Molecular mechanism and evolution of guanylate kinase regulation by (ppp)ppGpp. *Mol. Cell* **57**, 735–749 (2015).
46. Bittner, A. N., Kriel, A. & Wang, J. D. Lowering GTP level increases survival of amino acid starvation but slows growth rate for *Bacillus subtilis* cells lacking (p)ppGpp. *J. Bacteriol.* **196**, 2067–2076 (2014).
47. Kriel, A. et al. Direct regulation of GTP homeostasis by (p)ppGpp: A critical component of viability and stress resistance. *Mol. Cell* **48**, 231–241 (2012).
48. Kriel, A. et al. GTP dysregulation in *Bacillus subtilis* cells lacking (p)ppGpp results in phenotypic amino acid auxotrophy and failure to adapt to nutrient downshift and regulate biosynthesis genes. *J. Bacteriol.* **196**, 189–201 (2014).
49. Moser, C., Mol, O., Goody, R. S. & Sinning, I. The signal recognition particle receptor of *Escherichia coli* (FtsY) has a nucleotide exchange factor built into the GTPase domain. *Proc. Natl Acad. Sci. USA* **94**, 11339–11344 (1997).
50. Ataíde, S. F. et al. The crystal structure of the signal recognition particle in complex with its receptor. *Science* **331**, 881–886 (2011).
51. Bange, G. et al. Structural basis for the molecular evolution of SRP-GTPase activation by protein. *Nat. Struct. Mol. Biol.* **18**, 1376–1380 (2011).
52. Sohnen, D. et al. Structure of the *Bacillus subtilis* 70S ribosome reveals the basis for species-specific stalling. *Nat. Commun.* **6**, 6941 (2015).
53. Beckert, B. et al. Translational arrest by a prokaryotic signal recognition particle is mediated by RNA interactions. *Nat. Struct. Mol. Biol.* **22**, 767–773 (2015).
54. Jomaa, A., Boehringer, D., Leibundgut, M. & Ban, N. Structures of the *E. coli* translating ribosome with SRP and its receptor and with the translocon. *Nat. Commun.* **7**, 10471 (2016).
55. Halic, M. et al. Structure of the signal recognition particle interacting with the elongation-arrested ribosome. *Nature* **427**, 808–814 (2004).
56. Halic, M. et al. Following the signal sequence from ribosomal tunnel exit to Signal Recognition Particle. *Nature* **444**, 507–511 (2006).

57. Voorhees, R. M. & Hegde, R. S. Structures of the scanning and engaged states of the mammalian SRP-ribosome complex. *eLife* **4**, 1–21 (2015).
58. Kater, L. et al. Partially inserted nascent chain unzips the lateral gate of the Sec translocon. *EMBO Rep.* **20**, e48191 (2019).
59. Kedrov, A. et al. Structural dynamics of the YidC-ribosome complex during membrane protein biogenesis. *Cell Rep.* **17**, 2943–2954 (2016).
60. Vinogradova, D. S. et al. How the initiating ribosome copes with ppGpp to translate mRNAs. *PLoS Biol.* **18**, 1–25 (2020).
61. Haseltine, W. A. & Block, R. Synthesis of guanosine tetra- and pentaphosphate requires the presence of a codon-specific, uncharged transfer ribonucleic acid in the acceptor site of ribosomes. *Proc. Natl Acad. Sci. USA* **70**, 1564–1568 (1973).
62. Kuroda, A., Murphy, H., Cashel, M. & Kornberg, A. Guanosine tetra- and pentaphosphate promote accumulation of inorganic polyphosphate in *Escherichia coli*. *J. Biol. Chem.* **272**, 21240–21243 (1997).
63. Potrykus, K. & Cashel, M. (p)ppGpp: still magical? *Annu. Rev. Microbiol.* **62**, 35–51 (2008).
64. Schreiber, G. et al. Overexpression of the *relA* gene in *Escherichia coli*. *J. Biol. Chem.* **266**, 3760–3767 (1991).
65. Svitils, A. L., Cashel, M. & Zyskindsl, J. W. Guanosine tetraphosphate inhibits protein synthesis in vivo. *J. Biol. Chem.* **268**, 2307–2311 (1993).
66. Pausch, P. et al. Structural basis for (p)ppGpp-mediated inhibition of the GTPase RbgA. *J. Biol. Chem.* **293**, 19699–19709 (2018).
67. Takada, H. et al. Ribosome association primes the stringent factor Rel for tRNA-dependent locking in the A-site and activation of (p)ppGpp synthesis. *Nucleic Acids Res.* **49**, 444–457 (2020).
68. Ross, W. et al. ppGpp binding to a site at the RNAP-DksA interface accounts for its dramatic effects on transcription initiation during the stringent response. *Mol. Cell* **62**, 811–823 (2016).
69. Wood, A., Irving, S. E., Bennisson, D. J. & Corrigan, R. M. The (p)ppGpp-binding GTPase Era promotes rRNA processing and cold adaptation in *Staphylococcus aureus*. *PLOS Genet.* **15**, e1008346 (2019).
70. Corrigan, R. M., Bellows, L. E., Wood, A. & Gründling, A. ppGpp negatively impacts ribosome assembly affecting growth and antimicrobial tolerance in Gram-positive bacteria. *Proc. Natl Acad. Sci. USA* **113**, E1710–E1719 (2016).
71. Bennisson, D. J. et al. The stringent response inhibits 70S ribosome formation in *Staphylococcus aureus* by impeding GTPase-ribosome interactions. *mBio* <https://doi.org/10.1128/mbio.02679-21> (2021).
72. Diez, S., Ryu, J., Caban, K., Gonzalez, R. L. & Dworkin, J. The alarmone (p)ppGpp directly regulate translation initiation during entry into quiescence. *Proc. Natl Acad. Sci. USA* **117**, 15565–15572 (2020).
73. Wood, H., Luirink, J. & Tollervey, D. Evolutionary conserved nucleotides within the *E. coli* 4.5S RNA are required for association with P48 in vitro and for optimal function in vivo. *Nucleic Acids Res.* **20**, 5919–5925 (1992).
74. Braig, D. et al. Signal sequence-independent SRP-SR complex formation at the membrane suggests an alternative targeting pathway within the SRP cycle. *Mol. Biol. Cell* **22**, 2309–2323 (2011).
75. Braig, D., Bär, C., Thumfart, J.-O. & Koch, H.-G. Two cooperating helices constitute the lipid-binding domain of the bacterial SRP receptor. *J. Mol. Biol.* **390**, 401–413 (2009).
76. Hoffschulte, H. K., Drees, B. & Müller, M. Identification of a soluble SecA/SecB complex by means of a subfractionated cell-free export system. *J. Biol. Chem.* **269**, 12833–12839 (1994).
77. Nishiyama, K. I. et al. A derivative of lipid A is involved in signal recognition particle/SecYEG-dependent and -independent membrane integrations. *J. Biol. Chem.* **281**, 35667–35676 (2006).
78. Welte, T. et al. Promiscuous targeting of polytopic membrane proteins to SecYEG or YidC by the *Escherichia coli* signal recognition particle. *Mol. Biol. Cell* **23**, 464–479 (2012).
79. Knüpfper, L. et al. Molecular mimicry of SecA and signal recognition particle binding to the bacterial ribosome. *mBio* **10**, 1–17 (2019).
80. Wienken, C. J., Baaske, P., Rothbauer, U., Braun, D. & Duhr, S. Protein-binding assays in biological liquids using microscale thermophoresis. *Nat. Commun.* **1**, 100 (2010).
81. Theveneau, P. et al. The upgrade programme for the structural biology beamlines at the European synchrotron Radiation Facility-High throughput sample evaluation and automation. *J. Phys. Confer. Ser.* **425**, 012001 (2013).
82. Kabsch, W. Integration, scaling, space-group assignment and post-refinement. *Acta Crystallogr. Sect. D: Biol. Crystallogr.* **66**, 133–144 (2010).
83. McCoy, A. J. Solving structures of protein complexes by molecular replacement with Phaser. *Acta Crystallogr. Sect. D: Biol. Crystallogr.* **63**, 32–41 (2006).
84. Emsley, P. & Cowtan, K. Coot: model-building tools for molecular graphics. *Acta Crystallogr. Sect. D: Biol. Crystallogr.* **60**, 2126–2132 (2004).
85. Liebschner, D. et al. Macromolecular structure determination using X-rays, neutrons and electrons: Recent developments in Phenix. *Acta Crystallogr. Sect. D: Struct. Biol.* **75**, 861–877 (2019).
86. Freymann, D. M., Keenan, R. J., Stroud, R. M. & Walter, P. Functional changes in the structure of the SRP GTPase on binding GDP and Mg²⁺+GDP. *Nat. Struct. Biol.* **6**, 793–801 (1999).
87. DeLano, W. L. *The PyMOL Molecular Graphics System, Version 1.8 Schrödinger, LLC.* (Delano Scientific, 2002).
88. Moriarty, N. W. et al. Interactive comparison and remediation of collections of macromolecular structures. *Protein Sci.* **27**, 182–194 (2018).
89. Schäfer, H. et al. The alarmone (p)ppGpp are part of the heat shock response of *Bacillus subtilis*. *PLOS Genet.* **16**, e1008275 (2020).
90. Seidelt, B. et al. Structural insight into nascent polypeptide chain-mediated translational stalling. *Science* **326**, 1412–1415 (2009).
91. Zheng, S. Q. et al. MotionCor2: Anisotropic correction of beam-induced motion for improved cryo-electron microscopy. *Nat. Methods* **14**, 331–332 (2017).
92. Rohou, A. & Grigorieff, N. CTFIND4: Fast and accurate defocus estimation from electron micrographs. *J. Struct. Biol.* **192**, 216–221 (2015).
93. Zhang, C. & Lai, L. Automatch: Target-binding protein design and enzyme design by automatic pinpointing potential active sites in available protein scaffolds. *Proteins: Struct., Funct. Bioinforma.* **80**, 1078–1094 (2012).
94. Zivanov, J., Nakane, T. & Scheres, S. H. W. Estimation of high-order aberrations and anisotropic magnification from cryo-EM data sets in RELION-3.1. *IUCr* **7**, 253–267 (2020).
95. Punjani, A., Rubinstein, J. L., Fleet, D. J. & Brubaker, M. A. CryoSPARC: Algorithms for rapid unsupervised cryo-EM structure determination. *Nat. Methods* **14**, 290–296 (2017).
96. Wagner, T. et al. SPHIRE-crYOLO is a fast and accurate fully automated particle picker for cryo-EM. *Commun. Biol.* **2**, 1–13 (2019).
97. Petersen, E. F. et al. UCSF Chimera-A visualization system for exploratory research and analysis. *J. Computational Chem.* **25**, 1605–1612 (2004).
98. Goddard, T. D. et al. UCSF ChimeraX: Meeting modern challenges in visualization and analysis. *Protein Sci.* **27**, 14–25 (2018).
99. Crowe-McAuliffe, C. et al. Structural basis for antibiotic resistance mediated by the *Bacillus subtilis* ABCF ATPase VmlR. *Proc. Natl Acad. Sci. USA* **115**, 8978–8983 (2018).

Acknowledgements

The authors thank C. Ungewickell and S. Rieder for technical assistance, L. Kater and K. Best for support with the pre-processing pipeline of cryo-EM data. We also gratefully acknowledge the support of the Core Facility “Protein Spectroscopy” of the Medical School of the Philipps-University Marburg. We thank the European Synchrotron Radiation Facility (ESRF, Grenoble, France) and the Deutsche Elektronen Synchrotron (DESY, Hamburg, Germany) for excellent support. G.B. acknowledges support from the Deutsche Forschungsgemeinschaft (DFG) from the priority program SPP1879 “Nucleotide second messenger signaling in bacteria”. G.B. thanks the Max-Planck society for generous support. R.B. was supported by the DFG (BE1814/15-1 and TRR174) and the Center for Integrated Protein Science Munich (CiPS-M) to. H.K. is supported by a DFG fellowship through the Graduate School of Quantitative Bioscience Munich (QBM). H.G.K. was supported by the (DFG) through the grants KO2184/8, KO2184/9 (SPP2002); SFB1381, Project-ID 403222702, and RTG 2202, Project-ID 278002225.

Author contributions

Conceptualization: G.B., L.C.; Investigation: C.N.M., H.F.E., H.G.K., H.K., J.M., L.C., O.B., P.G., P.S., W.S.; Visualization: C.N.M., G.B., H.F.E., H.K., L.C.; Funding acquisition: G.B., H.G.K., R.B.; Supervision: G.B., L.C., H.G.K., R.B.; Writing: G.B., H.G.K., H.K., L.C., R.B.; All authors have read and commented on the manuscript.

Funding

Open Access funding enabled and organized by Projekt DEAL.

Competing interests

The authors declare no competing interests.

Additional information

Supplementary information The online version contains supplementary material available at <https://doi.org/10.1038/s41467-022-28675-0>.

Correspondence and requests for materials should be addressed to Laura Czech or Gert Bange.

Peer review information *Nature Communications* thanks the anonymous reviewers for their contribution to the peer review of this work.

Reprints and permission information is available at <http://www.nature.com/reprints>

Publisher's note Springer Nature remains neutral with regard to jurisdictional claims in published maps and institutional affiliations.



Open Access This article is licensed under a Creative Commons Attribution 4.0 International License, which permits use, sharing, adaptation, distribution and reproduction in any medium or format, as long as you give appropriate credit to the original author(s) and the source, provide a link to the Creative Commons license, and indicate if changes were made. The images or other third party material in this article are included in the article's Creative Commons license, unless indicated otherwise in a credit line to the material. If material is not included in the article's Creative Commons license and your intended use is not permitted by statutory regulation or exceeds the permitted use, you will need to obtain permission directly from the copyright holder. To view a copy of this license, visit <http://creativecommons.org/licenses/by/4.0/>.

© The Author(s) 2022

Publication #3

Title: Structural and mechanistic divergence of the small (p)ppGpp synthetases RelP and RelQ


Authors: Wieland Steinchen, Marian S. Vogt, Florian Altegoer, Pietro I. Giammarinaro, Petra Horvatek, Christiane Wolz & Gert Bange.

Journal: Scientific Reports

Year: 2018

Contributions: W.S. and G.B. designed research. W.S., M.S.V., F.A., P.I.G. and P.H. performed experiments. W.S., F.A., C.W. and G.B. analyzed data. W.S. and G.B. prepared the manuscript. All authors commented on the manuscript.

SCIENTIFIC REPORTS



OPEN

Structural and mechanistic divergence of the small (p)ppGpp synthetases RelP and RelQ

Wieland Steinchen¹, Marian S. Vogt¹, Florian Altegoer¹, Pietro I. Giammarinaro¹, Petra Horvatek², Christiane Wolz² & Gert Bange¹

The nutritional alarmones ppGpp and pppGpp (collectively: (p)ppGpp) are nucleotide-based second messengers enabling bacteria to respond to environmental and stress conditions. Several bacterial species contain two highly homologous (p)ppGpp synthetases named RelP (SAS2, YwaC) and RelQ (SAS1, YjbM). It is established that RelQ forms homotetramers that are subject to positive allosteric regulation by pppGpp, but structural and mechanistic insights into RelP lack behind. Here we present a structural and mechanistic characterization of RelP. In stark contrast to RelQ, RelP is not allosterically regulated by pppGpp and displays a different enzyme kinetic behavior. This discrepancy is evoked by different conformational properties of the guanosine-substrate binding site (G-Loop) of both proteins. Our study shows how minor structural divergences between close homologues result in new functional features during the course of molecular evolution.

Microorganisms are able to cope with a broad variety of environmental challenges such as nutrient limitation, antibiotics or changes in abiotic factors like varying pH values or temperatures. To do so, they adapt their metabolism at many different dogmatic processes, e.g. replication, transcription, translation and ribosomal biogenesis^{1–3}. The ‘stringent response’ (SR) is highly conserved among bacteria^{4–6} and plant chloroplasts^{7–9} and although historically only referring to the adaptation to nutrient depletion^{10,11} it has since also been demonstrated to affect virulence^{2,12,13}, biofilm formation¹⁴, development of cellular heterogeneity^{15,16}. Moreover, in some microorganisms the SR has been suggested to affect persister cell formation^{17–19}. Central to the stringent response are the two unusual nucleotides ppGpp and pppGpp (collectively (p)ppGpp or alarmones). Proteins of the RelA/SpoT homology (RSH) superfamily²⁰ catalyze the pyrophosphate transfer from ATP onto the 3'-OH group of GDP or GTP, yielding ppGpp or pppGpp, respectively.

RSH-type synthetases fall into the two classes of ‘long’ and ‘short’ RSH (Fig. 1a^{1,20}). Long RSH-type synthetases are typically composed of multiple domains and harbor a (p)ppGpp hydrolase followed by a (p)ppGpp synthetase domain in their N-terminal part (NTD). Their C-terminal portion (CTD) is highly variable and comprises domains involved in the binding of ribosomes and regulation of the opposing activities found within the NTD^{21–24}. In contrast, short RSH-type alarmone synthetases only contain a synthetase domain and lack the hydrolase domain as well as regulatory domains found within the CTD of long RSH proteins (Fig. 1a). Members of this ‘small alarmone synthetase’ (SAS) family fall into the RelQ (also: SAS1) and RelP (also: SAS2) subclasses and are found in a wide range of bacteria including *Bacillus subtilis*, *Staphylococcus aureus*, *Enterococcus faecalis* and *Listeria monocytogenes*^{20,25–30}. Furthermore, there is evidence for a third class of SAS proteins named RelV in *Vibrio cholerae*³¹. Noteworthy, SAS proteins typically occur in pairs (RelP and RelQ) in the same organism. Nevertheless, despite being highly similar on the amino acid sequence level (Fig. 1a), RelP/RelQ proteins seem to exhibit different functional roles as evidenced from disparate transcriptional profiles and their dependence on different stress signals^{25,27,32}.

So far, only RelQ from *B. subtilis* and *Enterococcus faecalis* have been functionally characterized^{29,30,33}. *BsRelQ* shares the conserved synthetase fold with the long RSH Rel, but in contrast to the monomeric Rel, *BsRelQ* forms highly symmetric homotetramers. Clarification of the catalytic mechanism of *BsRelQ* showed that the

¹Philipps-University Marburg, LOEWE Center for Synthetic Microbiology & Department of Chemistry, Hans-Meerwein-Straße, 35043 Marburg, Germany. ²University of Tübingen, Interfaculty Institute of Microbiology and Infection Medicine, Elfriede-Aulhorn-Straße 6, 72076 Tübingen, Germany. Correspondence and requests for materials should be addressed to W.S. (email: wieland.steinchen@synmikro.uni-marburg.de) or G.B. (email: gert.bange@synmikro.uni-marburg.de)

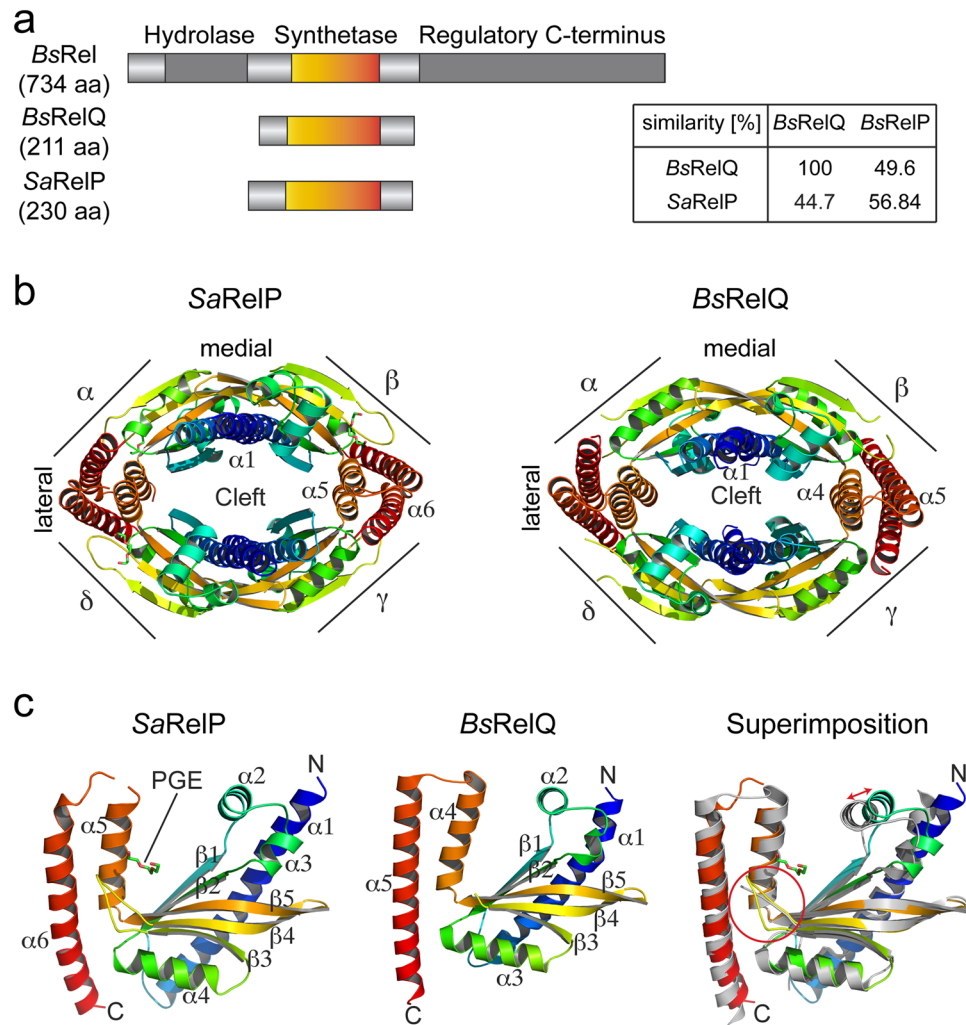


Figure 1. Structural analysis of RelP. **(a)** Domain architecture of the (p)ppGpp synthetases *BsRel*, *BsRelQ* and *SaRelP* drawn to scale. The inset depicts amino acid similarities between RelP and RelQ proteins from *Bacillus subtilis* (*Bs*) and *Staphylococcus aureus* (*Sa*). **(b)** Cartoon representation of the crystal structures of the *SaRelP* (this study) and *BsRelQ* (PDB: 5DEC³³) homotetramers. Each monomer (α - δ) is rainbow-colored from its N- to its C-terminus. **(c)** The (p)ppGpp synthetase monomers of *SaRelP* (left; this study), *BsRelQ* (middle; PDB: 5DEC³³) and their superimposition (right) coloured in rainbow from N- to C-terminus.

enzyme binds ATP and GDP/GTP in a sequential order with ATP being the first substrate and arranges them in a near-attack conformation within the active site to catalyze immediate pyrophosphate transfer. A remarkable feature of the *BsRelQ* homotetramer is the presence of a pronounced cleft in its center providing the binding site for two allosteric pppGpp molecules that, when present, elevate the (p)ppGpp synthetase activity of *BsRelQ*³³. Up to date, no structural characterization of RelP proteins is available. Also, it is unknown whether the (p)ppGpp synthesizing activity of RelP is subject to regulation. Therefore, we set out to provide a structural and biochemical comparison of RelP/RelQ proteins that might explain their divergent functional roles in bacteria.

Results

RelP and RelQ share an equal architecture. To better understand RelP at the molecular level, we determined the crystal structures of RelP homologues from *S. aureus* (*Sa*) and *B. subtilis* (*Bs*) at 2.25 and 3.3 Å resolution, respectively (Table S1). Both, *SaRelP* and *BsRelP* form highly symmetrical and oval-shaped homotetramers with a prominent cleft in their centers highly reminiscent of *BsRelQ* (Figs 1b and S1a). Helix α_1 at the N-terminus of each monomer stabilizes the medial sides of the homotetramer interface via hydrogen bonds and salt bridges (buried surface area of ~ 1200 Å²). Helices α_5 and α_6 at the C-terminus of each monomer establish the lateral sides of the homotetramer interface mainly due to polar contacts (buried surface area of ~ 1200 Å²). The (p)ppGpp synthetase monomers of *SaRelP* and *BsRelP* are highly identical and consist of a mixed β -sheet build by five β -strands (β_1 – β_5) that is surrounded by alpha helices (α_1 – α_6 , Figs 1c and S1b).

Structural comparison of RelP and RelQ reveals the architecture of the homotetramer as well as each of the monomers is highly similar (r.m.s.d. of 1.292 over 138 C α atoms for the RelP and RelQ monomers). However,

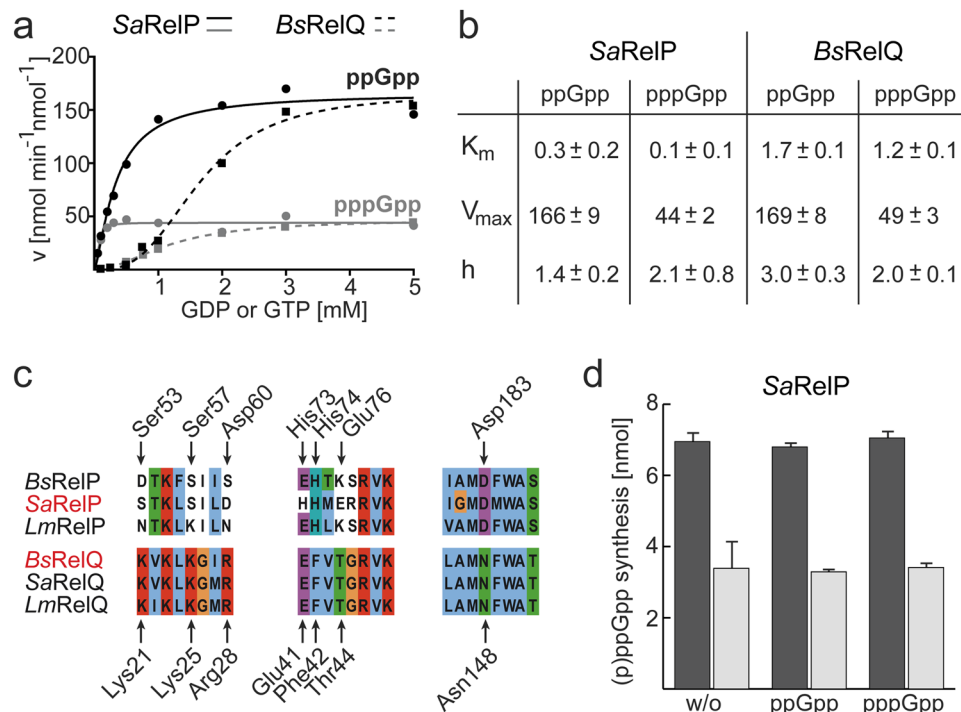


Figure 2. Enzymatic properties of RelP. **(a)** Velocity/substrate (v/S) characteristic of SaRelP (solid lines) and BsRelQ (dashed lines) for ppGpp (black) and pppGpp (grey). Velocity is given in nmol per minute per nmol SaRelP/BsRelQ. The data for BsRelQ have been re-plotted from³³ to enable direct comparison of both enzymatic activities. Data of one representative experiment are shown. **(b)** Kinetic parameters of (p)ppGpp synthesis by SaRelP and BsRelQ. **(c)** Amino acid sequence alignment of residues conferring pppGpp binding to the allosteric cleft of RelQ and their equivalent positions in RelP proteins from *Bacillus subtilis* (*Bs*), *Staphylococcus aureus* (*Sa*) and *Listeria monocytogenes* (*Lm*). Amino acid numberings relate to SaRelP (above) and BsRelQ (below). **(d)** Synthesis of ppGpp (black) and pppGpp (grey) by SaRelP is unaffected by the presence of ppGpp or pppGpp. Error bars indicate the SD of three independent replicates.

RelP and RelQ differ in the orientation of helix α_2 , which appears to be shifted approximately 3 Å towards the active site center in RelQ when compared to RelP (Fig. 1c; right panel). Another interesting observation is that the loop connecting β_3 and β_4 , which is disordered in the structure of BsRelQ, could be resolved in both structures of RelP (Fig. 1c). Taken together, RelQ and RelP share highly conserved ternary and quaternary structures, but also reveal subtle differences that might be of functional relevance (see below).

RelP and RelQ differ in their (p)ppGpp synthetase activity. The most distinguished features of BsRelQ lie in the apparent positive cooperativity of (p)ppGpp synthesis and its susceptibility to allosteric stimulation of by pppGpp but not ppGpp³³. To test whether both features would also be present in RelP, we performed an *in-depth* kinetic analysis. We used the same buffer composition for characterization of SaRelP as previously for BsRelQ to ensure maximal comparability. SaRelP was incubated together with 5 mM ATP and varying concentrations of GDP or GTP (Of note: BsRelP exhibited no (p)ppGpp synthetase activity under our assay conditions for unclear reasons). SaRelP synthesized ppGpp more efficiently than pppGpp as evidenced from an approximately 4-fold higher V_{max} value (Fig. 2a and b). A similar preference for the product ppGpp was previously observed for BsRelQ³³ and RelQ from other organisms^{25,30}. However, the K_m values for (p)ppGpp synthesis drastically differ between both enzymes in that they are significantly lower for SaRelP (i.e. 0.3 ± 0.2 for GDP and 0.1 ± 0.1 for GTP) than for BsRelQ (i.e. 1.7 ± 0.1 for GDP and 1.2 ± 0.1 for GTP; Fig. 2b). It also seemed to us that SaRelP monomers displays less cooperativity within the tetramer than BsRelQ indicated by Hill coefficients closer to 1 (Fig. 2b).

Amino acid sequence analysis of RelP shows that the amino acid residues required for allosteric binding of pppGpp to RelQ are replaced in RelP proteins (Fig. 2c). Indeed, this different set of amino acids found in SaRelP seems incapable to coordinate pppGpp in similar fashion as BsRelQ (Fig. S2) strongly suggesting to us that SaRelP cannot be allosterically stimulated by the alarmone. In agreement with our structural analysis, no change in the enzymatic activity of SaRelP was observed in the absence and the presence of ppGpp or pppGpp (Fig. 2d). Taken together, RelQ and RelP do not differ much in their V_{max} values of (p)ppGpp synthesis, while significantly differing in the K_m values. Moreover, RelP is not subject to allosteric stimulation by pppGpp.

ATP-binding to RelP and RelQ is identical. To gain further insights into the disparate enzymatic activities of RelQ and RelP, we attempted to solve the structure of SaRelP in presence of the non-hydrolysable ATP analogue AMPCPP (α,β -methyleneadenosine 5'-triphosphate) and GDP or GTP. However, we could only obtain crystals and solve the structure of SaRelP in presence of AMPCPP (Fig. S3a and Table S1). Coordination of

AMPCPP within all the four active sites of *SaRelP* is guided by π -stacking interactions of the adenine base with the arginine residues 78 and 112 of *SaRelP* (Fig. S3b). The ribose moiety of the adenosine is coordinated by hydrogen bonding via His190. Interactions with the phosphate moieties of AMPCPP are mainly established by lysine and arginine residues residing in $\beta 1$ and $\alpha 2$ (i.e. Lys80, Lys88 and Arg91) and Ser84 contacting the 5' α -phosphate. AMPCPP adopts a kinked conformation that is enforced by a magnesium ion coordinated by Asp107 and Glu174 (Fig. S3b). An identical conformation of AMPCPP is observed in the active site of *BsRelP* (Fig. S3c). As all ATP-coordinating and catalytic amino acid residues are strictly conserved among RelP/RelQ proteins (Fig. S3d), we suspect a common ATP-binding mode and mode of catalysis.

G-Loop rigidity governs the activity of RelP and RelQ. If binding of ATP to RelP and RelQ is identical (see above), then the different enzymatic properties of both enzymes should originate from differences in binding of GDP/GTP and/or a different susceptibility to allosteric stimulation by pppGpp. As mentioned above, our structural analysis of RelP and RelQ indicated a different conformational flexibility of the loop connecting strands $\beta 3$ and $\beta 4$ (Fig. 1c). This loop contains a conserved tyrosine residue (i.e. Tyr151 in *SaRelP* and Tyr116 in *BsRelQ*, Fig. 3a) critical to guanosine nucleotide binding in all (p)ppGpp synthetases. Therefore, we decided to term the loop connecting $\beta 3$ and $\beta 4$ 'G-Loop'. To our surprise, the different configurations of the G-Loop seem to be a common theme among RelP/RelQ proteins. In the apo- and ATP-bound states of *BsRelQ*, the G-Loop is disordered, and could therefore not be modeled in these structures (Fig. 3b). In stark contrast, the G-Loop of *SaRelP* was well-ordered and could be unambiguously modeled in its apo- and ATP-bound structures (Fig. 3c). We speculated that the difference in enzymatic activity between RelQ and RelP is founded in the different conformational properties of the G-Loop.

Inspection of the amino acids of the G-Loop reveals the presence of proline in RelP proteins with no correspondent in RelQ (Fig. 3a). We hypothesized that the absence of this proline in RelQ renders the G-Loop less rigid, while its presence in RelP results in a well-ordered G-Loop that might easily facilitate GDP/GTP coordination (Fig. 3d). We challenged this notion by introducing proline into the disordered G-Loop of RelQ (i.e. *BsRelQ*-H111P). *BsRelQ*-H111P produces (p)ppGpp as efficient as *SaRelP* and the V_{\max} (i.e. 243 ± 9 and 194 ± 8 $\text{nmol min}^{-1} \text{nmol}^{-1}$ for ppGpp and pppGpp, respectively), K_m (i.e. 0.4 ± 0.2 for GDP and 1.9 ± 0.2 for GTP) and Hill-coefficient (i.e. 1.6 ± 0.2 for GDP and 1.0 ± 0.1 for GTP) of *BsRelQ*-H111P more resemble *SaRelP* than *BsRelQ* (Fig. 3e and compare to Fig. 2a and b). Moreover and unlike *BsRelQ*, *BsRelQ*-H111P is not amenable to allosteric stimulation by pppGpp (Fig. 3f). These results demonstrate a strong dependence of RelP/RelQ activity on the rigidity of the G-Loop.

Allosteric stimulation of RelQ by pppGpp acts via the G-Loop. Our results indicated that RelP proteins synthesize (p)ppGpp more efficiently than RelQ, because RelP can more readily bind the GDP/GTP substrate through increased rigidity of the G-Loop. Moreover, pppGpp stimulates the activity of RelQ, while it does not for RelP (Figs 2d and 3f). Therefore, we hypothesized that binding of pppGpp to the central cleft of RelQ might be translated into an increased (p)ppGpp synthesis via the G-Loop. Superimposition of the crystal structures of apo-*BsRelQ* and pppGpp-bound *BsRelQ* (PDB: 5DEC and 5DED³³, respectively) allowed tracing a structurally possible path, which would connect the presence of pppGpp within the allosteric cleft of RelQ with the G-loop (Fig. 4). In short, two opposing subunits of the *BsRelQ* tetramer are involved in coordination of one allosteric pppGpp in the central cleft^{1,33}. Coordination of pppGpp leads to a displacement of Phe42, Thr44 and Asn148 by $\sim 1\text{--}2$ Å towards the cleft (Figs 4b; S2). Helix $\alpha 4$ comprising Asn148 follows this movement and rotates by approximately 15° in a counterclockwise manner. This movement is relayed onto helix $\alpha 5$ through the hydrophobic core between both helices constituted by Phe149 ($\alpha 4$), Leu183 and Met187 (both $\alpha 5$, Fig. 4c). Rotation of $\alpha 5$ turns Glu178 towards the G-Loop and enables formation of a salt bridge between Glu178 and Arg117 (Fig. 4c). Further contacts between $\alpha 5$ and the G-Loop are established between His111/Glu178 and Glu113/Gln174 (Fig. 4d).

To probe the participation of these amino acids, we replaced them by alanine and measured the (p)ppGpp synthesis of the resulting *BsRelQ* variants in pppGpp-dependent manner (Figs 4e and S4). Variation of His111 and Glu113 does not affect stimulation of *BsRelQ*. However, upon replacement of Gln174 and Glu178 the pppGpp-stimulatory effect is decreased and completely abolished when Arg117 is replaced (Figs 4e and S4).

Finally, we tested how the allosteric pppGpp affects the enzyme kinetic behaviour of *BsRelQ* by determining the (p)ppGpp synthesis *BsRelQ* in presence of different concentrations of pppGpp (i.e. 0, 2.5, 10, 25, 100, 250 μM). While addition of increasing amounts of pppGpp to *BsRelQ* does only slightly elevate V_{\max} of (p)ppGpp synthesis, the K_m values for the substrates GDP and GTP decrease dramatically (Figs 4f and S5). Also, *BsRelQ* displays a less cooperative behaviour indicated by a loss of the sigmoidal shape of the v/S characteristic when pppGpp is present. It therefore appears to us that the apparent cooperativity of *BsRelQ* rather originates from pppGpp produced during the enzymatic reaction rather than from a positive cooperativity between the four active sites of *BsRelQ* (compare to Fig. 2a and ref.²⁹). Noteworthy, at the highest concentration of pppGpp tested (i.e. 250 μM), the enzyme kinetic behavior of *BsRelQ* is highly similar to *BsRelQ*-H111P and *SaRelP*.

These results show that allosteric binding of pppGpp causes structural rearrangements of *BsRelQ* that are translated into an increased (p)ppGpp synthetase activity via an induced structural rigidity of the G-Loop.

Discussion

Two small alarmone synthetases (i.e. RelP/SAS2 and RelQ/SAS1) are typically found together in members of the Firmicutes phylum e.g. *B. subtilis*, *S. aureus* or *L. monocytogenes*²⁰. RelP and RelQ share similarities of ~ 50 percent on the amino acid sequence level. Our structural analysis shows that RelP and RelQ possess a highly similar (p)ppGpp synthetase domain and both establish highly similar homotetrameric complexes (Fig. 1b and c). Nevertheless, both enzymes decisively differ in their ability to produce (p)ppGpp in that RelP is much more active

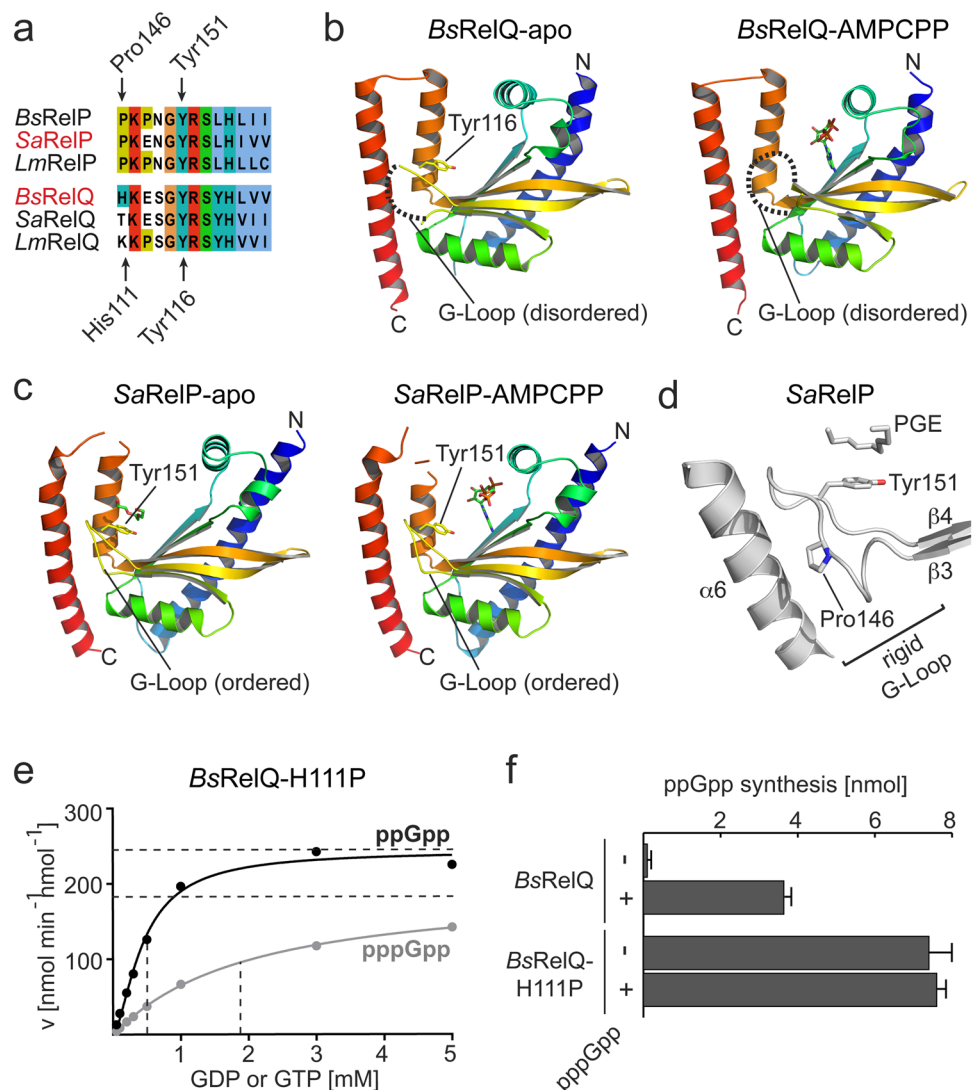


Figure 3. G-loop rigidity dictates the activity of RelP and RelQ. **(a)** Amino acid sequence alignment of the G-Loops found in RelP and RelQ proteins from *Bacillus subtilis* (*Bs*), *Staphylococcus aureus* (*Sa*) and *Listeria monocytogenes* (*Lm*). Amino acid numberings relate to *SaRelP* (above) and *BsRelQ* (below). **(b)** Crystal structures of the apo- and AMPCPP-bound state of *BsRelQ* (PDB: 5DEC and 5F2V³³, respectively) show a disordered G-Loop (dashed line). **(c)** Crystal structures of the apo- and AMPCPP-bound state of *SaRelP* (this study) show a clearly ordered G-Loop. **(d)** The presence of Pro146 in *SaRelP* confers a high rigidity of the G-Loop. **(e)** The v/S characteristic of ppGpp (black) and pppGpp (grey) synthesis of the *BsRelQ*-H111P variant. Velocity is given in nmol per minute per nmol *BsRelQ*-H111P. Dashed lines indicate the K_m and V_{max} values. Data of one representative experiment are shown. **(f)** ppGpp synthesis of *BsRelQ* and its variants in absence (–) and presence (+) of pppGpp. Error bars indicate the SD of three independent replicates.

than RelQ (Fig. 2a). Why is that the case? Our analysis demonstrates that binding of ATP proceeds in identical fashion in RelP/RelQ proteins, because both proteins harbor an identical architecture of their ATP-coordination site (Fig. S3). However, RelP and RelQ inherently differ in their ability to coordinate the GDP and GTP substrates. This is caused by a different structural flexibility of their G-Loops. While the G-loop of RelQ is highly disordered, the equivalent region of RelP is highly ordered and can therefore readily coordinate GDP/GTP (Fig. 3). However, the activity of RelQ can be enhanced by coordination of pppGpp within the central cleft³³. This pppGpp results in a rearrangement of helices α_4 and α_5 at the lateral sides of the RelQ homotetramer and, by establishing a salt bridge between Glu178 (α_5) and Arg117 (G-Loop) (Fig. 4), results in a more ordered (and active) conformation of the G-Loop. The (p)ppGpp synthetase activity of the so-stimulated RelQ resembles RelP. Notably, the K_m values obtained for *SaRelP* (Fig. 2a and b) and allosterically stimulated *BsRelQ* (Figs S4 and S5) accord with the intracellular concentrations of GDP and GTP, estimated as 200–500 μ M and 1–5 mM, respectively^{34,35}. Under these conditions, both enzymes are highly sensitive to small changes in GDP/GTP levels. Non-stimulated *BsRelQ*, in contrast, appears rather insensitive to changes in GDP/GTP levels because of its high K_m values for both substrates (Fig. 2a and b). In summary, RelP always appears as a highly active alarmone synthetase, while

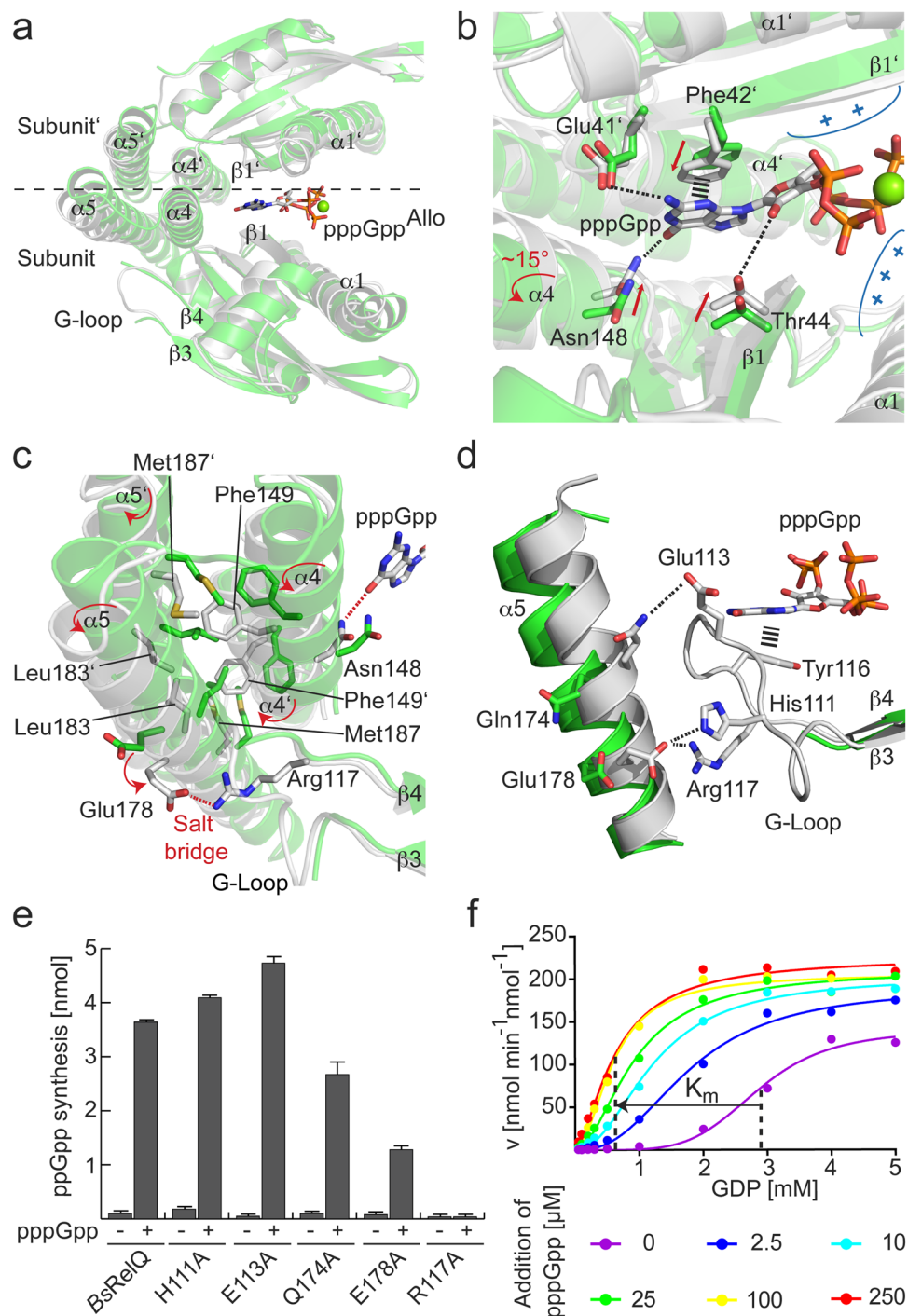


Figure 4. Allosteric binding of pppGpp to RelQ stabilizes the G-Loop. **(a)** Superimposition of one half of the tetramers of BsRelQ (white, PDB: 5DEC³³) and BsRelQ-pppGpp (green, PDB: 5DED³³). **(b)** Coordination of pppGpp in the central cleft of BsRelQ by amino acids residing in $\alpha 1$, $\beta 1$ and $\alpha 4$ results in conformational changes (indicated by red arrows). **(c)** Interaction of Asn148 with pppGpp causes a rotation of $\alpha 4$ that is transmitted onto $\alpha 5$ through the hydrophobic core established by Phe149, Leu183 and Met187 from two subunits of BsRelQ. Concerted rotation of helices $\alpha 4$ and $\alpha 5$ enables formation of a salt bridge between Glu178 and Arg117. **(d)** Interactions between amino acid side chains from $\alpha 5$ and the G-Loop of BsRelQ are only established in presence of pppGpp and result in ordering of the G-Loop. **(e)** ppGpp synthesis by BsRelQ and BsRelQ variants in absence (–) and presence (+) of pppGpp. Error bars indicate the SD of three independent replicates. **(f)** The v/S characteristic of ppGpp synthesis by BsRelQ in presence of different amounts of pppGpp. The velocity is given in nmol per minute per nmol BsRelQ. The K_m values of BsRelQ in absence and presence of 250 μ M pppGpp are indicated by dashed lines. Data of one representative experiment are shown.

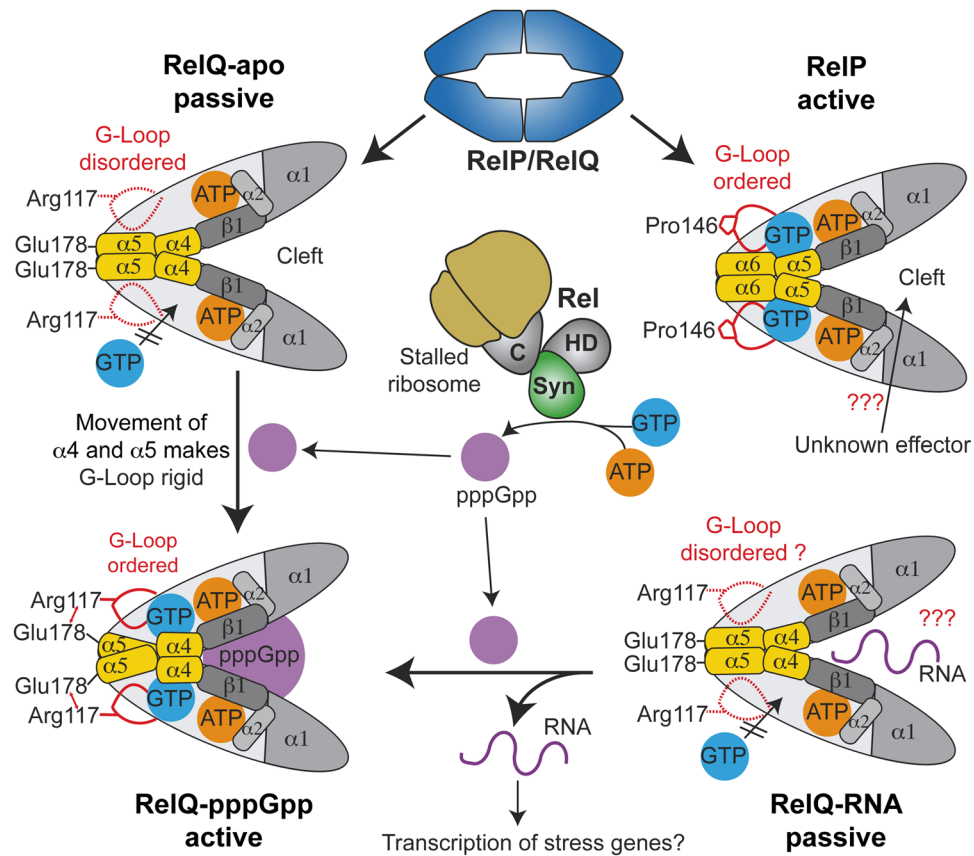


Figure 5. Mechanistic framework of Rel, RelP and RelQ. Three states of RelQ differing in (p)ppGpp synthetase activity are known: apo-RelQ and the RNA-bound RelQ are catalytically passive states, while RelQ bound to the alarmone pppGpp is an active (p)ppGpp synthetase. In both passive states, RelQ readily binds ATP (orange). However, GTP (blue) is only poorly coordinated, because of the disordered nature of the G-Loop. Binding of pppGpp (violet) into the allosteric cleft of RelQ results in a concerted rearrangement of $\alpha 4$ and $\alpha 5$ (yellow) that rigidifies the G-Loop, enables tight coordination of GTP and renders RelQ highly active. Such pppGpp molecules might originate from Rel's (p)ppGpp synthetase activity, which is enhanced under conditions of amino acid starvation. In such a case, pppGpp might bind into to the unoccupied central cleft of apo-RelQ or could competitively replace an RNA molecule from the cleft as shown previously²⁹. The G-Loop of RelP is always ordered enforcing the active state of RelP. Whether an RNA or any other unknown effector molecule can bind into the central cleft of RelP is not known.

RelQ can switch between a passive state with low and an active (i.e. pppGpp-stimulated) state with high (p)ppGpp synthetase activity.

Having elucidated the different properties of RelP and RelQ, we wondered how this divergence might be relevant for the bacterial cell. In our current understanding, RelQ can appear in two passive states. In the apo-state, RelQ's central cleft is unoccupied while in the RNA-bound state a so far uncharacterized RNA^{29,36} might reside in the central cleft (Fig. 5). We suspect that RelQ is predominantly found in either of those passive states in nutrient-rich conditions, because the (p)ppGpp hydrolytic activity of Rel should keep (p)ppGpp levels below the limit of RelQ stimulation. When the microorganism is suddenly confronted with nutrient limitation, Rel will recognize and bind to stalled ribosomes. When doing so, Rel could provide the pppGpp needed to bring RelQ into its active (i.e. pppGpp-bound) state by the intricate mechanism involving helical rearrangements and loop stabilization (Fig. 5). RelQ would then simply serve as an amplifier of the stress signal given by Rel. Additionally, the RNA bound to RelQ would be outcompeted by pppGpp and might result in the transcription of stress genes. Unfortunately, it is unclear so far, which genes might be differentially regulated, as the 'real' RNA bound by RelQ *in vivo* still remains to be identified^{29,36}. Seemingly, RelQ's activity is intensively coupled to Rel (Fig. 5). Although experimental data for this functional link of Rel and RelQ are missing so far, the outlined scenario would provide an elegant way for an instant rise of (p)ppGpp levels dominated by the activity Rel and aided by RelQ.

RelP, in contrast to RelQ, is always a highly active enzyme that possesses all features enabling efficient (p)ppGpp synthesis, mainly an ordered G-Loop (Fig. 5). RelP should therefore not rely on the signal provided by Rel but might rather work independently. The presence of a central cleft within the tetramer of RelP nevertheless allows hypothesizing that an unknown factor might regulate the activity of RelP (Fig. 5). Noteworthy, the different activities of RelP and RelQ seem to be perfectly matched with their disparate transcriptional profiles. The switchable RelQ, predominantly transcribed during logarithmic growth²⁷, can counteract a sudden nutrient limitation

with the help of the Rel protein. The presence of RelP during logarithmic growth, however, might be detrimental for the microorganism. Consequently, RelP transcripts appear only during early stationary phase and in response to treatment with antibiotics, ethanol, high salt and acidic or alkaline pH stress conditions^{25,37,38}. Also, RelP has been implicated in mediating inactivation of ribosomes by forming translation-inactive ribosome dimers thereby providing an elegant and fast shutdown mechanism for the bacterial metabolism^{32,39}. In conclusion, our study strengthens the understanding of disparate roles of RelP/RelQ proteins and sets the stage for future investigations on this class of (p)ppGpp synthetases.

Materials and Methods

Cloning and mutagenesis. Genes encoding for RelP (*ywaC* and SA2297, respectively) were amplified from *B. subtilis* PY79 and *S. aureus* strain Newman genomic DNA by polymerase chain reaction using Phusion High-Fidelity DNA polymerase (NEB) according to the manufacturer's manual. The *forward* primer for SA2297 encoded a hexahistidine-tag in frame with the DNA sequence of *relP*. The *forward* primer for *ywaC* encoded a strep-tag in frame with the DNA sequence. The resulting PCR fragments were cloned into the pET24d(+) vector (Novagen) at the *NcoI/XhoI* restriction sites. Mutations within RelP were generated by overlapping PCR.

Protein Production and Purification. *Escherichia coli* BL21 (DE3) (NEB) carrying the plasmids for His-tagged proteins were grown in lysogeny broth (LB)-medium supplemented with 50 µg/ml kanamycin and 12.5 g/l D(+)-lactose-monohydrate for 20 h at 30 °C. Cells were harvested by centrifugation (3500 × g, 20 min, 4 °C), resuspended in lysis buffer (20 mM of HEPES-Na pH 8.0, 250 mM NaCl, 40 mM imidazole, 20 mM MgCl₂, 20 mM KCl) and lysed by two passages through the M-110L Microfluidizer (Microfluidics). After centrifugation (47850 × g, 20 min, 4 °C), the clear supernatant was loaded on a 1-ml HisTrap column (GE Healthcare) equilibrated with 10 column volumes (CV) lysis buffer. After washing with 10 CV of lysis buffer, the protein was eluted with 5 CV elution buffer (lysis buffer containing 500 mM imidazole). The protein was concentrated (Amicon Ultracel-10K (Millipore)) and applied to size-exclusion chromatography (SEC) on a HiLoad 26/600 Superdex 200 pg column (GE Healthcare) equilibrated in SEC buffer (20 mM of HEPES-Na, pH 7.5, 200 mM NaCl 20 mM MgCl₂, 20 mM KCl). Protein containing fractions were pooled, concentrated (Amicon Ultracel-10K (Millipore)), deep-frozen in liquid nitrogen and stored at −80 °C. Protein concentration was determined by a spectrophotometer (NanoDrop Lite, Thermo Scientific).

BsRelP was purified by a similar procedure using a 1-ml StrepTrap column (GE Healthcare). Lysis buffer without imidazole was employed for cell lysis, column equilibration and washing and elution from the column was conducted with 5 CV of SEC buffer containing 2.5 mM desthiobiotin.

Preparation of ppGpp and pppGpp. (p)ppGpp was produced essentially as described previously³³. In brief, 5 µM SAS1 were incubated in SEC buffer together with 10 mM ATP and 10 mM GDP for 30 min at 37 °C to produce ppGpp or together with 10 mM ATP and 10 mM GTP for 2 h at 37 °C to produce pppGpp. Afterwards, the reaction was mixed with the same volume of chloroform and centrifuged (17300 × g, 5 min, 4 °C). The aqueous phase was removed and the organic phase mixed with one volume of double-distilled water and centrifuged (17300 × g, 5 min, 4 °C). The combined aqueous phases were subjected to anion-exchange chromatography using a ResourceQ. 6-ml column (GE Healthcare) at a flow rate of 6 ml/min and the nucleotides eluted with a gradient of NaCl. Fractions containing ppGpp or pppGpp were pooled followed by addition of lithium chloride with a concentration of 1 M and four volumes of ethanol. The suspension was then incubated at −20 °C for 20 min and centrifuged (5000 × g, 20 min, 4 °C). The resulting pellets were washed with absolute ethanol, dried and stored at −20 °C. Quality of the so-prepared alarmones was controlled by HPLC and yielded ppGpp and pppGpp in purities of 98% and 95%, respectively.

Kinetic analysis of RelP/RelQ. The enzyme kinetic behavior of RelP and RelQ (compare to Figs 2a, 3e, 4f and S5), were monitored by HPLC. Reactions were prepared in SEC buffer supplemented with 100 mM HEPES-Na pH 7.5 by incubating 0.2 µM protein together with 5 mM ATP and varying concentrations of GDP or GTP (i.e. 0.05, 0.1, 0.2, 0.3, 0.5, 1, 3 and 5 mM; 2 and 4 mM were included where necessary). For the analysis of pppGpp affecting the kinetic behavior of *BsRelQ*, pppGpp was also added to the reaction in concentrations of 0/2.5/10/25/100/250 µM. Samples were taken after different time points (i.e. 2, 4, 6, 8 and 10 minutes) and stopped as follows: two volume parts of chloroform were added to the sample, thoroughly mixed for 15 seconds, kept at 95 °C for 15 seconds and flash-frozen in liquid nitrogen. While thawing, the samples were centrifuged (17300 × g, 30 min, 4 °C) and the aqueous phase used for analysis. HPLC measurements were conducted on an Agilent 1100 Series system (Agilent technologies) equipped with a C18 column (EC 250/4.6 Nucleodur HTec 3 µM; Macherey-Nagel). Nucleotides were eluted isocratically with a buffer containing 50 mM KH₂PO₄, 50 mM K₂HPO₄, 10 mM TPAB (tetrapentylammonium bromide) and 20% (v/v) acetonitrile and detected at 260 nm wavelength in agreement with standards. Analysis of enzymatic measurements was performed with GraphPad Prism version 6.04 for Windows, (GraphPad Software, San Diego, California, USA). The velocity of (p)ppGpp synthesis was obtained by linear regression of the amount of AMP quantified after different incubation times. Kinetic parameters (K_m , V_{max} and the Hill coefficient (h) ± standard deviation) were obtained from the fit of the v/S characteristic according to the equation $v = V_{max} S^h / (K_m^h + S^h)$.

Stimulation of RelP/RelQ by (p)ppGpp. In experiments probing the stimulatory effect of (p)ppGpp (compare to Figs 2d, 3f, 4e and S4), 0.2 µM RelP/RelQ were incubated together with 5 mM ATP and 0.25 mM GDP/GTP in presence or absence of 200 µM (p)ppGpp for 10 minutes at 37 °C. The reactions were stopped and analyzed as described above.

Crystallization and structure determination. Crystallization was carried out at room temperature by sitting drop vapor diffusion in SWISSCI MRC 2-well plates (Jena Bioscience) with a reservoir volume of 50 μ l and the drop containing 0.5 μ l of protein and crystallization solution each. Crystals of *BsRelP* were obtained from a 10 mg/ml solution after 1 week from 0.1 M CHES pH 9.5 and 30% (w/v) PEG 3000. Crystals of *SaRelP* were obtained from a 15 mg/ml solution after 1 week in 0.1 M CHES pH 9.5 and 40% (v/v) PEG600. For crystallization of *SaRelP*-AMPCPP, a 15 mg/ml concentrated protein solution was incubated together with 5 mM AMPCPP for 30 minutes on ice. Crystals of *SaRelP*-AMPCPP were obtained after 2 days from 0.1 M Tris pH 8.5, 0.2 M lithium sulfate and 30% (w/v) PEG4000.

To harvest crystals, 0.5 μ l of a cryo-protecting solution containing mother liquor supplemented with 20% (v/v) glycerol was added to the drop, crystals looped and flash-frozen in liquid nitrogen. Diffraction data were collected at the European Synchrotron Radiation Facility (ESRF) Grenoble, France, at beamlines ID23-1 and ID29 under laminar nitrogen flow at 100 K (Oxford Cryostream 700 Series) with a DECTRIS PILATUS 6M detector. Data were processed with XDS⁴⁰ and CCP4-implemented SCALA⁴¹. Crystal structures were determined by molecular replacement (MR) employing *BsRelQ* (PDB: 5DEC³³) as search model using the CCP4-implemented PHASER⁴¹. Structures were manually built in COOT⁴² and refined with PHENIX⁴³. Figures were prepared with PYMOL (www.pymol.org).

Accession Codes

Atomic coordinates and structure factors were deposited in the Protein Data Bank (PDB) under 6FGJ (apo-*SaRelP*), 6FGK (apo-*BsRelP*) and 6FGX (AMPCPP-bound *SaRelP*).

References

- Steinchen, W. & Bange, G. The magic dance of the alarmones (p)ppGpp. *Molecular microbiology* **101**, 531–544, <https://doi.org/10.1111/mmi.13412> (2016).
- Dalebroux, Z. D. & Swanson, M. S. ppGpp: magic beyond RNA polymerase. *Nature reviews. Microbiology* **10**, 203–212, <https://doi.org/10.1038/nrmicro2720> (2012).
- Kanjee, U., Ogata, K. & Houry, W. A. Direct binding targets of the stringent response alarmone (p)ppGpp. *Molecular microbiology* **85**, 1029–1043, <https://doi.org/10.1111/j.1365-2958.2012.08177.x> (2012).
- Boutte, C. C. & Crosson, S. Bacterial lifestyle shapes stringent response activation. *Trends in microbiology* **21**, 174–180, <https://doi.org/10.1016/j.tim.2013.01.002> (2013).
- Potrykus, K. & Cashel, M. (p)ppGpp: still magical? *Annual review of microbiology* **62**, 35–51, <https://doi.org/10.1146/annurev.micro.62.081307.162903> (2008).
- Liu, K., Bittner, A. N. & Wang, J. D. Diversity in (p)ppGpp metabolism and effectors. *Current opinion in microbiology* **24**, 72–79, <https://doi.org/10.1016/j.mib.2015.01.012> (2015).
- Masuda, S. *et al.* The bacterial stringent response, conserved in chloroplasts, controls plant fertilization. *Plant & cell physiology* **49**, 135–141, <https://doi.org/10.1093/pcp/pcm177> (2008).
- van der Biezen, E. A., Sun, J., Coleman, M. J., Bibb, M. J. & Jones, J. D. Arabidopsis RelA/SpoT homologs implicate (p)ppGpp in plant signaling. *Proceedings of the National Academy of Sciences of the United States of America* **97**, 3747–3752, <https://doi.org/10.1073/pnas.060392397> (2000).
- Takahashi, K., Kasai, K. & Ochi, K. Identification of the bacterial alarmone guanosine 5'-diphosphate 3'-diphosphate (ppGpp) in plants. *Proceedings of the National Academy of Sciences of the United States of America* **101**, 4320–4324, <https://doi.org/10.1073/pnas.0308555101> (2004).
- Stent, G. S. & Brenner, S. A genetic locus for the regulation of ribonucleic acid synthesis. *Proceedings of the National Academy of Sciences of the United States of America* **47**, 2005–2014 (1961).
- Cashel, M. The control of ribonucleic acid synthesis in *Escherichia coli*. IV. Relevance of unusual phosphorylated compounds from amino acid-starved stringent strains. *The Journal of biological chemistry* **244**, 3133–3141 (1969).
- Weiss, L. A. & Stallings, C. L. Essential roles for *Mycobacterium tuberculosis* Rel beyond the production of (p)ppGpp. *Journal of bacteriology* **195**, 5629–5638, <https://doi.org/10.1128/JB.00759-13> (2013).
- Vogt, S. L. *et al.* The stringent response is essential for *Pseudomonas aeruginosa* virulence in the rat lung agar bead and *Drosophila melanogaster* feeding models of infection. *Infection and immunity* **79**, 4094–4104, <https://doi.org/10.1128/IAI.00193-11> (2011).
- He, H., Cooper, J. N., Mishra, A. & Raskin, D. M. Stringent response regulation of biofilm formation in *Vibrio cholerae*. *Journal of bacteriology* **194**, 2962–2972, <https://doi.org/10.1128/JB.00014-12> (2012).
- Ababneh, Q. O. & Herman, J. K. RelA inhibits *Bacillus subtilis* motility and chaining. *Journal of bacteriology* **197**, 128–137, <https://doi.org/10.1128/JB.02063-14> (2015).
- Ababneh, Q. O. & Herman, J. K. CodY Regulates SigD Levels and Activity by Binding to Three Sites in the *fla/che* Operon. *Journal of bacteriology* **197**, 2999–3006, <https://doi.org/10.1128/JB.00288-15> (2015).
- Lewis, K. Persister cells. *Annual review of microbiology* **64**, 357–372, <https://doi.org/10.1146/annurev.micro.112408.134306> (2010).
- Amato, S. M., Orman, M. A. & Brynildsen, M. P. Metabolic control of persister formation in *Escherichia coli*. *Molecular cell* **50**, 475–487, <https://doi.org/10.1016/j.molcel.2013.04.002> (2013).
- Conlon, B. P. *et al.* Persister formation in *Staphylococcus aureus* is associated with ATP depletion. *Nature microbiology* **1**, 16051, <https://doi.org/10.1038/nmicrobiol.2016.51> (2016).
- Atkinson, G. C., Tenson, T. & Hauryliuk, V. The RelA/SpoT homolog (RSH) superfamily: distribution and functional evolution of ppGpp synthetases and hydrolases across the tree of life. *PLoS one* **6**, e23479, <https://doi.org/10.1371/journal.pone.0023479> (2011).
- Brown, A., Fernandez, I. S., Gordiyenko, Y. & Ramakrishnan, V. Ribosome-dependent activation of stringent control. *Nature* **534**, 277–280, <https://doi.org/10.1038/nature17675> (2016).
- Arenz, S. *et al.* The stringent factor RelA adopts an open conformation on the ribosome to stimulate ppGpp synthesis. *Nucleic acids research* **44**, 6471–6481, <https://doi.org/10.1093/nar/gkw470> (2016).
- Loveland, A. B. *et al.* Ribosome*RelA structures reveal the mechanism of stringent response activation. *eLife* **5**, <https://doi.org/10.7554/eLife.17029> (2016).
- Mechold, U., Murphy, H., Brown, L. & Cashel, M. Intramolecular regulation of the opposing (p)ppGpp catalytic activities of Rel(Seq), the Rel/Spo enzyme from *Streptococcus equisimilis*. *Journal of bacteriology* **184**, 2878–2888 (2002).
- Geiger, T., Kastle, B., Gratani, F. L., Goerke, C. & Wolz, C. Two small (p)ppGpp synthetases in *Staphylococcus aureus* mediate tolerance against cell envelope stress conditions. *Journal of bacteriology* **196**, 894–902, <https://doi.org/10.1128/JB.01201-13> (2014).
- Lemos, J. A., Lin, V. K., Nascimento, M. M., Abranches, J. & Burne, R. A. Three gene products govern (p)ppGpp production by *Streptococcus mutans*. *Molecular microbiology* **65**, 1568–1581, <https://doi.org/10.1111/j.1365-2958.2007.05897.x> (2007).
- Nanamiya, H. *et al.* Identification and functional analysis of novel (p)ppGpp synthetase genes in *Bacillus subtilis*. *Molecular microbiology* **67**, 291–304, <https://doi.org/10.1111/j.1365-2958.2007.06018.x> (2008).

28. Srivatsan, A. *et al.* High-precision, whole-genome sequencing of laboratory strains facilitates genetic studies. *PLoS genetics* **4**, e1000139, <https://doi.org/10.1371/journal.pgen.1000139> (2008).
29. Beljantseva, J. *et al.* Negative allosteric regulation of *Enterococcus faecalis* small alarmone synthetase RelQ by single-stranded RNA. *Proceedings of the National Academy of Sciences of the United States of America* **114**, 3726–3731, <https://doi.org/10.1073/pnas.1617868114> (2017).
30. Gaca, A. O. *et al.* From (p)ppGpp to (pp)pGpp: Characterization of Regulatory Effects of pGpp Synthesized by the Small Alarmone Synthetase of *Enterococcus faecalis*. *Journal of bacteriology* **197**, 2908–2919, <https://doi.org/10.1128/JB.00324-15> (2015).
31. Das, B., Pal, R. R., Bag, S. & Bhadra, R. K. Stringent response in *Vibrio cholerae*: genetic analysis of spoT gene function and identification of a novel (p)ppGpp synthetase gene. *Molecular microbiology* **72**, 380–398, <https://doi.org/10.1111/j.1365-2958.2009.06653.x> (2009).
32. Tagami, K. *et al.* Expression of a small (p)ppGpp synthetase, YwaC, in the (p)ppGpp(0) mutant of *Bacillus subtilis* triggers YvyD-dependent dimerization of ribosome. *Microbiology Open* **1**, 115–134, <https://doi.org/10.1002/mbo3.16> (2012).
33. Steinchen, W. *et al.* Catalytic mechanism and allosteric regulation of an oligomeric (p)ppGpp synthetase by an alarmone. *Proceedings of the National Academy of Sciences of the United States of America* **112**, 13348–13353, <https://doi.org/10.1073/pnas.1505271112> (2015).
34. Varik, V., Oliveira, S. R. A., Haurlyuk, V. & Tenson, T. HPLC-based quantification of bacterial housekeeping nucleotides and alarmone messengers ppGpp and pppGpp. *Scientific reports* **7**, 11022, <https://doi.org/10.1038/s41598-017-10988-6> (2017).
35. Bennett, B. D. *et al.* Absolute metabolite concentrations and implied enzyme active site occupancy in *Escherichia coli*. *Nature chemical biology* **5**, 593–599, <https://doi.org/10.1038/nchembio.186> (2009).
36. Haurlyuk, V. & Atkinson, G. C. Small Alarmone Synthetases as novel bacterial RNA-binding proteins. *RNA biology* **14**, 1695–1699, <https://doi.org/10.1080/15476286.2017.1367889> (2017).
37. Thackray, P. D. & Moir, A. SigM, an extracytoplasmic function sigma factor of *Bacillus subtilis*, is activated in response to cell wall antibiotics, ethanol, heat, acid, and superoxide stress. *Journal of bacteriology* **185**, 3491–3498 (2003).
38. Zweers, J. C., Nicolas, P., Wiegert, T., van Dijk, J. M. & Denham, E. L. Definition of the sigma(W) regulon of *Bacillus subtilis* in the absence of stress. *PLoS one* **7**, e48471, <https://doi.org/10.1371/journal.pone.0048471> (2012).
39. Beckert, B. *et al.* Structure of the *Bacillus subtilis* hibernating 100S ribosome reveals the basis for 70S dimerization. *The EMBO journal* **36**, 2061–2072, <https://doi.org/10.15252/embj.201696189> (2017).
40. Kabsch, W. X. *Acta crystallographica. Section D, Biological crystallography* **66**, 125–132, <https://doi.org/10.1107/S0907444909047337> (2010).
41. Winn, M. D. *et al.* Overview of the CCP4 suite and current developments. *Acta crystallographica. Section D, Biological crystallography* **67**, 235–242, <https://doi.org/10.1107/S0907444910045749> (2011).
42. Emsley, P. & Cowtan, K. Coot: model-building tools for molecular graphics. *Acta crystallographica. Section D, Biological crystallography* **60**, 2126–2132, <https://doi.org/10.1107/S0907444904019158> (2004).
43. Adams, P. D. *et al.* PHENIX: a comprehensive Python-based system for macromolecular structure solution. *Acta crystallographica. Section D, Biological crystallography* **66**, 213–221, <https://doi.org/10.1107/S0907444909052925> (2010).

Acknowledgements

We thank the European Synchrotron Radiation Facility (ESRF), Grenoble, France for support during data collection. We thank the SFB987 of the Deutsche Forschungsgemeinschaft (DFG) for financial support (to G.B.). We are grateful to Uwe Linne (Marburg) for advice.

Author Contributions

W.S. and G.B. designed research. W.S., M.S.V., F.A., P.I.G. and P.H. performed experiments. W.S., F.A., C.W. and G.B. analyzed data. W.S. and G.B. prepared the manuscript. All authors commented on the manuscript.

Additional Information

Supplementary information accompanies this paper at <https://doi.org/10.1038/s41598-018-20634-4>.

Competing Interests: The authors declare that they have no competing interests.

Publisher's note: Springer Nature remains neutral with regard to jurisdictional claims in published maps and institutional affiliations.



Open Access This article is licensed under a Creative Commons Attribution 4.0 International License, which permits use, sharing, adaptation, distribution and reproduction in any medium or format, as long as you give appropriate credit to the original author(s) and the source, provide a link to the Creative Commons license, and indicate if changes were made. The images or other third party material in this article are included in the article's Creative Commons license, unless indicated otherwise in a credit line to the material. If material is not included in the article's Creative Commons license and your intended use is not permitted by statutory regulation or exceeds the permitted use, you will need to obtain permission directly from the copyright holder. To view a copy of this license, visit <http://creativecommons.org/licenses/by/4.0/>.

© The Author(s) 2018

Discussion

Ap4A is a central component in thermoresistance of *Bacillus subtilis*

Nucleotide-based second messenger molecules play important roles in the responses to changing intra- and extracellular conditions, often also referred to as “stress”. Already in the 1960s, a study reported the presence of the universally conserved dinucleotide diadenosine 5',5''-P1,P4-tetraphosphate (Ap4A)¹. Ap4A is primarily produced by aminoacyl-tRNA synthetases (aaRS) with lysyl-tRNA synthetase being the most prominent member^{2,3}, by a side reaction when ATP reacts with the activated complex aminoacyl adenylate-aaRSs¹. Moreover, Ap4A is degraded by the ApaH phosphohydrolase in *Escherichia coli*⁴ and by PrpE in *Bacillus subtilis*⁵.

In human, Ap4A is also generated by the aaRS enzymes, and its physiological and pathological implications have been better explored. In particular Ap4A is involved in activating the microphthalmia-associated transcription factor during allergic-response-IgE^{6,7} and inhibiting the cGAS-STING pathway⁸. Additionally, Ap4A has been shown to bind the P2Y2 receptors in the ocular tissue and has been suggested as a potential treatment in eye diseases^{9,10}. The human genome possesses also Nudix hydrolases to eventually break down Ap4A to ATP and AMP¹¹. In the bacterial kingdom, over the past decades a variety of studies suggest important and pleiotropic roles of Ap4A: in the model organism *E. coli*, Ap4A affects the timing of cell division, motility, catabolite repression, the response to heat-/oxidative stress and aminoglycoside antibiotics^{4,12-15}. Similar findings eventually reported roles of Ap4A in the sporulation of *Myxococcus xanthus*³, heat-shock and ethanol stress and cell oxidation in the pathogen *Salmonella*

typhimurium^{12,16}, the biofilm of *Pseudomonas aeruginosa*¹⁷, and the survival of *Helicobacter pylori* to oxidative stress¹⁸. Given the pleiotropic effects associated with the Ap4A nucleotide, it is not surprising that it acts centrally within the bacterial metabolism. However, no detailed mechanistic or structural information were available for bacterial effectors of Ap4A. On the same line, the Publication #1 here included demonstrated the impact and consequences of the interaction between Ap4A and the inosine monophosphate dehydrogenase in *Bacillus subtilis*. We show that Ap4A inhibits the catalytic activity of the Inosine-5'-monophosphate dehydrogenase (IMPDH), which catalyzes the oxidative conversion of inosine-monophosphate (IMP) to xanthosine-monophosphate (XMP). Our structural and biochemical analysis shows that Ap4A executes its inhibitory action *via* the regulatory cystathionine β -synthetase (CBS) domain of IMPDH. Our kinetic analysis demonstrates that Ap4A regulates IMPDH allosterically in a non-competitive manner and promotes octamer formation from tetramers of IMPDH. Comparing the crystal structures of *Bs*IMPDH in complex with Ap4A and the apo *Bs*IMPDH- Δ CBS domains, it is blatant the disorder active site of the enzyme when it is bound to Ap4A. In fact, Ap4A induces allosterically a dislocation of the catalytic loop containing the essential residue Cys308, moreover the catalytic flap that coordinates the NAD⁺ cofactor is fully disordered. As ultimate consequence, Ap4A induces octamer formation gluing monomers of IMPDH between their CBS domains.

Disrupting the Ap4A-coordination mutating the arginines 141/144 to alanines, or lysine 202 to alanine would lead to a loss of thermoresistance as proved by our *in vivo* studies. A full deletion of the CBS domain has the same outcome. The mutants R141A/R144A, K202A and Δ CBS also showed an altered ratio of the guanosine/adenosine pool: without Ap4A

regulation the general guanosine de novo synthesis increases independently from the heat shock.

Our data reveals the necessity of *Bacillus subtilis* to downregulate its guanosine pathway, when facing an increase of temperature. This scenario is compatible with the possible activation of the heat shock response. At suboptimal temperatures, cells need to cope with aggregation and unfolding of the proteome, where a large amount of ATP is requested by the heat shock chaperones and proteases. Decreasing the levels GTP would support *de novo* biosynthesis of ATP in case of lack. Lower levels of GTP would also decelerate protein production since many GTPases support translation.

Regulation of eukaryotic and prokaryotic IMPDH enzymes

The human genome contains two genes that encode for two IMPDH enzymes (IMPDH1 and IMPDH2). Both enzymes, as the eukaryotic and bacterial IMPDHs, contain a catalytic domain for the conversion of IMP to XMP and a regulatory domain (CBS domains) that can bind two or more nucleotides. Authors already reported how the Human IMPDH1 can bind Ap4A 5 times stronger than ATP, but the interaction does not lead to a significant inhibition of the enzymatic activity¹⁹. Instead, human IMPDHs are regulated by GTP/GDP and ATP/ADP binding in the CBS domains^{20,21}. Moreover, human IMPDHs are cable of filament-formation in response to a high demand of guanosines. In this form they do not respond to allosteric regulation nucleotide-mediated in their regulatory domains^{20,21}. Also, the IMPDH enzyme of the fungus *Ashbya gossypii* is regulated by guanosine nucleotides *in vitro*, but in cell experiments are still lacking²². Diversely, prokaryotic IMPDHs have been divided in two different classes according

to their oligomerization states and kinetics²³. Class I is mainly present in proteobacteria, characterized by stable octamers and sigmoidal kinetics. Instead, the class II IMPDHs are in equilibrium between tetramers and octamers. The substrates NAD⁺ and IMP, binding to the active site, shift the oligomers to the tetrameric form. The class II does not have cooperativity among monomers and is described by Henri-Michaelis-Menten kinetic. The *Pseudomonas aeruginosa* IMPDH belongs to the first class. It generally has a weak enzymatic activity and requires ATP to stimulate the active site. Also, in this case two molecules of ATP bind the CBS domains and induces an open conformation of the octamer²⁴. As discussed in the Publication #1, Ap4A binds the *Bacillus subtilis* IMPDH in the same site and conformation of ATP molecules in the *Pseudomonas aeruginosa* IMPDH.

IMPDH and (p)ppGpp

In the second messengers' world, crosstalks between nucleotides are known. Recently Fung D.K. *et al.*²⁵ reported that Ap4A accumulates in strains of *Bacillus subtilis* overexpressing small alarmone synthetases. However, a direct relation between (p)ppGpp and Ap4A was not possible. Other authors in Fernández-Justel *et al.* proposed IMPDH as a crosstalk point between (p)ppGpp and ATP in *Bacillus subtilis* and in *Streptomyces coelicolor*²⁶. In their study, (p)ppGpp could only inhibit the firmicute IMPDHs in presence of ATP. Similarly, in their study, the proteobacterial IMPDHs of *Escherichia coli* and *Pseudomonas aeruginosa* were inhibited by GTP/GDP when ATP was present in the reaction mixture. Sadly, they do not include any *in vivo* data that could confirm their *in vitro* findings and no affinities were determined between (p)ppGpp and IMPDH or GTP/GDP

and IMPDH. Altogether, the authors suggested (p)ppGpp as modulator the guanosine pathway in a housekeeping fashion, but no correlations with heat shock or stringent response were offered, probably due to the lack of *in vivo* data. Controversially, precedent studies do not report inhibition of *Bs*IMPDH activity by (p)ppGpp^{27,28}, while it was instead shown that it can inhibit the inosine guanosine-kinase of *E. coli*²⁷.

In our study, Publication #1, we could instead monitor the Ap4A concentrations increasing from exponential phase and no thermal shock (24 μ M) to heat shock (51 °C tested) for 30 minutes (ca. 50 μ M). Correlating the basal Ap4A concentration with the K_D (7.4 ± 2.1 μ M) and K_i (15.8 μ M) values obtained *in vitro* for the IMPDH-Ap4A interaction. We instead believe that Ap4A has a strong role in the downregulation of the *de novo* guanosine-biosynthesis pathway (**Fig. 3**).

It would be more fascinating to explore, instead, the role of (p)ppGpp in the other side of the purine biosynthesis, where the adenylosuccinate synthase (PurA in *B. subtilis*) converts IMP to adenylosuccinate. In fact, authors already demonstrated how PurA is inhibited by (p)ppGpp²⁹. In this scenario a guanosine based alarmone ((p)ppGpp) would inhibit the adenosine pathway, while Ap4A would control the guanosine *de novo* biosynthesis (**Fig. 3**).

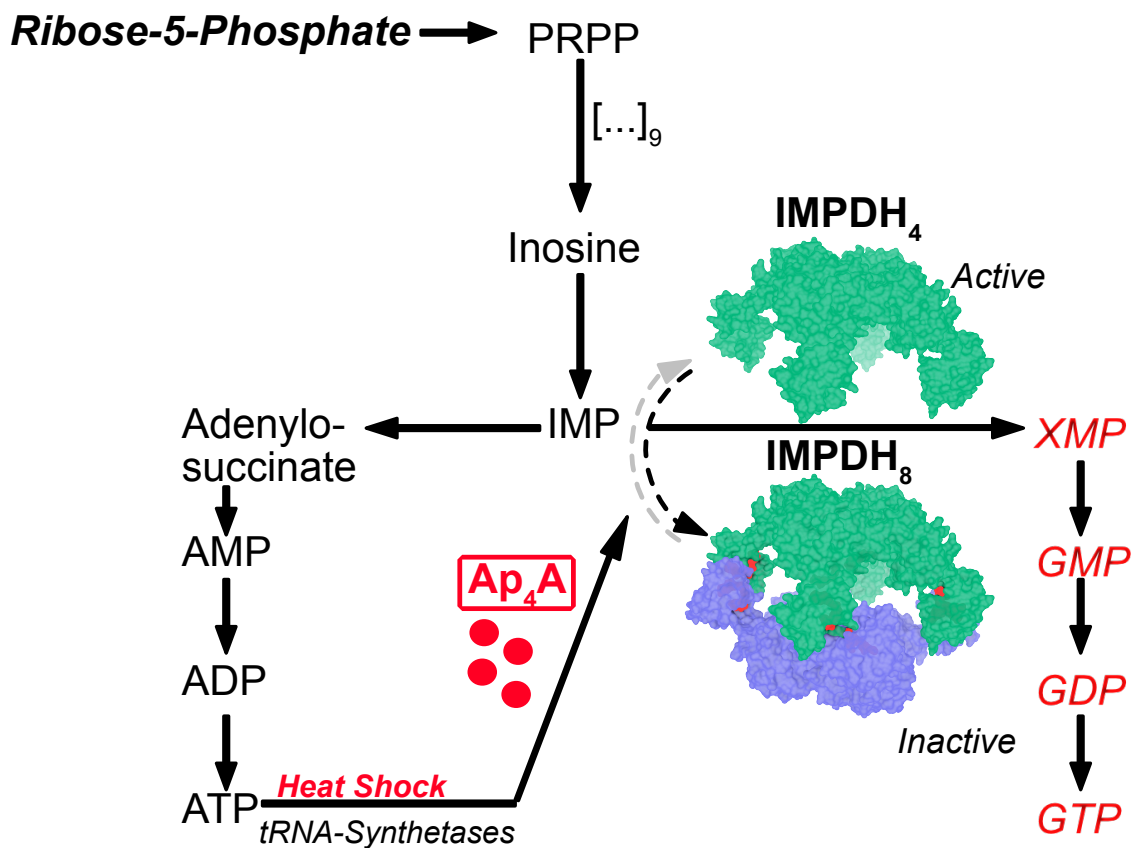


Fig. 3: *De novo* biosynthesis of purines derives from the metabolism of sugars. The inosine metabolite (IMP) sits at the branching point between guanosine and adenosine nucleotides. The IMPDH enzyme converts IMP to xanthosine monophosphate (XMP). During heat shock in *Bacillus subtilis*, the dinucleotide Ap₄A inhibits IMPDH by promoting its oligomerization from tetramer to octamer. This in turn leads to a decrease in the pool of guanosine nucleotides (red label).

Priorities in Stringent Response

Adaptation to Stringent Response (SR) evolved divergently among different bacterial species. In fact, (p)ppGpp is a strict inhibitor of the proteobacterial RNA polymerase but does not interfere with the firmicute counterpart. In this case, the anabolic pathway of GTP is targeted at the level of the guanylate kinase GMK³⁰.

Nevertheless, (p)ppGpp alarmones remain the master regulators whenever bacteria must deal with face carbon, amino acid, or lipid starvation. Scientific literature documented a wide spectrum of targets of (p)ppGpp that have been characterized among gram-positives and gram-negatives until current date (reviewed in ³¹).

Most commonly, (p)ppGpp targets are enzymes involved in essential cellular processes and most of them are GTPases. The (p)ppGpp inhibition-mechanism of GTPase enzymes is based on a direct competition for the active site. (p)ppGpp, according to its affinity for the target, can displace the GTP substrate.

The SRP protein Ffh and its receptor FtsY are GTPases as well and constitute part of a conserved mechanism for membrane protein insertion and secretion. In our study (Publication #2), we described how (p)ppGpp can inhibit both Ffh and Ftsy and prevent the heterodimerization between them. Our inhibition model demonstrates that (p)ppGpp directly competes with the substrate GTP in the active site of Ffh and Ftsy. Here, the phosphates δ - and ϵ on the 3'O of the (p)ppGpp ribose would impede the dimer formation of the GTPases by means of repulsion and steric hindrance when the NG domains of the SRP and its receptor are in a face-to-face position. In such

manner, (p)ppGpp prevents co-translational and post-translational insertion of membrane proteins.

In our study, both Ffh and Ftsy showed higher affinities to GDP rather than to (p)ppGpp and to GTP, measured with ITC and MST. Such measurements would collocate the SRP inhibition in a scenario of rather high starvation when the GTP and GDP pools are mostly converted by Rel/RelA to ppGpp and pppGpp. However, the obtained K_D values do not exclude a possible local inhibition of the SRP system when it is ribosome-associated. There, the Rel/RelA enzymes would be the source of (p)ppGpp in stalled ribosomes.

First, our study (Publication #2) suggests that proteobacteria and firmicutes could display the same inhibition mechanisms of the SPR-dependent membrane protein insertion. Secondly, our CryoEM studies suggest that pppGpp interferes with the flexibility of the *Bacillus subtilis* Ffh NG-domain, however, we could not observe the same dynamic in the *Escherichia coli* counterpart. This evidence might implicate that proteobacteria do not need the same additional modes of regulation.

It seems not the case for *Bacillus subtilis*, where (p)ppGpp can reduce the conformational freedom of the SRP complex when it recognizes the signal sequence of the nascent chain and then it would also inhibit the Ffh hydrolysis activity and Ffh-FtsY dimerization.

Diversification in (p)ppGpp production

The source of ppGpp and pppGpp drastically changes in firmicutes and in proteobacteria. A long bifunctional Rel enzyme produces (p)ppGpp when bound to stalled ribosomes in firmicutes, and subsequently hydrolyses the alarmone to reprimarize the pools of GDP and GTP. Instead, proteobacteria encode in their genome two long RSH enzymes: RelA and SpoT. RelA is deputized to synthesis of (p)ppGpp while SpoT displays a weak synthesis activity and a more pronounced hydrolysis function.

The firmicute *Bacillus subtilis* can also rely on two additional small alarmone synthetases (RelP/SAS2 and RelQ/SAS1). In our study, Publication #3, we expanded the knowledge on how the SAS enzymes contribute in the response to nutritional and environmental stresses together with the Rel enzyme. We provided insights into the mechanisms of action of the enzymes RelP and RelQ on a biochemical level.

Despite RelQ and RelP sharing 50% homology in their sequences and existing in solution as homotetramers, we showed how they diverge in the (p)ppGpp production. In an identical fashion ATP binds the active site of both synthetases, but while the RelP enzyme possesses an organized G-loop to coordinate the substrates GTP or GDP, the RelQ requires the allosteric stimulation by pppGpp to reach the same K_m value as RelP. In particular, a molecule of pppGpp can bind the central cleft originated symmetrically by the subunits in the homotetramer to promote the recruitment of the catalytic G-loop onto the active site. In a natural consecution of events, the Rel enzyme would be the main producer of (p)ppGpp and then RelQ would amplify the alarmone production after allosteric stimulation offered by the (p)ppGpp pool already accumulated by the Rel enzyme. In such a way RelQ

co-works with RelP to finely control the alarmone levels in the exponential phase, also indicated by its transcription levels³². Other studies also suggested that an uncharacterized RNA motif can bind the *Enterococcus faecalis* RelQ in its cleft in order to inhibit (p)ppGpp production³³.

Diversely, RelP transcription is promoted by stresses originated by changes in pH, ethanol, high salts or antibiotic treatments and generally it is transcribed in early exponential phase³⁴⁻³⁶. Moreover, RelP does not need any stimulation *in vitro* activity, but this notion does not exclude that unknown factors might regulate its function *in vivo*.

Fine tuning of second messengers' concentrations is crucial to promptly react to cellular stresses and in this current picture, RelQ appears to be deeper characterized than RelP. Despite the fact that we do not know which RNA sequence can inhibit RelQ, we could assign it a role in the stress response, since its activity is linked to the amount of pppGpp present in the cell.

So far, we do not have evidence of possible regulator of RelP, and its function might logically sound redundant. Nevertheless, more recent studies suggested that RelP and RelQ are linked to the biofilm formation during cell wall stress³⁷. RelP was also linked to translation arrest promoting ribosome-dimerization³⁸. In this sense, RelP could diversify the general stress response not only producing alarmone but also shutting down the entire translational assembly. Anyway, more efforts are still required to explain how proteobacteria and firmicutes took such different paths in the stress response orchestration.

References of the Discussion

- 1 Zamecnik, P. G., Stephenson, M. L., Janeway, C. M. & Randerath, K. Enzymatic synthesis of diadenosine tetraphosphate and diadenosine triphosphate with a purified lysyl-sRNA synthetase. *Biochemical and Biophysical Research Communications* **24**, 91-97 (1966). [https://doi.org:https://doi.org/10.1016/0006-291X\(66\)90415-3](https://doi.org/10.1016/0006-291X(66)90415-3)
- 2 Charlier, J. & Sanchez, R. Lysyl-tRNA synthetase from *Escherichia coli* K12. Chromatographic heterogeneity and the lysU-gene product. *Biochem J* **248**, 43-51 (1987). [https://doi.org:10.1042/bj2480043](https://doi.org/10.1042/bj2480043)
- 3 Kimura, Y., Tanaka, C., Sasaki, K. & Sasaki, M. High concentrations of intracellular Ap4A and/or Ap5A in developing *Myxococcus xanthus* cells inhibit sporulation. *Microbiology (Reading)* **163**, 86-93 (2017). [https://doi.org:10.1099/mic.0.000403](https://doi.org/10.1099/mic.0.000403)
- 4 Farr, S. B., Arnosti, D. N., Chamberlin, M. J. & Ames, B. N. An apaH mutation causes AppppA to accumulate and affects motility and catabolite repression in *Escherichia coli*. *Proc Natl Acad Sci U S A* **86**, 5010-5014 (1989). [https://doi.org:10.1073/pnas.86.13.5010](https://doi.org/10.1073/pnas.86.13.5010)
- 5 Iwanicki, A., Herman-Antosiewicz, A., Pierechod, M., Séror, S. J. & Obuchowski, M. PrpE, a PPP protein phosphatase from *Bacillus subtilis* with unusual substrate specificity. *Biochem J* **366**, 929-936 (2002). [https://doi.org:10.1042/bj20011591](https://doi.org/10.1042/bj20011591)
- 6 Lee, Y. N., Nechushtan, H., Figov, N. & Razin, E. The function of lysyl-tRNA synthetase and Ap4A as signaling regulators of MITF activity in FcepsilonRI-activated mast cells. *Immunity* **20**, 145-151 (2004). [https://doi.org:10.1016/s1074-7613\(04\)00020-2](https://doi.org/10.1016/s1074-7613(04)00020-2)
- 7 Yannay-Cohen, N. *et al.* LysRS Serves as a Key Signaling Molecule in the Immune Response by Regulating Gene Expression. *Molecular Cell* **34**, 603-611 (2009). [https://doi.org:https://doi.org/10.1016/j.molcel.2009.05.019](https://doi.org/10.1016/j.molcel.2009.05.019)
- 8 Guerra, J. *et al.* Lysyl-tRNA synthetase produces diadenosine tetraphosphate to curb STING-dependent inflammation. *Sci Adv* **6**, eaax3333 (2020). [https://doi.org:10.1126/sciadv.aax3333](https://doi.org/10.1126/sciadv.aax3333)
- 9 Reigada, D. *et al.* Diadenosine tetraphosphate (Ap(4)A) inhibits ATP-induced excitotoxicity: a neuroprotective strategy for traumatic spinal cord injury treatment. *Purinergic Signal* **13**, 75-87 (2017). [https://doi.org:10.1007/s11302-016-9541-4](https://doi.org/10.1007/s11302-016-9541-4)

- 10 Crooke, A., Guzman-Aranguez, A., Carracedo, G., de Lara, M. J. P. & Pintor, J. Understanding the Presence and Roles of Ap4A (Diadenosine Tetraphosphate) in the Eye. *Journal of Ocular Pharmacology and Therapeutics* **33**, 426-434 (2017). <https://doi.org:10.1089/jop.2016.0146>
- 11 Marriott, A. S. *et al.* NUDT2 Disruption Elevates Diadenosine Tetraphosphate (Ap4A) and Down-Regulates Immune Response and Cancer Promotion Genes. *PLoS One* **11**, e0154674 (2016). <https://doi.org:10.1371/journal.pone.0154674>
- 12 Lee, P. C., Bochner, B. R. & Ames, B. N. AppppA, heat-shock stress, and cell oxidation. *Proc Natl Acad Sci U S A* **80**, 7496-7500 (1983). <https://doi.org:10.1073/pnas.80.24.7496>
- 13 Ji, X. *et al.* Alarmone Ap4A is elevated by aminoglycoside antibiotics and enhances their bactericidal activity. *Proceedings of the National Academy of Sciences* **116**, 9578-9585 (2019). <https://doi.org:doi:10.1073/pnas.1822026116>
- 14 Johnstone, D. B. & Farr, S. B. AppppA binds to several proteins in Escherichia coli, including the heat shock and oxidative stress proteins DnaK, GroEL, E89, C45 and C40. *Embo j* **10**, 3897-3904 (1991). <https://doi.org:10.1002/j.1460-2075.1991.tb04959.x>
- 15 Nishimura, A. *et al.* Diadenosine 5',5'''-P1,P4-tetraphosphate (Ap4A) controls the timing of cell division in Escherichia coli. *Genes Cells* **2**, 401-413 (1997). <https://doi.org:10.1046/j.1365-2443.1997.1300328.x>
- 16 Bochner, B. R., Lee, P. C., Wilson, S. W., Cutler, C. W. & Ames, B. N. AppppA and related adenylylated nucleotides are synthesized as a consequence of oxidation stress. *Cell* **37**, 225-232 (1984). [https://doi.org:10.1016/0092-8674\(84\)90318-0](https://doi.org:10.1016/0092-8674(84)90318-0)
- 17 Monds, R. D. *et al.* Di-adenosine tetraphosphate (Ap4A) metabolism impacts biofilm formation by Pseudomonas fluorescens via modulation of c-di-GMP-dependent pathways. *J Bacteriol* **192**, 3011-3023 (2010). <https://doi.org:10.1128/jb.01571-09>
- 18 Lundin, A. *et al.* The NudA protein in the gastric pathogen Helicobacter pylori is an ubiquitous and constitutively expressed dinucleoside polyphosphate hydrolase. *J Biol Chem* **278**, 12574-12578 (2003). <https://doi.org:10.1074/jbc.M212542200>
- 19 Fernández-Justel, D., Peláez, R., Revuelta, J. L. & Buey, R. M. The Bateman domain of IMP dehydrogenase is a binding target for dinucleoside polyphosphates. *J Biol Chem* **294**, 14768-14775 (2019). <https://doi.org:10.1074/jbc.AC119.010055>

- 20 Johnson, M. C. & Kollman, J. M. Cryo-EM structures demonstrate human IMPDH2 filament assembly tunes allosteric regulation. *Elife* **9** (2020). <https://doi.org:10.7554/eLife.53243>
- 21 Burrell, A. L. *et al.* IMPDH1 retinal variants control filament architecture to tune allosteric regulation. *Nat Struct Mol Biol* **29**, 47-58 (2022). <https://doi.org:10.1038/s41594-021-00706-2>
- 22 Buey, R. M. *et al.* Guanine nucleotide binding to the Bateman domain mediates the allosteric inhibition of eukaryotic IMP dehydrogenases. *Nature Communications* **6**, 8923 (2015). <https://doi.org:10.1038/ncomms9923>
- 23 Alexandre, T., Rayna, B. & Munier-Lehmann, H. Two Classes of Bacterial IMPDHs according to Their Quaternary Structures and Catalytic Properties. *PLOS ONE* **10**, e0116578 (2015). <https://doi.org:10.1371/journal.pone.0116578>
- 24 Labesse, G. *et al.* MgATP regulates allostery and fiber formation in IMPDHs. *Structure* **21**, 975-985 (2013). <https://doi.org:10.1016/j.str.2013.03.011>
- 25 Fung, D. K., Yang, J., Stevenson, D. M., Amador-Noguez, D. & Wang, J. D. Small Alarmone Synthetase SasA Expression Leads to Concomitant Accumulation of pGpp, ppApp, and AppppA in *Bacillus subtilis*. *Frontiers in Microbiology* **11** (2020). <https://doi.org:10.3389/fmicb.2020.02083>
- 26 Fernández-Justel, D. *et al.* Diversity of mechanisms to control bacterial GTP homeostasis by the mutually exclusive binding of adenine and guanine nucleotides to IMP dehydrogenase. *Protein Sci* **31**, e4314 (2022). <https://doi.org:10.1002/pro.4314>
- 27 Wang, B., Grant, R. A. & Laub, M. T. ppGpp Coordinates Nucleotide and Amino-Acid Synthesis in *E. coli* During Starvation. *Molecular Cell* **80**, 29-42.e10 (2020). <https://doi.org:https://doi.org/10.1016/j.molcel.2020.08.005>
- 28 Kriel, A. *et al.* GTP dysregulation in *Bacillus subtilis* cells lacking (p)ppGpp results in phenotypic amino acid auxotrophy and failure to adapt to nutrient downshift and regulate biosynthesis genes. *J Bacteriol* **196**, 189-201 (2014). <https://doi.org:10.1128/jb.00918-13>
- 29 Hou, Z., Cashel, M., Fromm, H. J. & Honzatko, R. B. Effectors of the Stringent Response Target the Active Site of *Escherichia coli* Adenylosuccinate Synthetase *. *Journal of Biological Chemistry* **274**, 17505-17510 (1999). <https://doi.org:10.1074/jbc.274.25.17505>

- 30 Liu, K. *et al.* Molecular mechanism and evolution of guanylate kinase regulation by (p)ppGpp. *Mol Cell* **57**, 735-749 (2015). <https://doi.org:10.1016/j.molcel.2014.12.037>
- 31 Steinchen, W., Zegarra, V. & Bange, G. (p)ppGpp: Magic Modulators of Bacterial Physiology and Metabolism. *Front Microbiol* **11**, 2072 (2020). <https://doi.org:10.3389/fmicb.2020.02072>
- 32 Nanamiya, H. *et al.* Identification and functional analysis of novel (p)ppGpp synthetase genes in *Bacillus subtilis*. *Mol Microbiol* **67**, 291-304 (2008). <https://doi.org:10.1111/j.1365-2958.2007.06018.x>
- 33 Beljantseva, J. *et al.* Negative allosteric regulation of *Enterococcus faecalis* small alarmone synthetase RelQ by single-stranded RNA. *Proceedings of the National Academy of Sciences* **114**, 3726-3731 (2017). <https://doi.org:doi:10.1073/pnas.1617868114>
- 34 Geiger, T., Kästle, B., Gratani, F. L., Goerke, C. & Wolz, C. Two small (p)ppGpp synthetases in *Staphylococcus aureus* mediate tolerance against cell envelope stress conditions. *J Bacteriol* **196**, 894-902 (2014). <https://doi.org:10.1128/jb.01201-13>
- 35 Thackray, P. D. & Moir, A. SigM, an extracytoplasmic function sigma factor of *Bacillus subtilis*, is activated in response to cell wall antibiotics, ethanol, heat, acid, and superoxide stress. *J Bacteriol* **185**, 3491-3498 (2003). <https://doi.org:10.1128/jb.185.12.3491-3498.2003>
- 36 Zweers, J. C., Nicolas, P., Wiegert, T., van Dijl, J. M. & Denham, E. L. Definition of the σ^W Regulon of *Bacillus subtilis* in the Absence of Stress. *PLOS ONE* **7**, e48471 (2012). <https://doi.org:10.1371/journal.pone.0048471>
- 37 Salzer, A., Keinhörster, D., Kästle, C., Kästle, B. & Wolz, C. Small Alarmone Synthetases RelP and RelQ of *Staphylococcus aureus* Are Involved in Biofilm Formation and Maintenance Under Cell Wall Stress Conditions. *Frontiers in Microbiology* **11** (2020). <https://doi.org:10.3389/fmicb.2020.575882>
- 38 Tagami, K. *et al.* Expression of a small (p)ppGpp synthetase, YwaC, in the (p)ppGpp⁰ mutant of *Bacillus subtilis* triggers YvyD-dependent dimerization of ribosome. *MicrobiologyOpen* **1**, 115-134 (2012). <https://doi.org:https://doi.org/10.1002/mbo3.16>